Supramolecular Anticancer Agents and their Effects on Cells and Biomolecules

Alexandra Jayne Pope

A thesis submitted to The University of Birmingham for the degree of

Doctor of Philosophy

Department of Chemistry

University of Birmingham

February 2011

Abstract

Metallo-drugs have been highly significant in the development of novel anticancer agents. Supramolecular drug agents allow the design and synthesis of a range of molecular architectures. The work in this thesis has built upon previous knowledge on this subject by undertaking novel biological studies on known metal supramolecular helicates as well as the design of a new helicate in order to improve upon existing drugs.

In chapter three, the DNA three-way junction binding of a number of supramolecular cylinders is described. Three-way junction binding is a new mode of DNA recognition and relevant to the DNA replication fork, present in dividing cells.

Chapter four outlines a number of novel *in vitro* studies on an iron supramolecular cylinder which indicate new, unsuspected and unprecedented biological actions.

In chapter five biological studies of unsaturated ruthenium(II) helicates are discussed. These complexes combine a cisplatin like coordinative binding mode with a helical supramolecular design.

Chapter six discusses the design of a synthetic route from an unsaturated ruthenium(II) complex to create a novel supramolecular compound with a tuneable ligand surface.

Acknowledgements

I would like to thank Professor Hannon, without whom this research would not have been possible.

A number of individuals and labs have also made this work achievable and enjoyable: the Hannon research group with its excellent work atmosphere and the many excuses for cake; the chemistry analytical department; those of the 4th floor biosciences and the Institute of Biophysics, Brno.

I would also like to say a big thanks to friends who have read parts of this thesis and especially to Helen and Liam for taking me in and keeping me sane (!)

Most importantly, I am so grateful to Dad and Mum, I couldn't have done this without you.

Papers Published from this Thesis

Issues surrounding standard cytotoxicity testing for assessing activity of non-covalent DNA-binding metallo-drugs.

A. J. Pope, C. Bruce, B. Kysela and M. J. Hannon, *Dalton Trans.,* 2010, **39**, 2772-2774.

Contents

Abbreviations

NMR	Nuclear Magnetic Resonance
ESI MS	Electrospray Ionisation Mass Spctrometry
CD	Circular Dichroism
LD	Linear Dichroism
MLCT	Metal to Ligand Charge Transfer
UV-Vis	Ultra-Violet, Visible spectroscopy
AFM	Atomic Force Microscopy
DNA / RNA	Deoxyribonucleic Acid / Ribonucleic Acid
A,T,C,G	Adenine, Thymine, Cytosine, Guanine
EB	Ethidium Bromide
EDTA	Ethylenediaminetetraacetic Acid
DCM	Dichloromethane
DMSO	Dimethylsulphoxide
CD_2Cl_2	Deuterated Dichloromethane
$CDCl_3$	Deuterated Chloroform
MeOD	Deuterated Methanol
DMSO-d6	Deuterated Dimethylsulphoxide
CD_3CN	Deuterated Acetonitrile
PBS	Phosphate Buffered Saline
RPMI / DMEM	Cell culture medium
MTT	3-[4,5-Dimethylthiazol-2-yl]-2,5-Diphenyl Tetrazolium Bromide
IC_{50}	50 % cell viability concentration
T47D, MDA-MB-231	Breast cancer cell lines
SKOV-3, A2780-P, A2780-R	Ovarian cancer cell lines
HL-60	Myeloid Leukaemia cell line
A-498	Kidney tumour cell line
TA98 / TA100	*Salmonella typhimurium* bacterial lines
SEM	Standard error of means

Chapter 1

Introduction

1.1 Supramolecular Chemistry

Supramolecular chemistry, first defined by Jean-Marie Lehn in 1978 as 'the chemistry of molecular assemblies and of the intermolecular bond'[1] is one of the fastest growing fields of chemistry. The Nobel Prize was won in 1987 by Donald J. Cram, Jean-Marie Lehn and Charles. J. Pedersen for their pioneering work in this area and subsequent advances in this field, notably by Hannon and co-workers (see section 1.7), have shown how the supramolecular approach can be a valuable tool for the design of new DNA recognition agents.[2] Supramolecular chemistry is able to bridge the size gap between synthetic chemistry and biology.

In this introduction, the principles of supramolecular chemistry and DNA recognition will be discussed and some examples of DNA binding metal complexes will be presented.

1.1.1 Supramolecular Helicate Classification and Design

Research into helicates was pioneered by Jean-Marie Lehn, in 1987.[3] The term helicate is used when one or more organic, covalent ligand strands are wrapped around metal ions, thus defining the helical axis.[4] These compounds are usually formed through self-assembly, a process by which specific components spontaneously assemble with high selectivity into a well-defined, discrete supramolecular architecture. This self assembly may be driven to completion by, for example, positive cooperativity or energy flow.[5]

Helicates may be classified as either homotopic or heterotopic, represented diagrammatically in Figure 1. 1. Helicates may also exist as two optical isomers. When a

molecule and its mirror image are not structurally identical it is termed to be chiral. In this case homotopic helicates can exist in two isomeric forms, heterotopic helicates in four.[4]

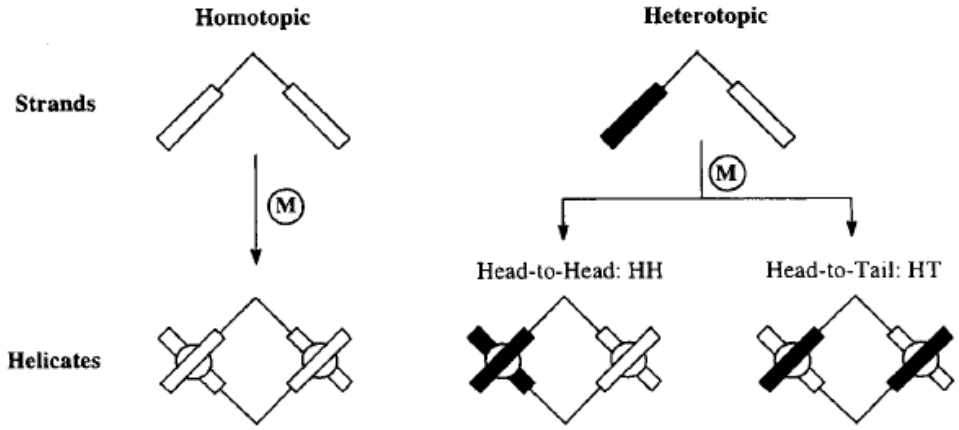

Figure 1. 1 Representation of homotopic and heterotopic helicates.[4]

When designing helical agents there are a number of factors that need to be taken into consideration. The ligand must be designed to have at least two binding sites which will be able to recognise and coordinate to the chosen metal ion. Furthermore, the ligand should be flexible enough between binding sites to allow it to wrap around the helical axis, but not too flexible so one ligand coordinates multiple times to the same metal ion.

1.2 Deoxyribonucleic Acid (DNA)

A well defined helix, formed through self assembly, is the DNA double helix. The focus herein will be on the B-form of the DNA helix which consists of two polynucleotide strands, comprising four different nucleotides, twisted together to form a right handed helix with a sugar phosphate backbone. The helix is held together via hydrogen bond interactions of the DNA bases, Figure 1. 2.

(1)

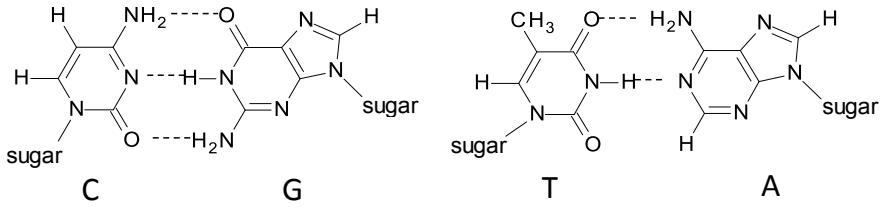

(2)

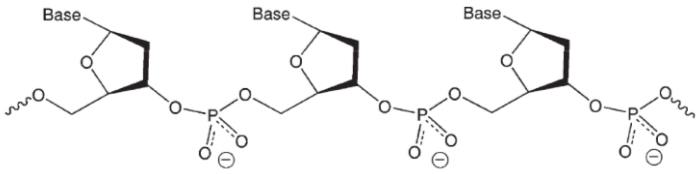

Figure 1. 2 (1) DNA bases and their hydrogen bond pairs. (2) The sugar phosphate backbone.

There are two distinct grooves in this double stranded structure, labelled the major and minor groove, Figure 1. 3. B-DNA has a wide, deep major groove, and a narrow, deep minor groove.

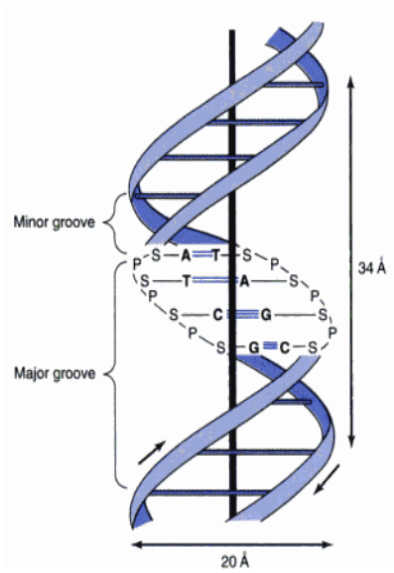

Figure 1. 3 The DNA helix, illustrating a major and minor groove.[6]

The DNA molecule may exist in various other forms, for example A- and Z-DNA, Figure 1. 4, however B-DNA is the most prevalent in biological systems.

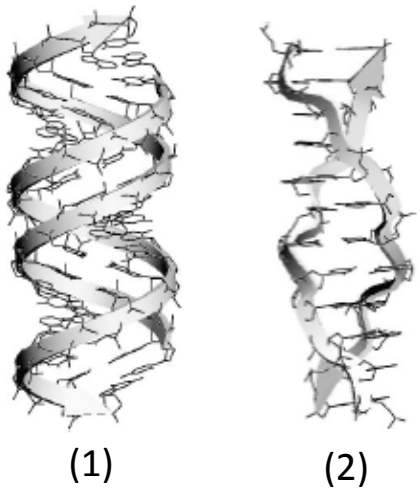

Figure 1. 4 A-DNA (1) and Z-DNA (2) structures.[6]

1. 2. 1 Other DNA Structures

Although the double stranded structure of DNA is the predominant form in biological systems, DNA can adopt other structures and levels of ordering which may then be recognised by a drug molecule. Triplex, quadruplex and junction structures are examples of higher order DNA structures. Triplex DNA, Figure 1. 5, is formed when duplex DNA associates with an additional polynucleotide strand. This lies in the major groove of the DNA and is held in place by hydrogen bonding interactions between base pairs.

Figure 1. 5 Schematic representation of triplex DNA.[6]

G-quadruplex DNA is a four-stranded DNA structure formed by non-Watson-Crick base pairing between stacked sets of guanine tetramers, Figure 1. 6.

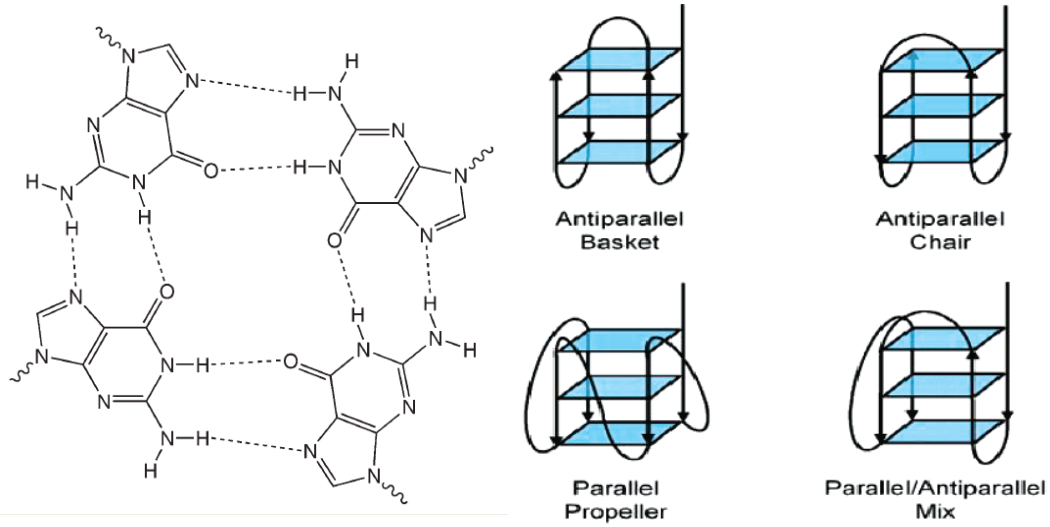

Figure 1. 6 Guanine tetramers (the basis for quadruplex formation) and possible DNA strand orientations for the formation of a G-quadruplex structure.[7]

DNA junction structures arise when two or more polynucleotide chains come together, illustrated in Figure 1. 7.

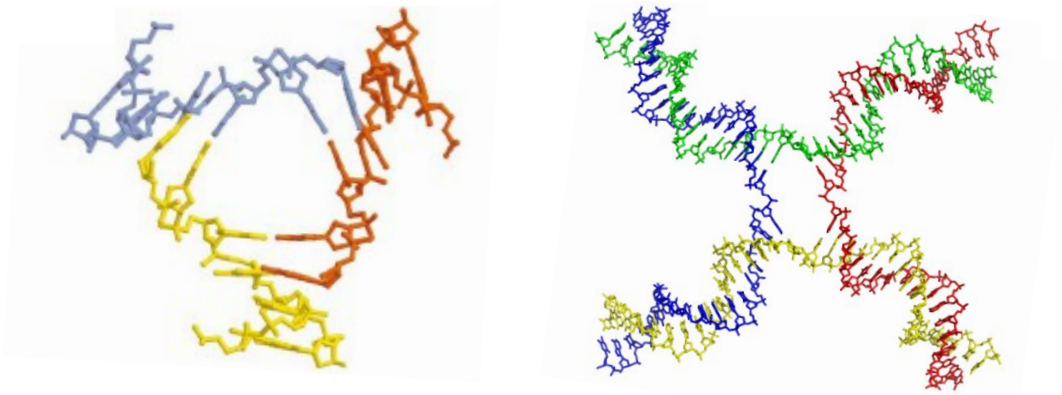

(1) (2)

Figure 1. 7 Examples of three-way (1)[8] *and four-way (2)*[9] *junction structures.*

DNA junctions such as these have been defined by David Lilley as 'branch points where double-helical segments intersect with axial discontinuities, such that strands are exchanged between the different helical sections.[9] Junction structures are present as intermediates in a number of genetic processes and are therefore of interest biologically. For example, an intermediate related to the DNA three-way junction structure is present during DNA replication and transcription, processes occurring in all living cells. Junction structures have also been implicated in the advancement of a number of diseases, for example Huntington's disease, which is characterised by a triplet repeat expansion in the DNA.[10]

1. 2. 2 DNA Recognition

Nature has a very accurate recognition system, beginning with the replication of DNA. Segments of the original DNA sequence are copied into RNA molecules, which in turn code for specific protein sequences. Each of these segments of DNA, corresponding to a final protein product is called a gene. Genes dictate the exact nature of the final protein, including the structure as well as under which conditions it will be produced. It is clear how much influence these genes have and hence why they are so important in disease states. Cancers for example, may occur when mutations in a subset of genes give a growth advantage to a group of cells. With the advent of genomic sequencing, medical research has turned to the ambitious idea of using the control of genes for the fight against disease. Theoretically, this may be achieved by creating synthetic agents (or utilising natural ones) that can bind selectively to genes in order to control their action.[2] Novel therapeutics may also be able to overcome drawbacks of current drugs such as toxic side effects or acquired resistance.

A number of DNA recognition modes have been investigated for their potential as key drug targets: major/minor groove binding, intercalation, backbone recognition, covalent binding to DNA bases and binding to DNA junctions or other DNA structures.

1.3 Metal Coordination Complexes as Anticancer Agents

Metal ions are a clear target for medicinal chemists attempting to make novel drug agents, especially ones that bind to DNA. The idea of using metal ions in drugs stems from the ubiquitous presence of metal ions in nature. Fe, Zn, Cu, Na, K and many others are present in the human body in trace amounts, however without them our bodies would not function. These ions are essential for many metabolic and catalytic processes. A particularly important example in this context is the zinc finger protein. The metal ion is used specifically for the structural configuration it confers to the protein.[11] This has parallels in the use of metals for drug design and gives an advantage over purely organic compounds.

Complexes of transition metal cations have become attractive targets in drug design due to their many possible structures, flexibility in ligand choice and the variety of DNA interactions and binding modes available. Currently, however, the only metal containing anticancer agents which have reached the clinic are the well known range of platinum compounds including cisplatin, carboplatin and oxaliplatin[12] (discussed in more detail in section 1.4). There are also a number of metal containing drugs undergoing clinical trials, for example the ruthenium compounds KP1019[13] and NAMI-A[14] (discussed in more detail in section 1.5.2.1) and many more in early stage research.

1.4 Platinum Anticancer Agents

1.4.1 Cisplatin and its Analogues

Cisplatin, Figure 1. 8, was first discovered by M. Peyrone in 1845[15], although it was not until the 1960s that its potential as an anticancer agent became apparent.

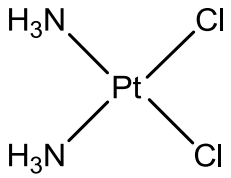

Figure 1. 8 *The structure of cisplatin.*

Cisplatin is now the most widely used anticancer agent worldwide[16] and therefore remains the benchmark for many researchers investigating novel anticancer agents, regardless of the compounds mode of action. Cisplatin acts through the loss of two *cis*-chloride groups on the platinum metal centre, either through aquation or binding to sulphur containing ligands. The labile nature of these ligands then allows the coordination to two neighbouring guanine molecules (usually through N-7) of the DNA chain, Figure 1. 9.

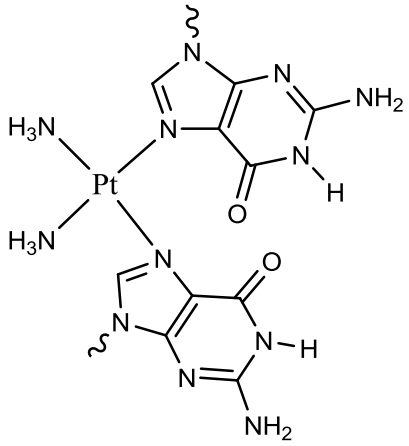

Figure 1. 9 *Cisplatin bound to two guanine molecules.*

This is a fast reaction and the DNA-Pt bond is kinetically inert. This causes a kink in the DNA, Figure 1. 10, and the subsequent inability of this DNA to be processed, leading to cell death through arrest of the cell cycle at G2 and apoptosis.[17]

Figure 1. 10 DNA with cisplatin bound illustrating the kink caused in the DNA structure.[18]

The details of the cellular uptake of cisplatin have yet to be fully elucidated. Early studies indicated passive diffusion to be an entry mechanism, with more recent work indicating that active copper transport proteins (influx CTR1 and efflux ATP7A and ATP7B) may play a role,[19] Figure 1. 11.

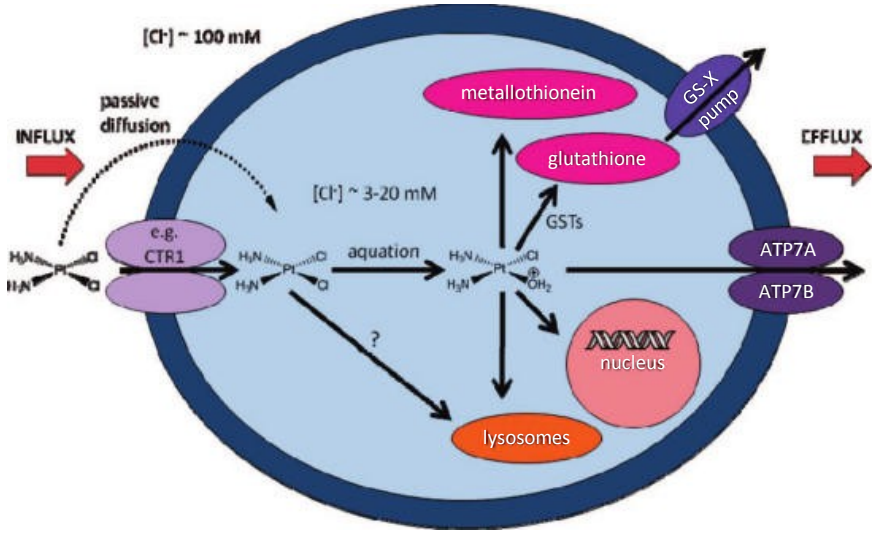

Figure 1. 11 Overview of the proposed pathway of cisplatin in the cell. [20]

Despite the obvious success of cisplatin, there are a number of drawbacks. The dose that can be administered is limited by kidney toxicity and although this may be ameliorated by hydrating the patient during treatment, this is not an ideal situation. Resistance to cisplatin caused by repair of the DNA-platinum lesion, reduced intracellular accumulation, or interaction with thiol containing molecules (such as glutathione) is also a problem. Furthermore, cisplatin is only active against a narrow spectrum of cancers, mostly notably testicular and ovarian.[21]

Second generation platinum drugs were initially designed to try and overcome some of the inherent toxicity of cisplatin. Carboplatin, Figure 1. 12, contains a cyclobutane dicarboxylic acid ligand. This ligand exhibits slower aquation, meaning less interaction with biological ligands en-route to DNA. This was found to reduce nephrotoxicity, however carboplatin has a similar clinical profile to cisplatin, therefore displaying cross resistance.[21] Oxaliplatin, Figure 1. 12, has the NH_3 moieties of cisplatin replaced with more inert nitrogen donor ligands. This increases water solubility and makes ligand exchange

reaction rates more favourable. First and second generation platinum drugs, however, are not orally bioavailable. In order to overcome this problem, the third generation drug, satraplatin, Figure 1. 12, was developed comprising a Pt(IV) octahedral centre. This drug is stable for days in biological media and remains unchanged until it reaches its biological target. Here it is converted to the more labile Pt(II) species by biological reductants (ascorbate, glutathione or NADPH), assisted by the hypoxic environment of solid tumours.[22] Satraplatin was indeed found to increase the oral bioavailability of the drug as well as showing some activity in cisplatin resistant tumour cell lines.[21] However, satraplatin has been unsuccessful in clinical trials. A further platinum drug designed to overcome cross resistance with cisplatin is picoplatin, Figure 1. 12, where the steric bulk of the methyl substituted pyridine slows reaction and substitution rates with thiol containing ligands, thus allowing more time for the drug to reach its target of DNA.[21]

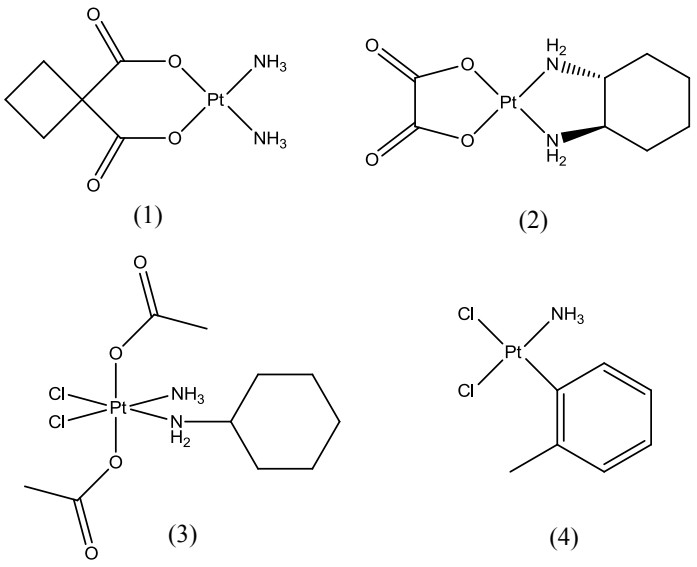

Figure 1. 12 Platinum second and third generation anticancer drugs: (1) carboplatin, (2) oxaliplatin, (3) satraplatin, (4) picoplatin.

1.4.2 Other Platinum Anticancer Agents

Extended analogues of cisplatin have also been investigated in order to improve upon existing agents further. The complex BBR3464 (triplatin) is a triplatinum tetracationic complex in which the metal centres are linked by flexible diamine chains,[23] Figure 1. 13. Interestingly, even though this complex does not contain platinum centres with *cis* leaving groups, it is more cytotoxic than cisplatin as well as displaying activity against cisplatin resistant cell lines.[24]

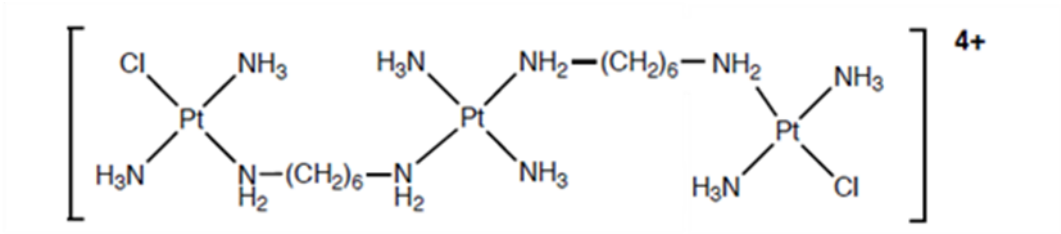

Figure 1. 13 Triplatin, a multinuclear cationic trans Pt(II) complex.

This complex binds to DNA forming inter- and intra-stand crosslinks as well as causing the reversible switching from a right handed B-DNA helix to a left handed Z-DNA structure.[25] This complex has undergone phase (II) clinical trials,[26] but is not proceeding further at this time.

An analogue of BBR3464, Figure 1. 14, is an octacationic trinuclear complex, where the reactive Pt-Cl moieties of BBR3464 have been replaced with amines. This changes the DNA binding of this complex dramatically, meaning only non-covalent, electrostatic binding is possible.

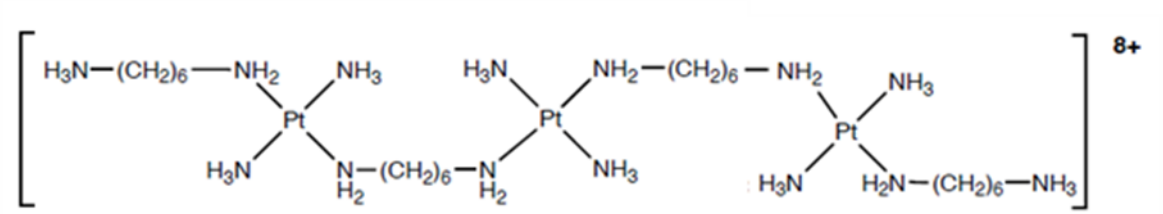

Figure 1. 14 Octacationic trinuclear platinum DNA backbone binder.

This complex binds to the DNA backbone through the formation of hydrogen bonds from two *cis* amine groups to one oxygen phosphate. This allows the complex to either track along the backbone or to bind spanning across the minor groove, making contacts with either side of the DNA backbone. This binding has been termed a phosphate clamp,[27] Figure 1. 15. Most importantly, this complex also shows good activity against cancer cell lines.[28]

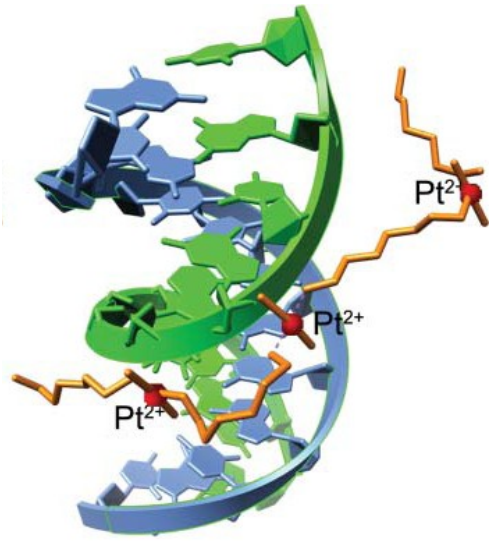

Figure 1. 15 DNA backbone tracking by a platinum phosphate clamp.[29]

1.5 Ruthenium Anticancer Agents

1.5.1 Ruthenium as a Metal Centre

Despite the continuing success of platinum anticancer agents, the fact remains that many of these complexes are toxic, mutagenic and act against a limited number of cancers. It has become apparent in recent years that new metal centres, with new structures and modes of action are needed. Desirable properties in a new metal centre include: additional coordination sites, the ability to change oxidation states and differing ligand affinities and substitution kinetics.[30] A ruthenium centre possesses all of these properties making this an interesting metal to investigate. Ruthenium drugs have historically been used for many medical applications including immunosuppressant, antibiotics and NO scavengers.

Few metallo-drugs remain unchanged, without interaction with biomolecules such as proteins or water, before they reach their biological target; therefore ligand lability is an important factor in determining biological activity. Ru(II) and Ru(III) have similar ligand exchange kinetics to Pt(II) complexes.[31] The coordination number of the metal centre is also important. For example Ru(II), (III) and (IV) complexes have a hexacoordinate metal centre, with octahedral geometry. This is markedly different to the well known platinum drugs where the metal usually has a square planar geometry. For this reason it was thought that the action of ruthenium drugs would be substantially different to those of cisplatin and its analogues.

Ruthenium (II), (III) and (IV) are all accessible under physiological conditions. Ru(II) complexes are generally the active species, with Ru(III) complexes being relatively biologically inert.[31] It is hypothesised that one way the inactive Ru(III) compounds may

enter cells is by mimicking iron and binding to biomolecules such as albumin and serum transferrin.[31] Rapidly dividing cells have a higher requirement for iron and have an increased number of transferrin receptors on their cell surfaces, hence facilitating selective toxicity and increased uptake within cancer cells,[32] Figure 1. 16.

Drug molecules administered as inert Ru(III) complexes may be activated, once inside the cell, by a process called activation by reduction.[33] Angiogenesis, the creation of new blood vessels around tumour sites, uses up oxygen and other nutrients. This hypoxia (low O_2 content) means cancer cells depend more heavily on glycolysis for their energy, creating an excess of lactic acid in the surrounding tumour tissues. This in turn lowers the pH of the local environment, favouring the production of Ru(II) with respect to Ru(III) within the cancer cells,[33] Figure 1. 16.

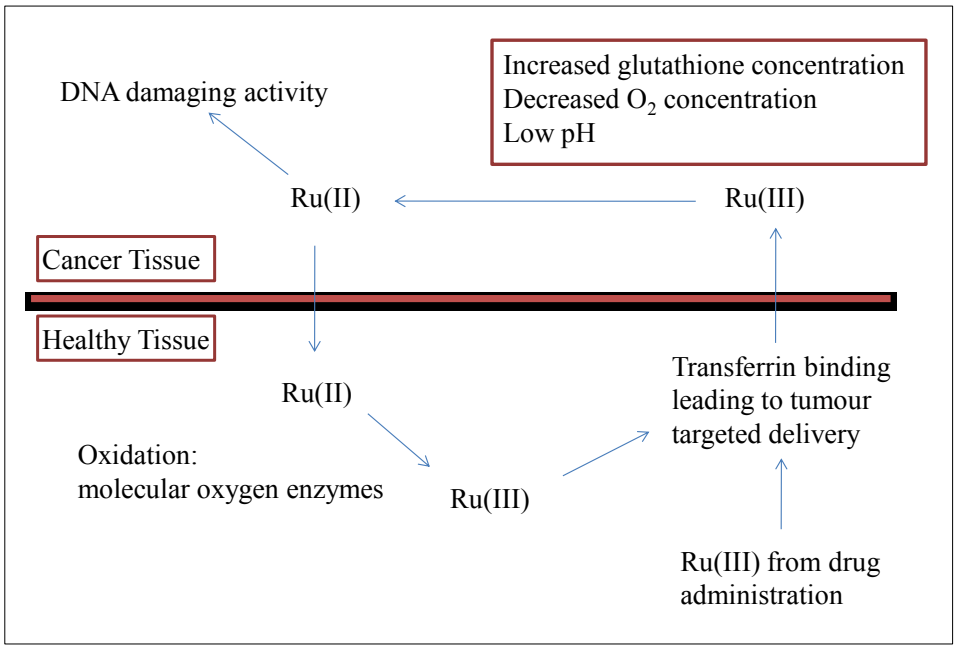

Figure 1. 16 Oxidation states of ruthenium in cancer cells and healthy tissues.[31]

Photoactivity, the ability to bind to and cause DNA damage in the presence of light, is a further desirable characteristic of many ruthenium complexes and may allow selectivity in DNA binding. In order for a compound to be suitable for this purpose it should conform to the following rules:[32] be stable towards aquation and relatively non toxic, accumulate preferentially in cancer versus normal cells, absorb strongly at relatively long wavelengths (640-850 nm) that are not significantly absorbed by biological tissues and produce high quantum yields of free radical intermediates or singlet O_2 upon irradiation.

1.5.2 Ruthenium Mononuclear Complexes

1.5.2.1 Ru (II)/(III) Chloride Complexes

Inspired by cisplatin, ruthenium drugs with chloride leaving groups have been extensively studied. The first example of a ruthenium anticancer complex was a Ru(II) ammine compound, $[RuCl_2(NH_3)_4]$, synthesised in the 80s.[33] Unfortunately, being uncharged, this complex was too insoluble for the clinic, however its activity sparked interest into the search for other ruthenium complexes for use as anticancer agents. The related analogue, *cis*-$[Ru(bpy)_2(NH_3)_2]^{2+}$ was shown to bind coordinatively to 9-methyl and 9-ethyl guanine through the formation of an aqua complex, under irradiation (λ_{irr} > 345 nm). Both single and double stranded DNA binding was observed.[34]

In order to overcome solubility issues of $[RuCl_2(NH_3)_4]$ the Ru (II) complex $[Ru(DMSO)_4Cl_2]$ (where DMSO is S bound) was explored. This complex is highly soluble. Isomers were investigated for anticancer activity as early as 1988, with the *trans* isomer being 20-fold more active than the *cis* isomer.[35] This compound was also found to localise in tumour cells more than normal tissue and has lower toxicity than cisplatin in normal

proliferating tissue.[36] Both isomers of $[Ru(DMSO)_4Cl_2]$ also exhibit photo-dependant cytotoxicity under UV illumination with the less anticancer active *cis* isomer thought to isomerise to the more active *trans* isomer upon irradiation.[37] This pro-drug approach is attractive as a method to reduce side effects.

Ruthenium drugs investigated for their antimetastatic properties include the range of chloride, indazole complexes; KP1019, KP1339 and NAMI-A, Figure 1. 17. NAMI-A and KP1019 have both progressed to clinical trials, with NAMI-A being the first ruthenium anticancer drug to progress this far.[13]

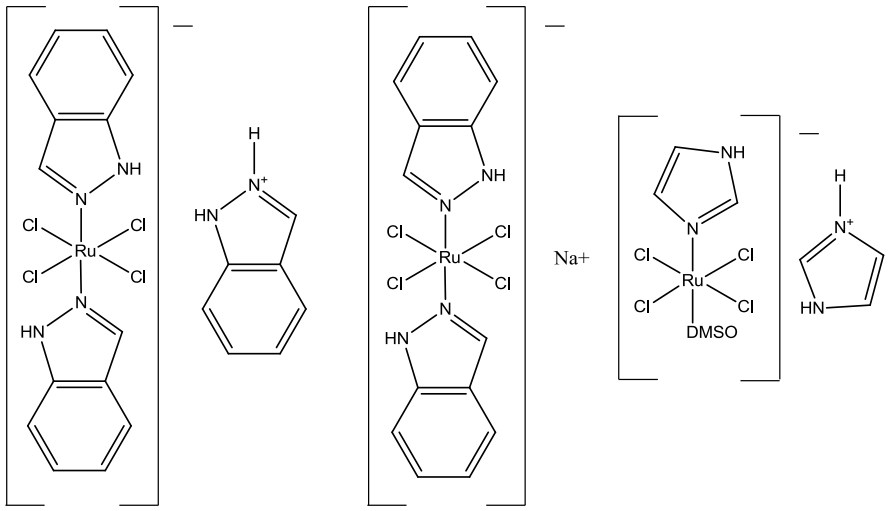

Figure 1. 17 The structures of (1) KP1019, (2) KP1339, (3) NAMI-A.

KP1019, indazolium *trans*[tetrachlorobis(1H-indazole)ruthenate(III)] is only moderately soluble in aqueous solutions and is therefore administered as the sodium salt, KP1339 which is used for in-situ preparation of KP1019.[38] The mechanism of uptake is thought to be through binding to the serum protein transferrin, with two ruthenium moieties residing in each iron binding site.[39] Apoptosis is induced via a mitochondrial pathway, which may

be produced via DNA binding, or through direct interaction with mitochondria.[39] Preclinical studies showed moderate activity with a high level of selectivity towards colorectal tumours. Clinical studies confirmed this.[40]

Despite being structurally similar to KP1019, NAMI–A, (H_2im)[*trans*-$RuCl_4(Him)(DMSO)$] exhibits a very different spectrum of activity. This complex displays limited activity against primary tumours but acts against the development and growth of metastases. This is associated with a number of biological processes including an increase of actin dependant cell adhesion, inhibition of matrix degradation by matrix metalloproteinases and reduction of cell invasiveness and migration.[41] The low *in vitro* cytotoxicity of this complex is attributed to the small number of metastatic cells present in the primary tumour.[40] With metastases of solid tumours representing the main reason for failure in cancer chemotherapy, compounds which possess this ability are very desirable.

Further ruthenium chlorido complexes include the pseudo-octahedral ruthenium 'pianostool' complexes, of general formula $[(\eta^6\text{-arene})Ru(X)(Y)(Z)]$, Figure 1. 18. Structure activity relationships have determined that a chelating ligand can help to control the stability and ligand-exchange kinetics of the complexes; the nature of the arene can influence cell uptake and interaction with biological targets; and the chloride or leaving group can help to control the timing of activation of the complexes.[42]

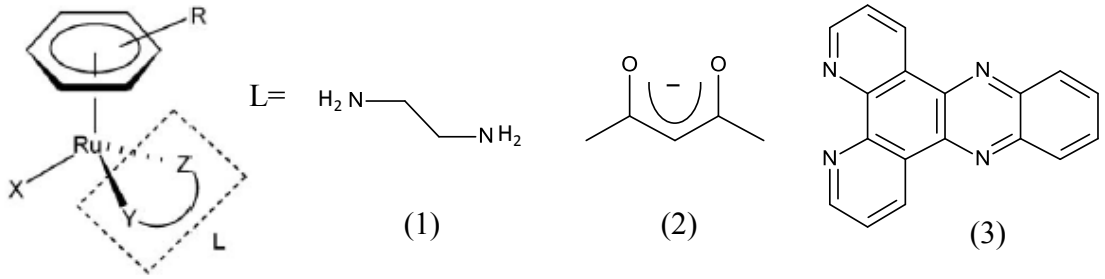

Figure 1. 18 Ruthenium 'pianostool' half sandwich complexes and examples of chelating ligands: (1) en, (2) acac, (3) dppz.

It appears that a more hydrophobic arene ligand and a single ligand exchange site, with the two other sites occupied by a bidentate chelating ligand, Figure 1. 19, increases cytotoxicity.[42] A mechanistic study showed initial aquation of the complex was followed by rapid binding to the 5'-phosphate group. A rearrangement then gives rise to nitrogen-bound adducts.[43]

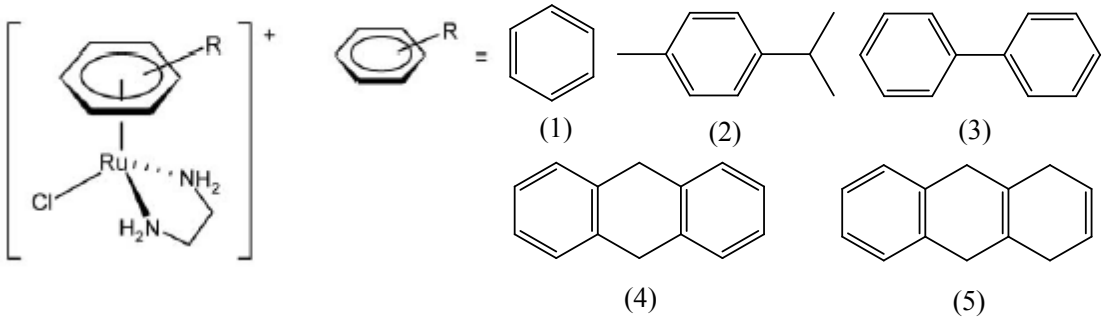

Figure 1. 19 Modified ruthenium 'pianostool' half sandwich complexes, with examples of R groups: (1) benzene, (2) p-cymene, (3) biphenyl, (4) dihydroanthracene, (5) tetrahydroanthracene.

These complexes do not show any cross resistance with cisplatin, so may have a distinct mode of action. Coordinative DNA binding is with a strong preference for guanine bases which may allow targeting of guanine rich portions of DNA such as G-quadruplexes, present in DNA telomeres.

A number of related Ru(II) complexes have also been investigated for their antimetastatic properties. A series of drugs of formula [Ru(II)(arene)Cl_2PTA], (RAPTA) where (PTA = 1,3,5-triaza-7- phospaadamantane) have been developed. A *p*-cymene derivative, RAPTA-C (1) and a toluene derivative, RAPTA-T (2), Figure 1. 20, show pH dependant DNA damage, meaning selectivity towards hypoxic tumour cells.[44]

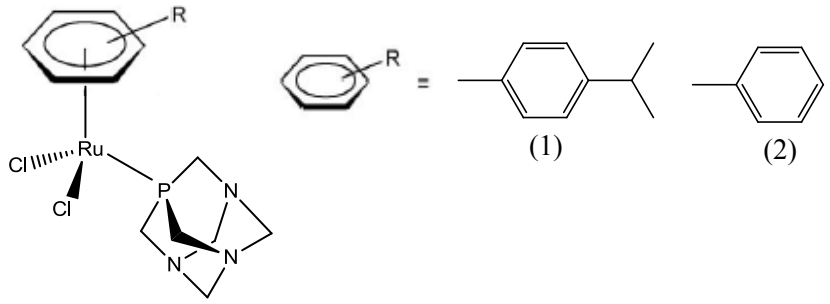

Figure 1. 20 The structures of RAPTA-C (1) and RAPTA-T (2)

These complexes showed relatively low activity *in vitro*, however *in vivo* RAPTA-T selectively reduced the growth of lung metastases.[44] The mechanism of action is thought to be through the inhibition of some steps of the metastatic process, such as detachment from the primary tumour, migration/invasion and re-adhesion to a new growth substrate. Unfortunately however, these complexes are prone to fast hydrolysis and in order to suppress this would have to be administered in saline. Second generation RAPTA complexes have therefore been developed employing bidentate carboxylate ligands, based on second generation Platinum drugs, Figure 1. 21. These drugs are resistant to hydrolysis and show similar DNA binding and antimetastatic activities to the original RAPTA complexes.[45]

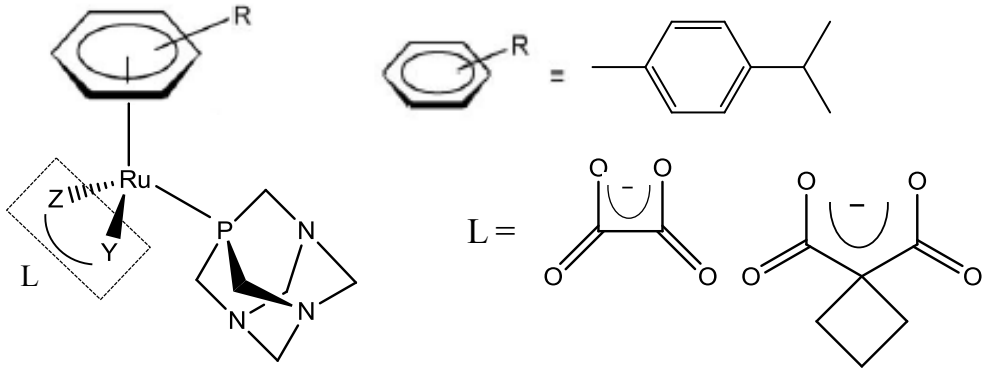

Figure 1. 21 Examples of second generation RAPTA complexes.

A further class of Ru(II) complexes have been developed, combining structural features of NAMI-A (imidazole ligands; imidazole, benzimidazole, *N*-methylimidazole, *N*-butylimidazole, *N*-vinylimidazole or *N*-benzoylimidazole) with the 'piano-stool' arene moiety, Figure 1. 22.[46]

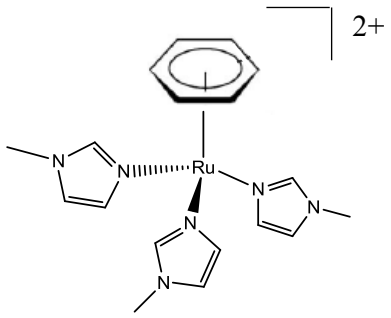

Figure 1. 22 Example of a RAPTA-NAMI complex.

These complexes displayed *in vitro* activities similar to those of the RAPTA complexes and several compounds were shown to be selective towards cancer cells as opposed to nontumorigenic cells. Two of these complexes, [Ru(η^6-*p*-cymene)Cl(vinylimid)$_2$][Cl], (vinylimid=*N*-vinylimidazole) and [Ru(η^6-benzene)(mimid)$_3$][BF4]$_2$, (mimid=*N*-methylimidazole) have been selected for more detailed *in vivo* evaluation.[47]

1.5.2.2 Ru(II) Polypyridyl Complexes

Ruthenium polypyridyl complexes have been extensively studied for their photophysical and DNA binding properties.[18] The simplest of these complexes, $[Ru(bpy)_3]^{2+}$ and $[Ru(phen)_3]^{2+}$ show stereospecific DNA binding.[48] For $[Ru(phen)_3]^{2+}$ there are two distinct binding modes; the D-enantiomer adopts an intercalative binding mode and prefers GC rich DNA, while the L-enantiomer binds in the minor groove and prefers AT rich DNA. [49] In contrast, the binding of $[Ru(bpy)_3]^{2+}$ is simply electrostatic as this complex does not have a ligand surface great enough for pi-stacking to DNA bases. DNA cleavage upon visible irradiation is, however, present for both complexes.[50]

Changing the ligand surface of these parent complexes has resulted in a range of compounds, Figure 1. 23. An increase in size of intercalator increases DNA binding, unwinding, luminescence and photocleavage.[51]

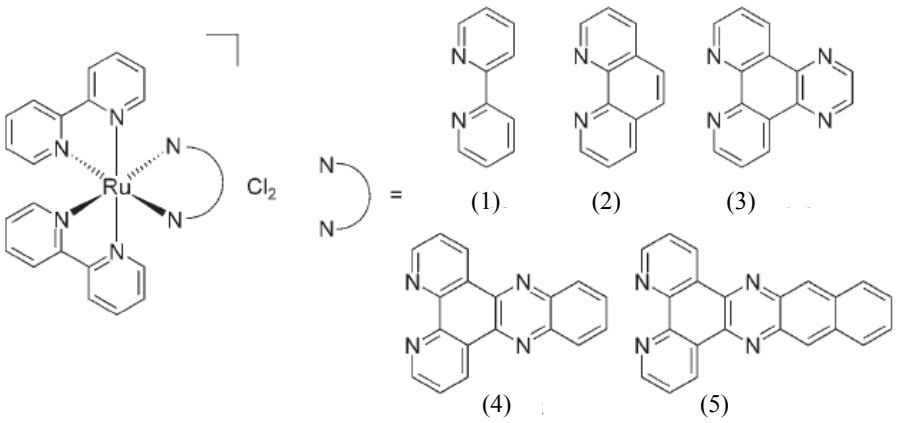

Figure 1. 23 Ruthenium polypyridyl complexes with examples of ligands: (1) bpy, (2) phen, (3) dpq, (4) dppz, (5) dppn.

The anticancer activities of this range of complexes have been investigated. The activity of complex 5 is the highest in the cell lines tested, with comparable activity to cisplatin.[52]

Unlike the chlorido complexes discussed previously, this range of compounds possess no leaving groups, so the mode of action is likely to be DNA intercalation.

The structurally similar dipyridophenazine complexes, $[RuL_2(dppz)]^{2+}$, Figure 1. 24, show a luminescence enhancement of several orders of magnitude upon DNA binding.[53] They have also been shown to be taken up into HeLa cells through flow cytometry. No loss of luminescence was observed, confirming the stability of these complexes in the intracellular environment. [54] This is critical for a drugs application as a therapeutic or diagnostic agent.

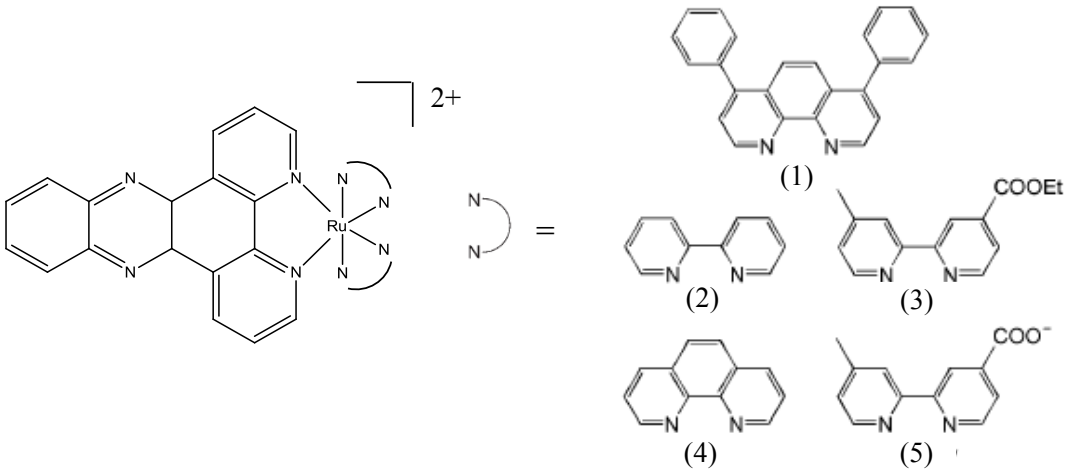

Figure 1. 24 Dipyridophenazine complexes with examples of ligands: (1) DIP, (2) bpy, (3) CO_2Et-bpy, (4) phen, (5) mcbpy.

There are a number of other similar complexes with extended aromatic surfaces which have shown specific interactions with DNA. $[Ru(bpy)_2L]Cl_2$ where L = tpqp or tactp, Figure 1. 25, bind selectively to DNA base mismatches. The bulky intercalating ligand is not able to bind to the normal form of B-DNA, but slots easily into the thermodynamically destabilised regions of DNA around base mismatches. [55] Base mismatches occur in the genome as a result of various cellular errors such as a polymerase error, as well as external

factors including UV/ionising radiation or genotoxic chemicals. Cellular failure to correct these errors is present in colon and some breast cancers.

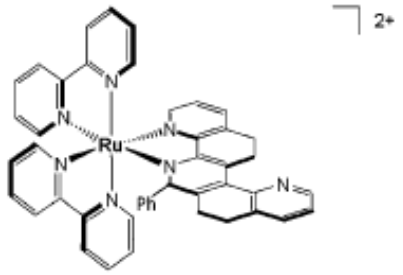

(1)

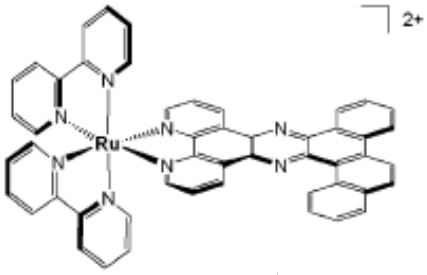

(2)

Figure 1. 25 Structures of $[Ru(bpy)_2(tpqp)]^{2+}$ (1) and $[Ru(bpy)_2(tactp)]^{2+}$ (2) [55]

A range of mononuclear azopyridyl complexes of the form $[Ru(azpy)_2Cl_2]$, an isomer of which is illustrated in Figure 1. 26, have been assessed for their cytotoxic activity. Many of the isomers have shown much higher activities than cisplatin.[56] These complexes are discussed in more detail in chapter 5.

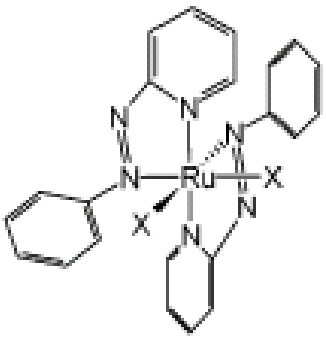

Figure 1. 26 The α-isomer of cis -$[Ru(azpy)_2Cl_2]$ (X= Cl, azpy= 2-(phenylazo)pyridine).

1.5.3 Ruthenium Dinuclear Complexes

Using a mononuclear drug complex as a template to create dinuclear complexes with different properties is a common method to follow. This approach has been used in the polypyridyl complexes 1 and 2, Figure 1. 27. Complex 1 showed low DNA binding

affinities,[53] however as with the mononuclear case the phenanthroline analogue, complex 2, conveyed stronger binding activity[57] with binding being mainly electrostatic.

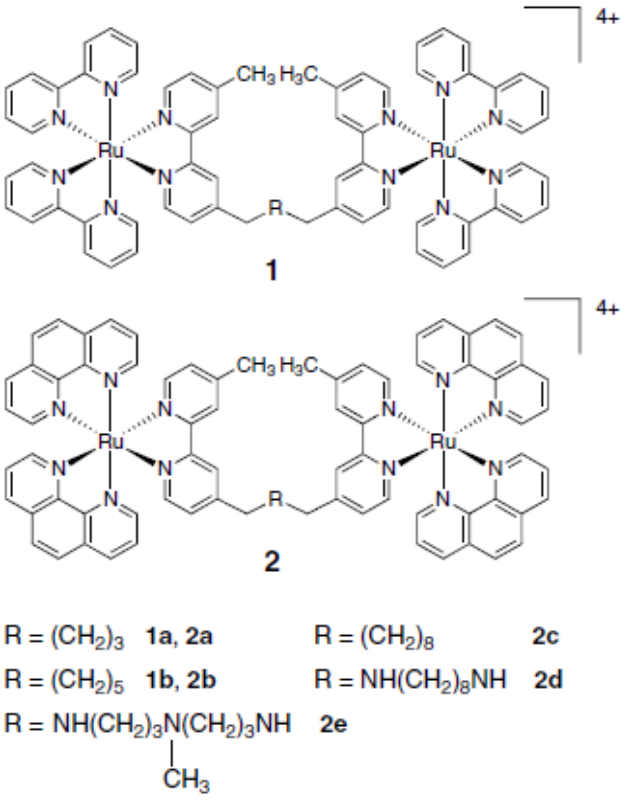

Figure 1. 27 Dinuclear ruthenium polypyridyl complexes.[53]

Investigating different chain lengths allowed optimum conditions for DNA binding to be found, with complex 2b exhibiting the strongest enhancement of binding affinity.[53] Luminescent enhancement upon DNA binding was also observed for all complexes of this family[58] and DNA photocleavage studies detected single strand breaks mediated by both type I (radical mediated) and type II (singlet oxygen mediated) cleavage.[59]

A range of similar dinuclear complexes comprising an intercalating portion are shown in Figure 1. 28. Much work has been carried out on these complexes and recently it has been shown that the kinetic recognition of AT rich DNA is possible. [60]

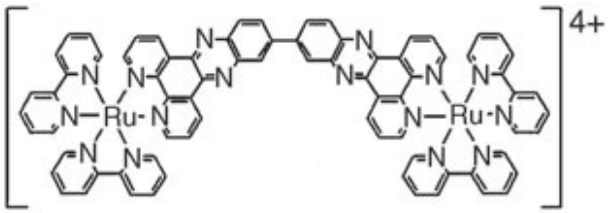

(1)

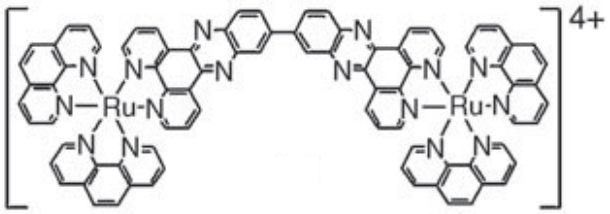

(2)

Figure 1. 28 Dinuclear polypyridyl complexes.[60]

Both enantiomeric forms of complexes (1) and (2) display fast binding through intercalation to poly(dAdT)$_2$.

A further complex comprising both phenanthroline moieties and an intercalating portion is the dinuclear threading intercalator,[61] Figure 1. 29, based on the mononuclear complex [Ru(phen)$_2$dppz]$^{2+}$. This compound has been investigated for anticancer activity and shows cytotoxicity in some cell lines. A three to four fold increase in cytotoxicity is shown over the mononuclear analogue.[18]

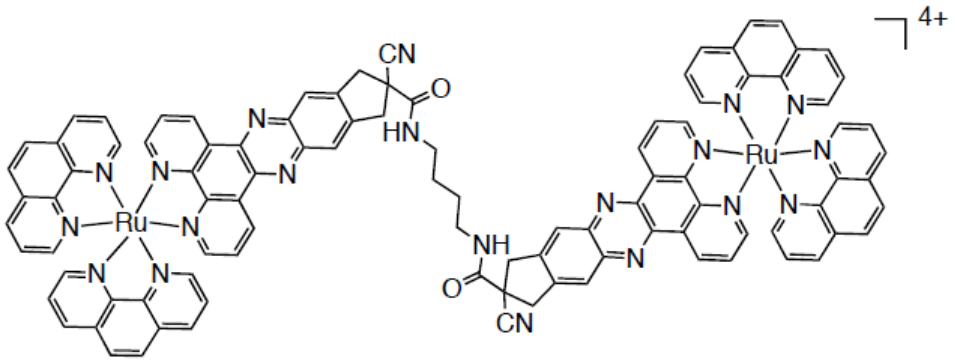

Figure 1. 29 A dinuclear threading bisintercalator constructed using a flexible dppz ligand.[18]

This complex binds to DNA through intercalation of the dppz moieties between DNA base pairs, with the rest of the molecule threading through the DNA. The observation of the DNA light switch effect is further evidence for this binding mode, as shielding of the dppz nitrogens from the aqueous environment upon DNA binding is required for emission.[62]

A dinuclear ruthenium complex, $[\{Ru(phen)_2\}_2\text{-}(\mu\text{-bpm})]^{4+}$, Figure 1. 30, was investigated for its ability to recognise and bind to DNA bulge sites. The *meso* (ΔΛ) diastereoisomer showed the strongest binding to the tridecanucleotide $d(CCGAGAATTCCGG)_2$ which contains a single adenine bulge site and was selective to this sequence compared with non-bulge containing nucleotides. [63]

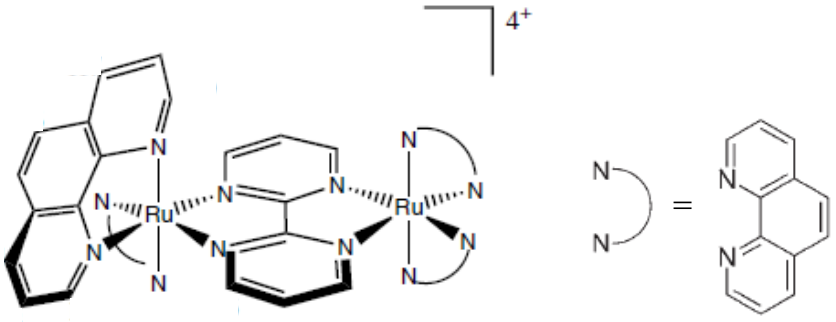

Figure 1. 30 The structure of ΔΔ-$[\{Ru(phen)_2\}_2\text{-}(\mu\text{-bpm})]^{4+}$.[63]

NMR analysis revealed that the binding of the *meso* isomer caused less structural perturbations in the DNA minor groove than the ΔΔ or ΛΛ isomers.[63] This study confirms the potential of dinuclear ruthenium complexes as DNA bulge probes.

Dinuclear derivatives of the pianostool organometallic ruthenium(II) complexes, Figure 1. 31, also show a good activity against cancer cell lines.[64]

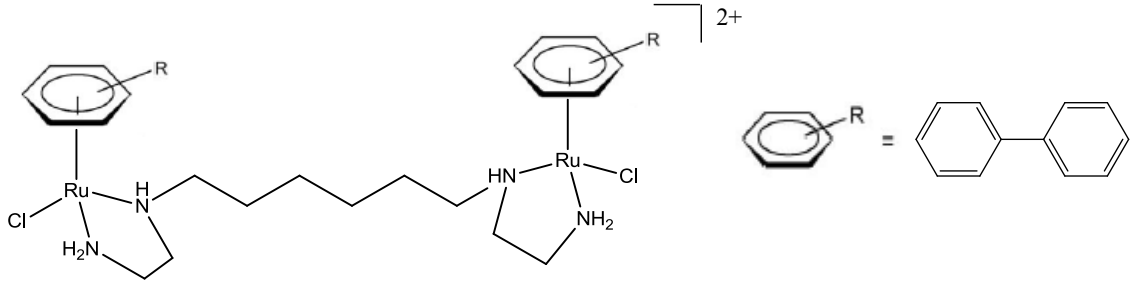

Figure 1. 31 Structure of the dinuclear pianostool ruthenium complex.

This complex caused an unwinding of plasmid DNA over twice that of the mononuclear counterpart and has been shown to inhibit DNA directed RNA synthesis *in vitro*. The compound gives rise to interstrand crosslinks of DNA, analogous to those caused by cisplatin.[64]

A dinuclear ruthenium(II) complex has been shown to promote the formation of and stabilise the human telomeric repeat AG3(T2AG3)3 quadruplex. The complex, $[Ru_2(obip)L_4]^{4+}$, where obip = 2-(2-pyridyl)imidazo[4,5-*f*][1,10]-phenanthroline and L=2,2′-bipyridine, Figure 1. 32, induced the formation of an antiparallel G-quadruplex structure in the absence of metal cations.[7]

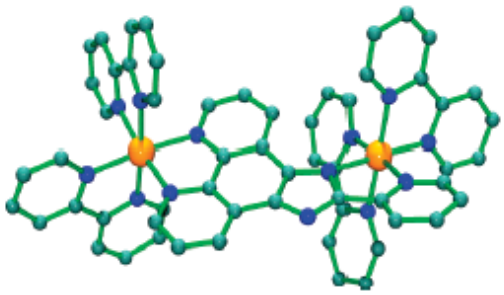

Figure 1. 32 Ball and stick representation of $[Ru_2(obip)L_4]^{4+}$.[7]

Binding stoichiometry was consistent with a 1:1 [quadruplex][complex] binding mode, suggesting interactions of the complex with a single guanine tetramer. Details of binding sites and biological activity are currently under investigation. It has been reported that telomerase inhibition activity of drugs is strongly related to their ability to stabilise the G-quadruplex structure. This complex is therefore a promising candidate for displaying anticancer activity.

1.6 Iron Anticancer Agents

1.6.1 Iron as a Metal Centre

To date, iron has not been widely used in the search for anticancer agents. This is perhaps surprising as it is essential in many biological processes and well tolerated by the body, unlike toxic heavy metals such as platinum or ruthenium. Iron is kinetically less inert than ruthenium, but being in the same periodic group this transition metal is interesting to investigate for its DNA binding and anticancer properties.

1.6.2 Iron Mononuclear Complexes

Well-established examples of iron anticancer agents are the ferrocene derivatives of the breast cancer drug tamoxifen, Figure 1. 33. This complex displays potent activity against

both estrogen-dependent and estrogen-independent breast cancer cell lines. Tamoxifen alone is active only against estrogen-dependent cells and ferrocene is not cytotoxic.[65] The activity of the ferrocene-tamoxifen derivatives (ferrocifens) in estrogen-independent cells is attributed to the redox properties of the Fe(II) complex causing oxidative damage to DNA. The mechanism of action of ferrocifens in estrogen-dependent cells is likely to be similar to that of tamoxifen itself.[66]

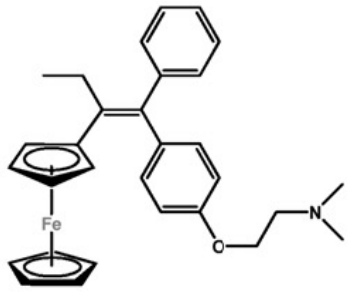

Figure 1. 33 Ferrocifen, a ferrocene derivative of tamoxifen.[66]

A recent study on ferrocene tamoxifen derivatives with modified side chains has established the minimal structural requirements to obtain cytotoxicity and it appears that the presence of both a ketone function adjacent to the ferrocene group and two phenols are needed for optimum activity, Figure 1. 34.[67]

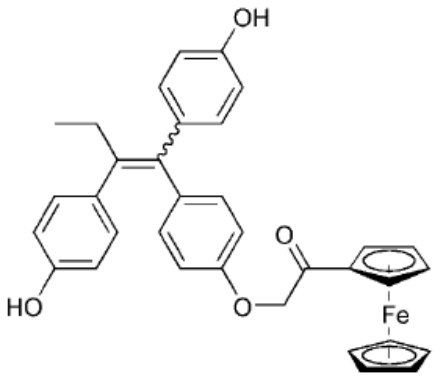

Figure 1. 34 A ferrocene tamoxifen derivative.[67]

A further example of an organic anticancer agent being linked to an iron moiety in order to covey differing activities is iron-bleomycin[68] (FeBLM), Figure 1. 35. Bleomycin binds to DNA in the minor groove or through partial intercalation.[69] The FeBLM complex, however, causes oxidative damage to DNA in the presence of O_2 and H_2O_2, causing DNA double strand scission.[70] It is likely that the coordinated iron(II) in this complex is oxidised in the Fenton reaction: $LFe^{2+} + H_2O_2 \rightarrow LFe^{3+} + HO\bullet + HO–$, (L= ligand bound to iron, in this case bleomycin). The production of highly reactive oxygen radical species is then damaging to DNA and other biomolecules.[71] Iron is the most abundant metal ion in biological systems likely to catalyse this reaction, therefore it is usually transported and stored in specific proteins such as ferritin in order to prevent or minimise this damaging reaction.[72]

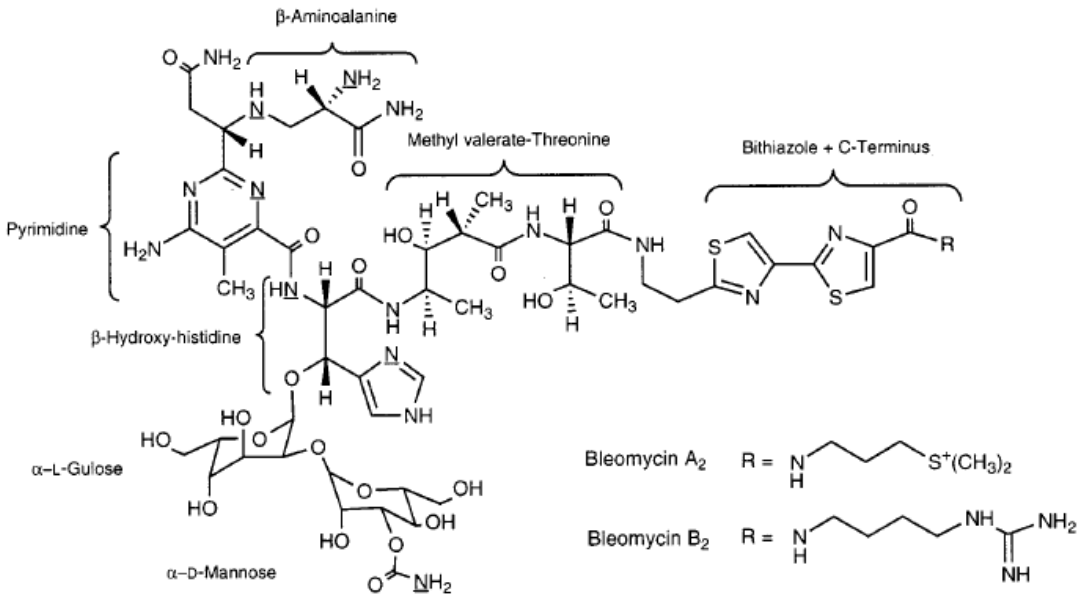

Figure 1. 35 The structures of bleomycin A_2 and B_2. Nitrogen atoms involved in metal ion binding are underlined.[70]

The Co(III)-bleomycin complex has been characterised,[73] however the exact structure of the iron-bleomycin complex remains a subject of discussion. A proposed binding mode is illustrated in Figure 1. 36.

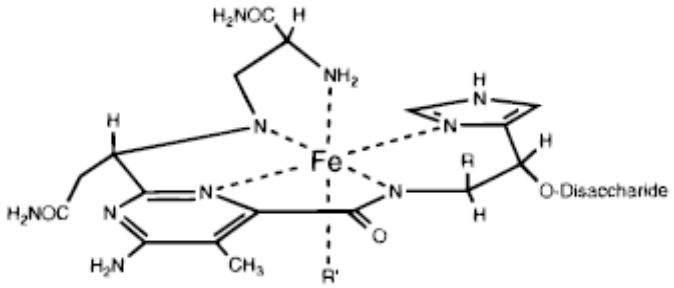

Figure 1. 36 Proposed structure of FeBLM.[70]

The addition of a nucleobase to a η^4-butadiene–$Fe(CO)_3$ [74] or a ferrocenyl group, [75] Figure 1. 37, conveys good cytotoxic activity and induces apoptosis. [76]

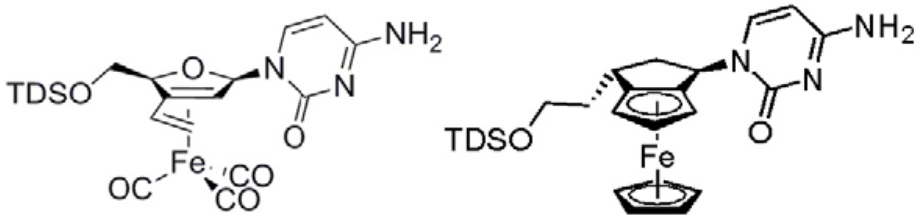

(1) (2)

Figure 1. 37 η^4-butadiene–$Fe(CO)_3$ (1) and ferrocene (2) complexes (where TDS= thexyldimethylsilyl) with an appended nucleobase.[76]

Complex 1 is also active against leukaemia cells resistant to common cytostatic drugs. The exact mechanism of action of these complexes is currently under investigation.

Iron(II) complexes containing a pentadentate ligand, Figure 1. 38, have been shown to display cytotoxicities in the range 0.13-68.5 μM. Complex (1) induces cell cycle arrest in

HeLa cells and causes cell death by apoptosis, possibly via the creation of reactive oxygen species. Both complexes cause DNA strand breaks.[77]

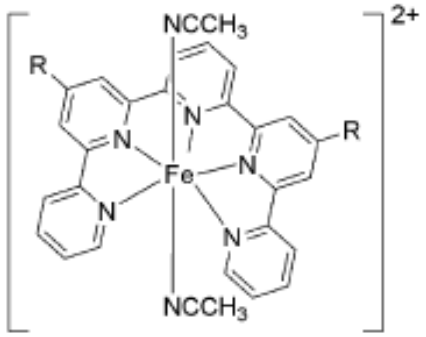

(1) R= H

(2) R = Ph

Figure 1. 38 Iron(II) complexes with pentapyridyl ligands.[77]

1.6.3 Iron Dinuclear Complexes

An additional example of an organometallo drug, created using a known organic compound is the Bis(Fe(II)EDTA-distamycin) fumaramide complex, [78] Figure 1. 39.

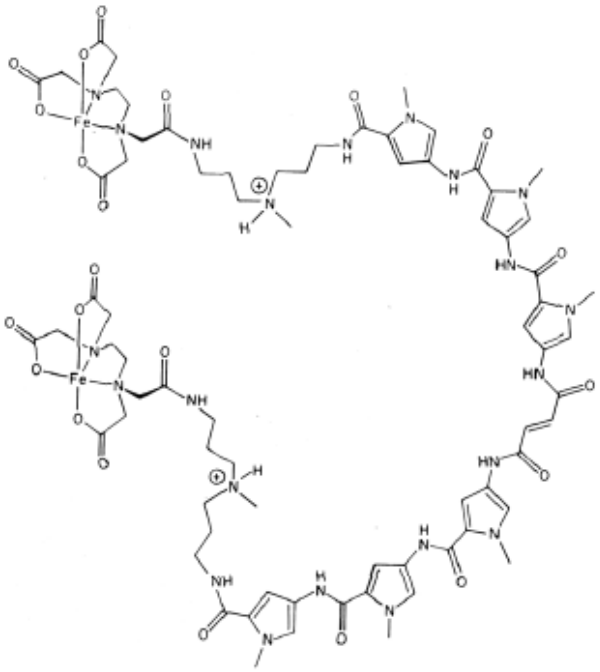

Figure 1. 39 The bis(Fe(II)EDTA-distamycin)furamamide complex.[78]

This complex shows sequence specific recognition of B-DNA, binding to sites of AT rich DNA in the minor groove, causing double stranded DNA cleavage.[79]

1.7 Supramolecular Helical Drug Agents

Hannon and co-workers have developed an extensive family of metallo-supramolecular helicates which interact with DNA in a number of ways and show activity against cancer cell lines. The parent complex of this group is the dinuclear iron(II) complex, $[Fe_2L_3]^{4+}$, where L = $C_{25}H_{20}N_4$, Figure 1. 40. This triple stranded complex was designed to mimic natural protein DNA recognition motifs, and is readily synthesised from commercially available starting materials.[80]

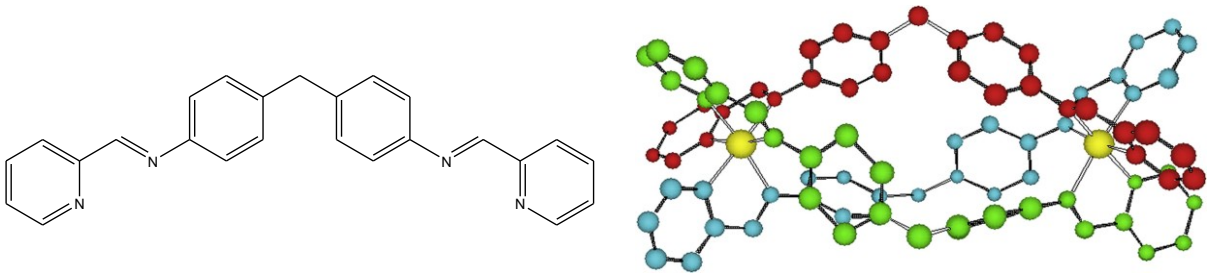

Figure 1. 40 Ligand L and X-ray crystal structure of the $[Fe_2L_3]^{4+}$ cation.[81]

$[Fe_2L_3]^{4+}$ binds to DNA and has also been shown to induce substantial DNA coiling in linear plasmid DNA, wrapping up the DNA duplex in an *intra*-molecular fashion,[82] Figure 1. 41. This remarkable structural effect is not observed with conventional small synthetic DNA binders.

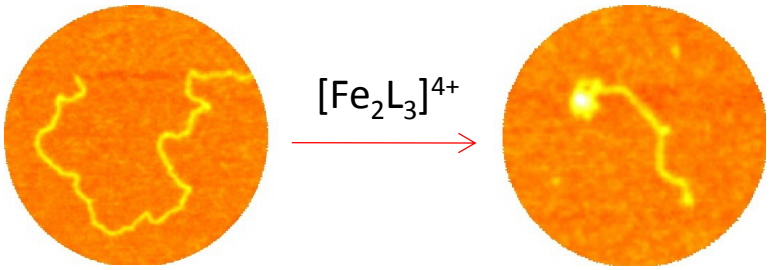

Figure 1. 41 AFM images showing coiling of linear plasmid DNA induced by $[Fe_2L_3]^{4+}$.[82]

$[Fe_2L_3]^{4+}$ has also been shown to bind in the heart of a DNA three-way junction structure, through electrostatic and π-π stacking interactions. This is an unprecedented new mode of DNA binding,[83] illustrated in Figure 1. 42. Furthermore, $[Fe_2L_3]^{4+}$ shows cytotoxic action, through cell stasis and apoptosis, with activity at concentrations comparable to those for cisplatin. $[Fe_2L_3]^{4+}$ was also found to be non-genotoxic and non-mutagenic, a desirable characteristic in a new anticancer agent.[81]

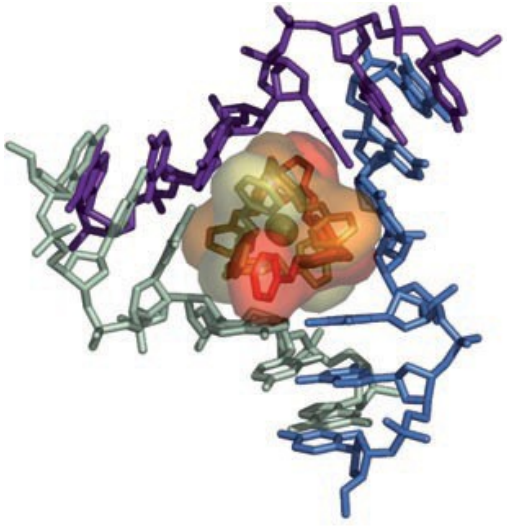

Figure 1. 42 Crystal structure of the major groove side view of $[Fe_2L_3]^{4+}$bound in the heart of a DNA three-way junction.[83]

It is important to note that $[Fe_2L_3]^{4+}$ exists as two enantiomers. Separation of enantiomers has been achieved using a cellulose column with sodium chloride solution as eluent.[84] The

differential binding of the M (left-handed / negatively twisted) and P (right handed) enantiomers has been studied through CD, LD and AFM imaging. These studies have shown that both enantiomers bind strongly to DNA with one of each enantiomer bound per helix turn.[85] The M-enantiomer is the stronger major groove binder, inducing severe DNA bending and coiling, while the P enantiomer shows much less dramatic binding.[86] Most recently the cylinder has been shown to possess antimicrobial activity, in both gram positive and negative bacteria.[87] $[Fe_2L_3]^{4+}$ is discussed in more detail in chapters 3 and 4.

A number of modifications have been made to the parent iron complex in order to investigate different DNA binding modes and cytotoxic activities, for example additions to the ligand, such as extra methyl groups[88] or the attachment of peptides.[89] These complexes show differing DNA binding to the parent complex, discussed in more detail in chapter 3.

The ruthenium analogue of the iron parent complex, $[Ru_2L_3]^{4+}$, Figure 1. 43, where L = $C_{25}H_{20}N_4$ has also been studied. DNA binding of this complex is similar to that of the parent, through non-covalent interactions, however the presence of ruthenium metal centres means an enhancement of luminescence is observed upon DNA binding.[90] Anticancer activity is also different to that of the parent cylinder with activity restricted to breast cancer cell lines. $[Ru_2L_3]^{4+}$is discussed in more detail in chapter 3.

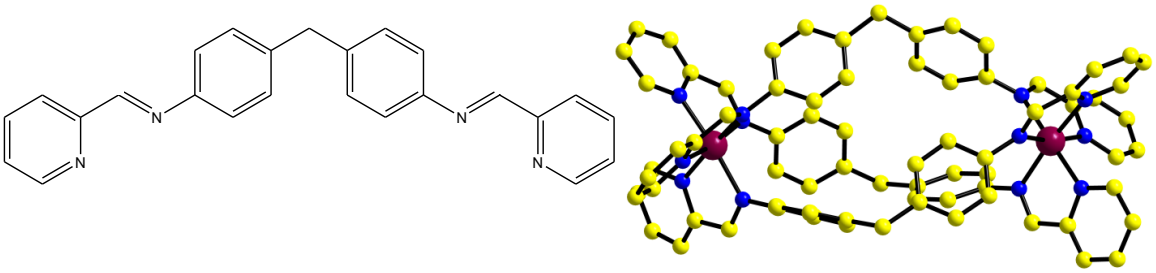

Figure 1. 43 Ligand L and X-ray crystal structure of the $[Ru_2L_3]^{4+}$ cation.[91]

A range of ruthenium(II) dinuclear isomers: γγ, γα, γβ, ββ and αα-$[Ru_2L_2Cl_4]$ where L^2=$C_{23}H_{18}N_6$, Figure 1. 44, have also been synthesised,[92] based on the mononuclear $[Ru(azpy)_2Cl_2]$ complexes.

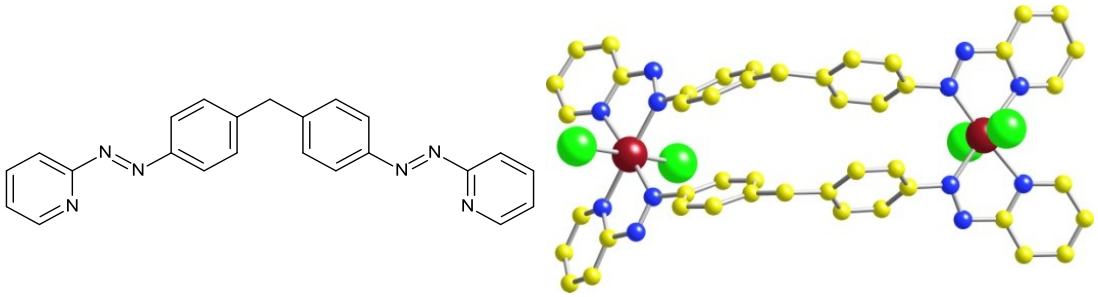

Figure 1. 44 Ligand L^2 and X-ray crystal structure of γγ-$[Ru_2L^2{}_2Cl_4]$, one of a range of isomers synthesised.[92]

These compounds have been investigated for their DNA binding and cytotoxic activities and display a broad range of activities, from the ββ isomer with no activity to the γγ isomer which displays ~40 times higher activity than cisplatin.[93] These complexes are discussed in more detail in chapters 5 and 6.

1.8 Summary

There have been many complexes synthesised and investigated to date, utilising a number of different metal centres to convey differing structures and properties. Complexes discussed in section 1.7 are molecules of study herein and in the following chapters the design, synthesis and characterisation of a novel metallo-supramolecular complex is also presented. The biological properties, including DNA binding of these anticancer agents will be reported. A number of these complexes have the potential to be used as DNA recognition agents and represent a promising step forward in the field of supramolecular drug design.

1.9 References

[1] *Supramolecular Chemistry*, ed. J. W. Steed and J. L. Atwood, Wiley, 2000.

[2] M. J. Hannon, *Chem. Soc. Rev*., 2006, **35**, 1-18.

[3] J. M. Lehn, A. Rigault, J. Siegel, J. Harrowfield and B. Chevrier, *Proc. Natl. Acad. Sci.*, 1987, **84**, 2565-2569.

[4] C. Piguet, G. Bernardinelli and G. Hopfgartner, *Chem. Rev.*, 1997, **97**, 2005-2062.

[5] A. Pfeil and J. M. Lehn, *J. Chem. Soc.*, 1992, 838-840.

[6] *DNA Topology*, ed. A. D. Bates and A. Maxwell, Oxford University Press, 2009.

[7] S. Shi, J. Liu, T. Yao, X. Geng, L. Jiang, Q. Yang, L. Cheng and L. Ji, *Inorg. Chem.,* 2008, **47**, 2910-2912.

[8] K. C. Woods, S. S. Martin, V. C. Chu and E. P. Baldwin, *J. Mol. Biol.*, 2001, **313**, 49-69.

[9] S. Kaur, PhD Thesis, University of Birmingham 2010.

[10] M. W. Becher, J. A. Kotzuk, A. H. Sharp, S. W. Davies, G. P. Bates, D. L. Price and C. A. Ross, *Neurobiology of Disease*, 1998, **4**, 387-397.

[11] N. P. Pavletich and C. O. Pabo, *Science*, 1993, **261**, 1701-1707.

[12] *Cisplatin Chemistry and Biochemistry of a Leading Anticancer Drug*, ed. B. Lippert, Wiley-VCH, 1999.

[13] C. G. Hartinger, S. Zorbas-Seifried, M. A. Jakupec, B. Kynast, H. Zorbas and B. K. Keppler, *J. Inorg. Biochem.,* 2006, **100**, 891-904.

[14] E. Alessio, G. Mestroni, A. Bergamo and G. Sava, *Curr. Topics in Med. Chem.,* 2004, **4**, 1525-1535.

[15] A. M. Peyrone, *Chemie. Pharm.,* 1845, **51**, 129.

[16] P. J. Dyson and G. Sava, *Dalton Trans.,* 2006*,* 1929-1933.

[17] P. M. Takahara, A. C. Rosenzweig, C. A. Frederick and S. J. Lippard, *Nature*, 1995, **377**, 649-652.

[18] M. J. Hannon, *Pure Appl. Chem*., 2007, **79**, 2243-2261.

[19] M. T. Kuo, H. Chen, I. S. Song, N. Savaraj and T. Ishikawa, *Cancer Metastasis Rev.*, 2007, **26**, 71-83.

[20] A. V. Klein and T. W. Hambley, *Chem. Rev.,* 2009, **109***,* 4911-4920.

[21] S. P. Fricker, *Dalton Trans.,* 2007, 4903-4917.

[22] M. D. Hall, H. R. Mellor, R. Callaghan and T. W. Hambley, *J. Med. Chem*., 2007, **50**, 3403-3411.

[23] C. Manzotti, G. Pratesi, E. Menta, R. Di Domenico, E. Cavalletti, H. H. Fiebig, L. R. Kelland, N. Farrell, D. Polizzi, R. Supino, G. Pezzoni, and F. Zunino, *Clin. cancer res.,* 2000, **6**, 2626-2634.

[24] P. Perego, L. Gatti, C. Caserini, R. Supino, D. Colangelo, R. Leone, S. Spinelli, N. Farrell and F. Zunino, *J. Inorg. Biochem*., 1999, **77**, 59-64.

[25] M. B. Kloster, J. C. Hannis, D. C. Muddiman and N. Farrell, *Biochemistry,* 1999, **38**, 14731-14737.

[26] D. Jodrell, T. Evans, W. Steward, D. Cameron, J. Prendiville, C. Aschele, C. Noberasco, M. Lind, J. Carmichael and N. Dobbs, *Eur. J. Cancer,* 2004, **40**, 1872-1877.

[27] S. Komeda, T. Moulaei, K. K. Woods, M. Chikuma, N. P. Farrell and L. D. Williams*, J. Am. Chem. Soc.,* 2006, **128**, 16092-16103.

[28] A. L. Harris, X. H. Yang, A. Hegmans, L. Povirk, J. J. Ryan, L. Kelland and N. P. Farrell, *Inorg. Chem.,* 2005, **44**, 9598-9600.

[29] R. Boer, A. Canals and M. Coll, *Dalton Trans.*, 2009, 399-414.

[30] M. J. Clarke, F. Zhu, and D. R. Frasca, *Chem. Rev.,* 1999, **99***,* 2511-2533.

[31] C. S. Allardyce and P. J. Dyson, *Platinum Metals Rev.*, 2001, **45**, 62-69.

[32] A. Levina, A. Mitra and P. A. Lay, *Metallomics*, 2009, **1**, 458-470.

[33] M. J. Clarke, *Coord. Chem. Rev.*, 2002, **232**, 69-93.

[34] T. N. Singh and C. Turro, *Inorg. Chem.*, 2004, **43**, 7260-7262.

[35] E. Alessio, G. Mestroni, G. Nardin, W. M. Attia, M. Calligaris, G. Sava and S. Zorzet, *Inorg. Chem.*, 1988, **27**, 4099-4106.

[36] M. Brindell, E. Kulis, S. K. C. Elmroth, K. Urbanska and G. Stochel, *J. Med. Chem.,* 2005, 7298-7304.

[37] W. H. Ang and P. J. Dyson, *Eur. J. Inorg. Chem.,* 2006, 4003-4018.

[38] P. Heffeter, K. Bock, B. Atil, M. Ali, R. Hoda, W. Korner, C. Bartel, U. Jungwirth, B. K. Keppler, M. Micksche, W. Berger, G. Koellensperger, *J. Biol. Inorg. Chem.*, 2010, **15**, 737-748.

[39] M. A. Jakupec, M. Galanski, V. B. Arion, C. G. Hartinger and B. K. Keppler, *Dalton Trans.*, 2008, 183-194.

[40] A. Bergamo and G. Sava*, Dalton Trans.*, 2007, 1267-1272.

[41] S. Pacor, S. Zorzet, M. Cocchietto, M. Bacac, M. Vadori, C. Turrin, B. Gava, A. Castellarin, and G. Sava, *Pharmacol. Exp. Ther.*, 2004, **310**, 737-744.

[42] Y. K. Yan, M. Melchart, A. Habtemariam and P. J. Sadler, *Chem. Commun*., 2005, 4764-4776.

[43] H. Chen, J. A. Parkinson, R. E. Morris and P. J. Sadler, *J. Am. Chem. Soc.,* 2003, **125**, 173-186.

[44] C. Scolaro, A. Bergamo, L. Brescacin, R. Delfino, M. Cocchietto, G. Laurenczy, T. J. Geldbach, G. Sava and P. J. Dyson, *J. Med. Chem.,* 2005, **48***,* 4161-4171.

[45] W. H. Ang, E. Daldini, C. Scolaro, R. Scopelliti, L. Juillerat-Jeannerat and P. J. Dyson, *Inorg. Chem*., 2006, **45**, 9006-9013.

[46] Cecile Moucheron, *New J. Chem*., 2009, **33**, 235-245.

[47] C. A. Vock, C. Scolaro, A. D. Phillips, R. Scopelliti, G. Sava and P. J. Dyson, *J. Med. Chem.,* 2006, **49**, 5552-5561.

[48] A. Yamagishi, *Chem. Commun.*, 1983, 572-573.

[49] B. M. Zeglis, V. C. Pierre and J. K. Barton, *Chem. Commun*., 2007, 4565-4579.

[50] J. M. Kelly, A. B. Tossi, D. J. McConnell and C. Ohuigin, *Nucleic Acid. Res.*, 1985, **13**, 6017-6034.

[51] A. M. Pyle, J. P. Rehmann, R. Meshoyrer, C. V. Kumar, N. J. Turro and J. K. Barton, *J. Am. Chem. Soc.*, 1989, **111**, 3051-3058.

[52] U. Schatzschneider, J. Niesel, I. Ott, R. Gust, H. Alborzinia and S. Wolfl, *ChemMedChem.*, 2008, **3**, 1104-1109.

[53] F. Pierard, A. Kirsch-De Mesmaeker, *Inorg. Chem. Commun*., 2006, **9**, 111-126.

[54] C. A. Puckett and J. K. Barton, *J. Am. Chem. Soc*., 2007, **129**, 46-47.

[55] E. Ruba, J. R. Hart and J. K. Barton, *Inorg. Chem.,* 2004, **43**, 4570-4578.

[56] A. C. G. Hotze, PhD Thesis, University of Leiden, 2003.

[57] F. M. O'Reilly and J. M. Kelly, *New J. Chem*., 1998, **22**, 215-217.

[58] F. M. O'Reilly and J. M. Kelly, *J. Phys. Chem. B,* 2000, **104***,* 7206-7213.

[59] F. M O'Reilly, J. Kelly and A. Kirsch-De Mesmaeker, *Chem. Commun.*, 1996, 1013-1014.

[60] P. Nordell, F. Westerlund, L. M. Wilhelmsson, B. Norden and P. Lincoln, *Angew. Chem. Int. Ed.,* 2007, **46**, 2203-2206.

[61] B. Onfelt, P. Lincoln, and B. Norden, *J. Am. Chem. Soc.,* 2001, **123***,* 3630-3637.

[62] B. Onfelt, P. Lincoln and B. Norden, *J. Am. Chem. Soc*., 1999, **121**, 10846-10847.

[63] J. L. Morgan, D. P. Buck, A. G. Turley, J. G. Collins and F. R. Keene, *Inorg. Chim. Acta.*, 2006, **359**, 888-898.

[64] H. Chen, J. A. Parkinson, O. Novakova, J. Bella, F. Wang, A. Dawson, R. Gould, S. Parsons, V. Brabec and P. J. Sadler, *PNAS,* 2003, **100**, 14623-14628.

[65] C. G. Hartinger and P. J. Dyson, *Chem. Soc. Rev*., 2009, **38**, 391-401.

[66] S. H. van Rijt and P. J. Sadler, *Drug Discov. Today*, 2009, 1-9.

[67] A. Nguyen, S. Top, P. Pigeon, A. Vessires, E. A. Hillard, M-A. Plamont, M. Huch, C. Rigamonti and G. Jaouen, *Chem. Eur. J*., 2009, **15**, 684-696.

[68] L. M. Mir, O. Tounekti and S. Orlowski, *Gen. Pharmac*., 1996, **27**, 745-748.

[69] S. T. Hoehn, H-D. Junker, R. C. Bunt, C. J. Turner and J. Stubbe, *Biochemistry,* 2001, **40***,* 5894-5905.

[70] C. A. Claussen and E. C. Long, *Chem. Rev.,* 1999, **99***,* 2797-2816.

[71] J. Prousek, *Pure Appl. Chem.*, 2007, **79**, 2325-2338.

[72] J. M. C. Gutteridge, *FEBS Letter*s, 1986, **201**, 291-295.

[73] K. D. Goodwin, M. A. Lewis, E. C. Long and M. M. Georgiadis, *PNAS,* 2008, **105**, 5052-5056.

[74] D. Schlawe, A. Majdalani, J. Velcicky, E. Heßler, T. Wieder, A. Prokop and H-G. Schmalz, *Angew. Chem. Int. Ed*., 2004, **43**, 1731-1734.

[75] P. James, J. Neudorfl, M. Eissmann, P. Jesse, A. Prokop and H-G. Schmalz, *Org. Lett*., 2006, **8**, 2763-2766.

[76] P. C. A. Bruijnincx and P. J Sadler, *Curr. Opin. in Chemical Biology,* 2008, **12**, 197-206.

[77] R. W-Y. Sun, D-L. Ma, E. L-M. Wong and C-M. Che, *Dalton Trans.*, 2007, 4884-4892.

[78] S. R. Youngquist and P. B. Dervan, *J. Am. Chem. Soc*., 1985, **107***,* 5528-5529.

[79] J. S. Taylor, P. G. Schultz and P. B. Dervan, *Tetrahedron*, 1984, **400**, 457-465.

[80] M. J. Hannon, V. Moreno, M. J. Prieto, E. Molderheim, E. Sletten, I. Meistermann, C. J. Isaac, K. J. Sanders and A. Rodger, *Angew. Chem. Intl. Ed.*, 2001, **40,** 879-884.

[81] A. C.G. Hotze, N. J. Hodges, R. E. Hayden, C. Sanchez-Cano, C. Paines, N. Male, M-K. Tse, C. M. Bunce, J. K. Chipman and M. J. Hannon, *Chemistry & Biology,* 2008*,* **15**, 1258-1267.

[82] M.J. Hannon and A. Rodger, *Pharmaceutical Visions*, 2002, Autumn issue*,* 14-16.

[83] A. Oleksi, A. G. Blanco, R. Boer, I. Usón, J. Aymami, A. Rodger, M. J. Hannon and M. Coll*, Angew. Chem., Int. Ed.,* 2006, **45**, 1227-1231.

[84] M. J. Hannon, I. Meistermann, C. J. Isaac, C. Blomme, J. R. Aldrich-Wright and A. Rodger, *Chem. Commun.*, 2001, 1078-1079.

[85] I. Meistermann, PhD Thesis, University of Warwick, 2001.

[86] I. Meistermann, V. Moreno, M. J. Prieto, E. Moldrheim, E. Sletten, S. Khalid, M. P. Rodger, J. C. Peberdy, C. J. Isaac, A. Rodger and M. J. Hannon, *PNAS*, 2002, **99**, 5069-5074.

[87] A. D. Richards, A. Rodger, M. J. Hannon and A. Bolhuis, *Int. J. Antimicrob. Agents*, 2009, **33**, 469-472.

[88] S. Khalid, M. J. Hannon, A. Rodger and M. Rodger, *J. Mol. Graphics and Modelling*, 2007, **25**, 794-800.

[89] L. Cardo and M.J. Hannon, *Inorg. Chim. Acta.*, 2009, **362**, 784-792.

[90] G. I. Pascu, A. C. G. Hotze, C. Sanchez-Cano, B. M. Kariuki, and M. J. Hannon, *Angew. Chem. Int. Ed.*, 2007, **46**, 4374-4378.

[91] G. Pascu, PhD Thesis, Univeristy of Birmingham, 2008.

[92] A. C. G. Hotze, B. M. Kariuki, and M. J. Hannon, *Angew. Chem. Int. Ed.*, 2006, **45**, 4839-4842.

[93] A. C. G. Hotze, A. J. Pope, B. M. Kariuki , and M. J. Hannon, unpublished work.

Chapter 2

Methods and Experimental Details

2.1. Chemicals

Unless otherwise stated, all chemicals and reagents were purchased from Sigma Aldrich (UK) of the highest quality available and used without further purification.

2.2 Physical Measurements

^{1}H NMR spectra were measured on a Bruker 400/300 DPX spectrometer. Spectra were recorded in the deuterated solvent stated and calibrated on residual solvent peaks. All spectra were obtained at 25 °C. Electrospray Ionisation (ESI) analyses were performed on a Micromass LCT Time of Flight Mass Spectrometer in positive ionisation mode.

2.3 Synthesis

2.3.1 Ligand Synthesis

2.3.1.1 Ligand L Synthesis

Ligand L (*N,N'*-bis(pyridin-2-ylmethylene)-4,4'-diaminodiphenylmethane), Figure 2. 1, was made according to literature procedure.[1] 4,4'–methylenedianiline (1.57 g, 8.00×10^{-3} mol) in 25 ml ethanol was added to two equivalents of pyridine-2-carboaldehyde (1.40 ml, 1.50×10^{-2} mol) in 25 ml ethanol and the solution stirred for four hours. The resulting yellow precipitate (1.95 g, 5.00×10^{-3} mol) was filtered and recrystallised from ethanol. Yield: 65 %

^{1}H NMR (CD_2Cl_2): δ 8.72 (2H, d, *J = 3.9 Hz*, H_6), δ 8.62 (2H, s, H_{im}), δ 8.23 (2H, d, *J = 8.1 Hz*, H_3), δ 7.85 (2H, t, *J = 7.5 Hz*, H_4), δ 7.41 (2H, t, *J = 7.0 Hz*, H_5), δ 7.30 (8H, m, $H_{a/b}$), δ 4.09 (2H, s, CH_2).

ESI MS: *m/z* 399 $[(C_{25}H_{20}N_4) + Na]^+$.

Ligand L has been previously synthesised,[1] therefore a full characterisation is not presented here.

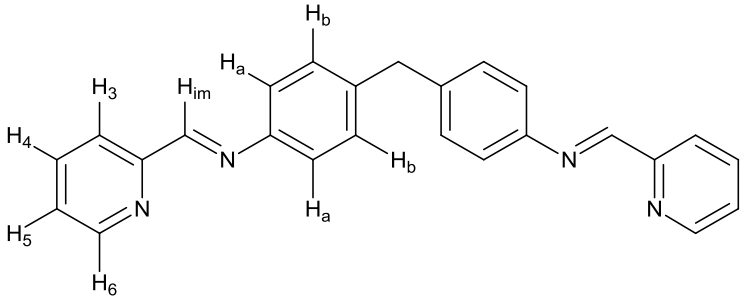

Figure 2. 1 Ligand L with NMR numbering scheme.

2.3.1.2 Ligand L[1] Synthesis

Ligand L[1] (*N,N'*-Bis(1-pyridin-2-yl-ethylidene)-4,4'-diaminodiphenylmethane), Figure 2. 2, was synthesised following literature procedure.[2] 4,4'–methylenedianiline (0.630 g, 3.00×10^{-3} mol) and 10 g 3Å dry molecular sieves were stirred in 100 ml toluene at room temperature for 10 minutes until dissolution of 4,4'–methylenedianiline. 2-Acetylpyridine (0.710 ml, 2.00×10^{-2} mol) was then added to the solution and the mixture left to stir at room temperature for three days. The solution was then filtered to remove the molecular sieves and the filtrate concentrated by rotary evaporation to yield a yellow oil (1.07 g, 3.00×10^{-3} mol). Yield: 84 %.

^{1}H NMR ($CDCl_3$): δ 8.68 (2H, d, *J = 4.0 Hz*, H_6), δ 8.04 (2H, broad d, *J = 7.9 Hz*, H_3), δ 7.97 (2H, td, *J = 7.5 Hz, J = 1.5 Hz*, H_4), δ 7.45 (2H, dd, *J = 7.5 Hz*, J = 1.3 Hz, H_5), δ 6.92 (2H, d, *J = 8.3 Hz*, H_b), δ 6.67 (2H, d, *J = 8.3 Hz*, H_a), δ 3.71 (2H, s, CH_2), 2.77 (6H, s, CH_3).

ESI MS: *m/z* 405 $[(C_{27}H_{24}N_4) + H]^+$.

Ligand L^1 has been previously synthesised,[2] therefore a full characterisation is not presented here.

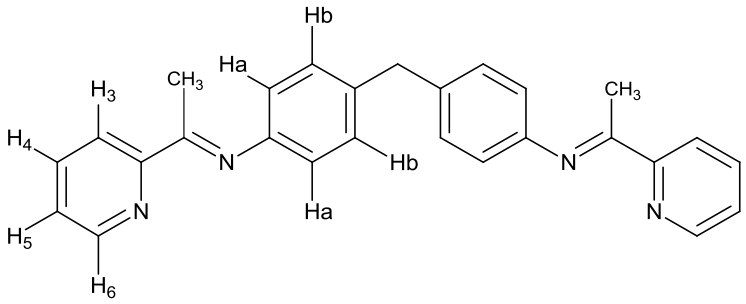

Figure 2. 2 Ligand L^1 with NMR numbering scheme.

2.3.1.3 Ligand L^2 Synthesis

Ligand L^2, (bis(1, 4-phenylazo-2-pyridine)), Figure 2. 3, was synthesised according to literature procedure,[3] and purified according to a new procedure. 2-Nitrosopyridine was synthesized as follows; 2-aminopyridine (9.40 g, 9.90×10^{-2} mol) with dimethylsulphide (8.00 ml, 0.108 mol) were dissolved in 100 ml dry DCM. n-chlorosuccinimide (13.3 g, 9.90×10^{-2} mol) was dissolved in 250 ml dry DCM and added dropwise to the above over one hour at -20 ºC. This solution was stirred at -20 ºC for an hour then at room temperature for a further hour. A solution of sodium methoxide (4.05 g, 7.50×10^{-2} mol) in 75 ml dry methanol was then added and stirred for 10 minutes at room temperature. Water (150 ml) was then added and stirred overnight. The organic (lower) layer was separated. The aqueous layer was washed with DCM (50 ml x 2), with DCM washes added to the organic layer. This was then washed with water (50 ml x 2) then dried with magnesium sulphate, filtered and evaporated on a rotary evaporator to yield an orange/ brown oil which was left in the fridge overnight. All of the oil was then dissolved in 100 ml dry DCM and added to a solution of meta chloro perbenzoic acid (20.1 g, 0.116 mol) in 500 ml dry DCM after cooling to 0 ºC. This was then stirred at 0 ºC for 90 minutes. Dimethylsulphide (4.00 ml,

5.40x10^{-2} mol) was then added and stirred at 0 ºC for 30 minutes. 500 ml saturated aqueous sodium carbonate solution was then added and stirred for one hour, followed by the separation of the green/yellow (lower) organic layer. The aqueous layer was washed with DCM (2x 50 ml) which was then added to the organic layer and washed with water (2 x 50 ml), dried with magnesium sulphate, filtered, evaporated to dryness and stored at 4 ºC overnight to yield dark brown crystals. These were recrystallised from ethanol (1.10 g, 1.00x10^{-2} mol).

2-Nitrosopyridine (0.100 g, 9.25x10^{-4} mol) was dissolved in 30 ml DCM. 4, 4-methylenedianiline (0.0910 g, 4.61x10^{-4} mol) was added, followed by 10 drops of glacial acetic acid at which point the solution turned orange. This mixture was stirred at room temperature for 18 hours. The resulting orange solution was evaporated to dryness and purified via an optimised isocratic HPLC method with a 10 % water, 90% methanol solvent system (Dionex Summit HPLC system with Chromeleon software, using a Summit P580P high pressure binary gradient pump and Summit UVD 170s UV/Vis Multi-channel detector with prep flow cell and Luna 10uC18 250 mm x 30 mm column, Phenomenex). Pure ligand L^2 (0.180 g, 4.76 x10^{-4} mol) has a retention time of 10.84 minutes. Yield: 51 %

^{1}H NMR ($CDCl_3$): δ 8.75 (2H, dq, *J = 4.7, 0.75 Hz*, H_6), 8.03 (4H, d, *J = 8.5 Hz*, $H_{a/b}$), 7.92 (2H, td, *J = 7.9, 1.9 Hz*, $H_{4/5}$), 7.83 (2H, dt, *J = 7.9, 1.0 Hz*, H_3), 7.40 (6H, m, $H_{a/b}$ + $H_{4/5}$), 4.17 (2H, s, CH_2).

ESI MS: *m/z* 379 $[(C_{23}H_{18}N_6) +H]^+$.

Ligand L^2 has been previously synthesised,[3] therefore a full characterisation is not presented here.

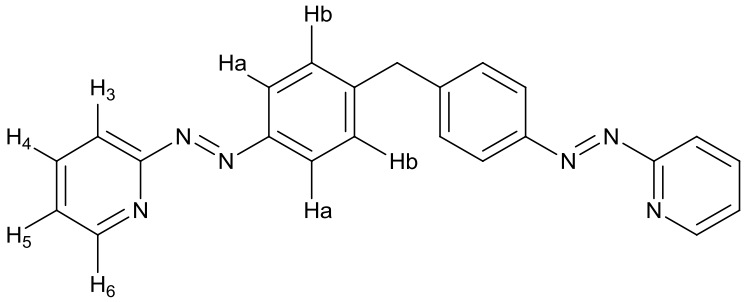

Figure 2. 3 Ligand L^2 with NMR numbering scheme.

2.3.2 Metal Complex Synthesis

Unless stated otherwise charged metal complexes were isolated with chloride counterions, due to good aqueous solubility and the fact that chloride ions are the most commonly used in commercial drugs.[4]

2.3.2.1 $[Fe_2L_3]^{4+}$ Synthesis

$[Fe_2L_3]^{4+}$ was synthesised according to literature procedure.[1] Ligand L (0.320 g, 8.55 x10^{-4} mol) in 50 ml methanol was stirred for 30 minutes to dissolve. Iron(II) chloride tetrahydrate (0.120 g, 5.91x10^{-4} mol) also in methanol was added and an immediate colour change to vivid purple was observed. The solution was refluxed for three hours, evaporated to dryness, re-dissolved and precipitated with ether, followed by filtration and washing (0.350 g, 2.54 x10^{-4} mol). Yield: 86%.

^{1}H NMR (MeOD): δ 9.21 (2H, s, H_{im}), δ 8.75 (2H, d, *J = 7.0 Hz*, H_3), δ 8.51 (2H, t, *J = 6.5 Hz*, H_4), δ 7.90 (2H, t, *J = 6.1 Hz*, H_5), δ 7.49 (2H, d, *J = 4.2 Hz*, H_6), δ 7.08 (4H, s, $H_{a/b}$), δ 5.62 (4H, s, $H_{a/b}$), δ 4.08 (2H, s, CH_2).

ESI MS: *m/z* 310 $[Fe_2(C_{25}H_{20}N_4)_3]^{4+}$.

UV-Vis in water, λ_{max}/nm (ε/ $dm^3mol^{-1}cm^{-1}$): 324 (32900), 570 [shoulder 525] (16900).

$[Fe_2L_3]^{4+}$ has been previously synthesised,[1] therefore a full characterisation is not presented here.

2.3.2.2 $[Fe_2L^1_3]^{4+}$ Synthesis

$[Fe_2L^1_3]^{4+}$ was synthesised according to literature procedure.[2] Ligand L^1 (0.199 g, 4.93 $x10^{-4}$ mol) in 50 ml methanol was added to iron(II) chloride tetrahydrate (0.0670 g, 3.36 $x10^{-4}$ mol) in 50 ml methanol. The solution immediately turned purple, characteristic of iron(II) tris-pyridylimine compounds, and was further refluxed for three days. The solution was then evaporated, precipitated with an excess of NH_4PF_6 (0.610 g, $4.00x10^{-3}$ mol) in methanol and stirred for two hours. This was then placed at 4 ºC for 45 minutes followed by filtration on a membrane filter. Ion exchange was then carried out by adding 3.08 g Dowex (chloride form) in 50 ml methanol. This was stirred at room temperature for three hours before filtering on filter paper and washing with methanol, giving a purple solid (0.180 g, $1.23x10^{-4}$ mol). Yield: 73.15 %.

^{1}H NMR (MeOD): 8.78 (2H, d, *J = 7.8 Hz*, H_3), δ 8.50 (2H, t, *J = 7.8 Hz*, H_4), δ 7.81 (2H, t, *J = 6.3 Hz*, H_5), δ 7.42 (2H, dd, *J = 6.3 Hz*, *J = 1.1 Hz*, $H_{a/a'/b/b'}$), δ 7.26 (2H, d, *J = 6.3 Hz*, H_6), δ 6.89 (2H, dd, J = 6.3 Hz, *J = 1.7 Hz*, $H_{a/a'/b/b'}$), δ 5.57 (2H, dd, *J = 8.3 Hz*, J = 1.5 Hz, $H_{a/a'/b/b'}$), δ 4.79 (2H, dd, *J = 8.3 Hz, J = 1.5 Hz*, $H_{a/a'/b/b'}$), δ 4.64 (6H, s, CH_3), δ 4.10 (2H, s, CH_2).

ESI-MS: *m/z* 331 $[Fe_2(C_{27}H_{24}N_4)_3]^{4+}$.

UV-Vis in water, λ_{max}/nm (ε/ $dm^3mol^{-1}cm^{-1}$): 324 (32900) 570 [shoulder 525] (16900).

$[Fe_2L^1_3]^{4+}$ has been previously synthesised,[2] therefore a full characterisation is not presented here.

2.3.2.3 $[Ru(DMSO)_4Cl_2]$ Synthesis

$[Ru(DMSO)_4Cl_2]$ was prepared according to literature procedure.[5] $RuCl_3$ (1.00 g, $5.00x10^{-3}$ mol) was refluxed in 5 ml DMSO for five minutes, cooled and evaporated to half volume. 20 ml acetone was added to precipitate a yellow powder which was filtered and dried (1.00 g, $2.00x10^{-3}$ mol). Yield: 43 %.

2.3.2.4 γγ -$[Ru_2L^2{}_2Cl_4]$ Synthesis

γγ -$[Ru_2L^2{}_2Cl_4]$ was synthesised according to published procedure[3] through a mixture of $[Ru(DMSO)_4Cl_2]$ (0.075 g, $1.55x10^{-4}$ mol) and the bispyridylazo ligand L^2 (0.0580 g, 1.54 $x10^{-4}$ mol) heated under reflux in 40 ml acetone for 18 hours. After ~ one hour a colour change to dark green was observed. The reaction was cooled after 18 hrs and the green precipitate isolated by filtration and washed with acetone and diethylether to afford 0.0520 g of crude product, consisting of the desired product and insoluble polymeric material. The crude product was purified on a neutral alumina (Brockman type I, Camag 100-250 mesh) column with DCM : acetonitrile (1:1) as eluent. The first fraction was collected (0.0100 g, 9.09 $x10^{-6}$ mol). Yield: 12 %.

^{1}H NMR (DMSO-d6) δ 9.07 (1H, d, *J = 5.6 Hz*, H_6), 8.76 (1H, d, *J = 7.7 Hz*, H_3), 8.43 (1H, t, *J = 7.7 Hz*, H4), 8.04 (1H, t, *J = 6.0 Hz*, H_5), 7.24 (2H, d, *J = 8.2 Hz*, H_a), 7,11 (2H, d, *J = 8.4 Hz*, H_b), 4.32 (2H, s, CH_2).

ESI-MS: *m/z* 1065 $[Ru_2L^2{}_2Cl_3]^+$.

UV-Vis in chloroform, λ_{max}/nm (ε/ $dm^3mol^{-1}cm^{-1}$): 304 (24800), 430 (17300), 642 (17100).

γγ -$[Ru_2L^2{}_2Cl_4]$ has been previously synthesised,[3] therefore a full characterisation is not presented here.

2.3.2.5 ββ-[$Ru_2L^2{}_2Cl_4$] Synthesis

ββ-[$Ru_2L^2{}_2Cl_4$] was synthesised according to procedure,[3] from a mixture of [$Ru(DMSO)_4Cl_2$] (0.230 g, $4.75x10^{-4}$ mol) and the bispyridylazo ligand L^2 (0.180 g, $4.76x10^{-4}$ mol) heated under reflux in 50 ml methoxyethanol for 24 hrs. After cooling, the solution was filtered and solvent removed by evaporation. The crude compound (0.0700 g) was dissolved in chloroform and isolated by precipitation with diethylether. The crude precipitate was purified via neutral alumina column chromatography (Brockman type I, Camag 100-250 mesh) eluted with DCM : acetonitrile (2:1). The first small light purple band was discarded and the second large purple band collected. Solvent was evaporated to half volume and the compound precipitated with diethyl ether, yielding a blue powder ($4.00x10^{-3}$ g, $3.27x10^{-6}$ mol). Yield: 1 %.

^{1}H NMR (CD_2Cl_2) (prime numbering is used for the pyridine ring and corresponding phenyl ring trans to Cl ligand) δ 9,61 (1H, d, *J = 5.70 Hz*, H_6), 8.62 (1H, d, *J = 7.49 Hz*, H_3), 8.61 (1H, d, *J = 7.49 Hz*, $H_{3'}$), 8.23 (1H, t, *J = 7.84, 1.43 Hz*, H_4), 8.05 (1H, t, *J = 8.20, 1.78 Hz,* $H_{4'}$), 7.88 (1H, t, *J = 7.49, 1.07 Hz*, H_5), 7.38 (2H, m, $H_{5'}$+ $H_{6'}$), 7.24 (2H, d, *J = 8.2 Hz*, $H_{a'}$), 7.17 (2H, d, *J = 8.20 Hz*, H_b), 7.17 (2H, d, *J = 8.55 Hz*, $H_{b'}$), 6.48 (2H, d, *J = 8.20 Hz*, H_a), 4.00 (2H, q, CH_2).

ESI-MS: *m/z* 1123 [($Ru_2L^2{}_2Cl_4$) + Na]$^+$.

UV-Vis in chloroform, λ_{max}/nm (ε/ $dm^3mol^{-1}cm^{-1}$): 300 (32200), 380 (39300), 572 (22200).

ββ-[$Ru_2L^2{}_2Cl_4$] has been previously synthesised,[3] therefore a full characterisation is not presented here.

2.3.2.6 ββ-[$Ru_2L^2_2(NO_3)_4$] Synthesis

ββ-[$Ru_2L^2_2(NO_3)_4$] was synthesised[6] from pure ββ-[$Ru_2L^2_2Cl_4$] ($4.00x10^{-3}$ g, $3.27x10^{-6}$ mol) in a minimum acetone and $AgNO_3$ ($2.00x10^{-3}$ g, $1.42 x10^{-5}$ mol) in 50 ml water. This was refluxed for three hours in the dark. The solution was then filtered to remove AgCl and evaporated to dryness. The product was taken up in chloroform and precipitated with diethylether to yield a blue/purple powder ($3.00x10^{-3}$ g, $2.24 x10^{-6}$ mol.) Yield: 68 %.

^{1}H NMR (acetone-d6) (prime numbering is used for the pyridine ring and corresponding phenyl ring trans to Cl ligand) δ 9,24 (1H, d, *J = 6.25 Hz*, H_6), 8.76 (1H, d, *J = 8.09 Hz*, H_3), 8.70 (1H, d, *J = 7.72 Hz*, $H_{3'}$), 8.53 (1H, t, *J = 8.46, 7.35 Hz*, H_4), 8.33 (1H, t, *J = 7.72 Hz*, $H_{4'}$), 8.19 (1H, t, *J = 7.72 Hz*, H_5), 7.67 (2H, d, *J = 8.46 Hz*, $H_{a'}$) 7.61 (1H, m, $H_{5'}$), 7.50 (1H, d, *J = 7.35 Hz*, $H_{6'}$), 7.20 (2H, d, *J = 8.82 Hz*, H_b), 7.14 (2H, d, *J = 8.46 Hz*, $H_{b'}$), 6.46 (2H, d, *J = 8.46 Hz*, H_a), 4.12 (2H, s, CH_2).

ESI-MS: *m/z* 1146 $[Ru_2L^2_2(NO_3)_3]^+$.

UV-Vis in acetone, λ_{max}/nm (ε/ $dm^3mol^{-1}cm^{-1}$): 270 (23700), 377 (30400), 529 (14800).

ββ-[$Ru_2L^2_2(NO_3)_4$] has been previously synthesised,[6] therefore a full characterisation is not presented here.

2.3.2.7 $[Ru_2L^2_2(bpy)_2]^{4+}$ Synthesis

$[Ru_2L^2_2(bpy)_2]^{4+}$ (NO_3^- counterions) was synthesised by a new procedure. To a solution of ββ- [$Ru_2L^2_2(NO_3)_4$] (0.0110 g, $9.11 x10^{-6}$ mol) in water, an excess of 2, 2-bipyridine (0.0350 g, $2.24 x10^{-4}$ mol) was added in acetone. The solution was refluxed for three hours, cooled and filtered to give a dark red solution. The solution was then evaporated and washed with chloroform to yield a red powder (0.0100 g, $6.58 x10^{-6}$ mol). Yield: 72 %.

^{1}H NMR (CD_3CN) (also see section 6.2.2) (C/E represent pyridine rings; A/D represent bipyridine rings; δ 8.99 (1H, d, *J = 8.19 Hz*, H_{3C}), 8.94 (1H, d, *J = 8.19 Hz*, H_{3E}), 8.50 (1H, m, *J = 8.19 Hz*, H_{4E}), 8.42 (1H, tt, *J = 7.94 Hz*, H_{4C}), 8.28 (1H, d, *J = 8.19 Hz*, H_{3A}), 8.21 (1H, t, *J = 7.94 Hz*, H_{4A}), 8.04 (1H, d, *J = 8.45 Hz*, H_{3D}), 7.96 (1H, t, *J = 7.17, 7.94 Hz*, H_{4D}), 7.91 (1H, d, *J = 5.63 Hz*, H_{6C}), 7.81 (2H, m, $H_{5/6E}$), 7.72 (2H, m, $H_{6D/5C}$), 7.61 (1H, t, *J = 5.63, 6.14 Hz*, H_{5A}), 7.56 (1H, t, *J = 7.43, 5.89 Hz*, H_{5D}), 7.20 (2H, d, *J = 8.19 Hz*, $H_{b'}$), 7.10 (1H, d, *J = 5.63 Hz*, H_{6A}), 6.94 (2H, d, *J = 8.45 Hz*, $H_{a'}$), 6.71 (2H, d, *J = 8.19 Hz*, H_b), 6.06 (2H, d, *J = 8.45 Hz*, H_a), 3.82 (2H, m, CH_2).

ESI-MS: *m/z* 318 $[Ru_2L^2{}_2(bpy)_2]^{4+}$, 424 $[Ru_2L^2{}_2(bpy)_2]^{3+}$, 636 $[Ru_2L^2{}_2(bpy)_2]^{2+}$.

UV-Vis in water, λ_{max}/nm (ε/ $dm^3mol^{-1}cm^{-1}$): 266 (44900), 382 (36400), 508 (18400).

IR: 2163, 1998, 1602, 1272 cm^{-1}.

2.4 DNA Binding Studies

2.4.1 UV-Visible Absorbance Spectroscopy

Information about the structure and environment of a species in a sample, or the identification of transitions between energy levels within a molecule can be determined using UV-Visible spectroscopy. More specifically, in metal complexes electromagnetic radiation in the range 200 nm to 700 nm can excite electrons from p-, d- and π- bonding or lone pair orbitals into unfilled non-bonding or anti-bonding orbitals. The wavelength at which the molecule absorbs is then a direct measure of the separation between the energy levels. The absorption of light in a solution is exponentially related to the number of molecules of the absorbant in solution and to the length of the light pathway through the sample, defined as:

$A = \log_{10} (I_0 / I)$, where I_0 = intensity of incident light, I = intensity of emergent light.

The absorbance may be used to find the concentration of a solution of a single absorbing species using the Beer-Lambert law[7]:

$$A = \varepsilon c l$$

A = absorbance (arbitrary units), ε = extinction coefficient (a constant for a particular wavelength of that species measured in mol^{-1} dm^3 cm^{-1}), c = concentration (mol dm^{-3}), l = path length of cell (cm).

DNA is commonly analysed using UV-Visible spectroscopy. The characteristic band of DNA, Figure 2. 4, has a maximum centred around 260 nm. This corresponds to the π→π* transitions of the delocalised π electrons from the DNA bases. Perturbations in this standard spectrum can give information about substrate binding or environment. Experimentally, UV-Visible spectroscopy has been used in this thesis for assessing stability of metal complexes, to assess isomerisation processes of complexes and in parallel with emission experiments to assess the effect on metal complexes due to DNA binding.

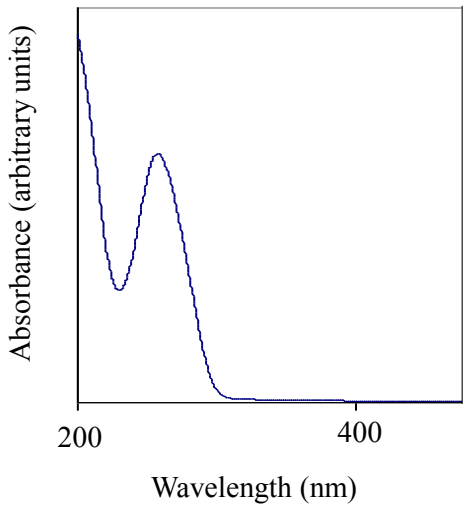

Figure 2. 4 UV-Visible spectrum of B-DNA.

UV-Visible spectra were recorded on a Cary 5000 UV-Vis-NIR Spectrophotometer (Varian).

2.4.2 Circular Dichroism

2.4.2.1 Principles of Circular Dichroism

Circular dichroism (CD) is a technique used to study the optical activity of chiral molecules and to probe their interactions with other compounds.[8] This method is therefore ideal for the study of DNA and its interaction with metal complexes. CD is defined as the difference in absorption (A) of left and right circularly polarised light, measured as a function of wavelength:

$$CD\ (\lambda) = A_l\ (\lambda) - A_r\ (\lambda)$$

Because chiral molecules do not have a reflection plane, the rearrangement of their electrons will not have one either. This means the interaction between the chiral molecule and left and right handed photons will be different, giving rise to a CD signal. Within DNA, the units responsible for inducing chirality are the ribose sugar moieties. However, this chiral sugar backbone has no important transitions in the spectral region and the CD spectrum of DNA arises from the CD induced into the transitions of the bases as a result of their coupling with the backbone sugars. For this reason the structural conformation of DNA, for example its polymorph forms B, Z and A can be easily deduced, Figure 2. 5. Peaks between 200 nm and 300 nm result from interactions of helically stacked bases.

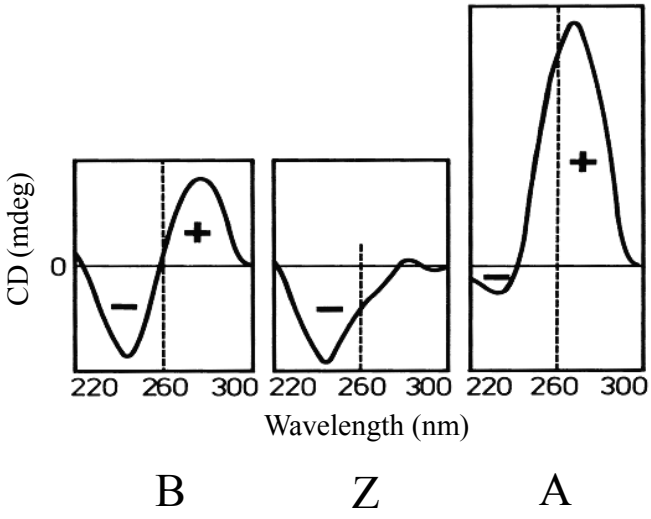

Figure 2. 5 Schematic CD spectra of B, Z and A DNA.[9]

As with the DNA bases, upon DNA binding achiral molecules acquire an induced CD signal (ICD) and the normal B-DNA signal may be perturbed, allowing interactions and DNA changes to be probed.

2.4.2.2 CD Experimental Procedure

Spectra were collected in 1 cm pathlength cuvettes using a Jasco J-715 spectropolarimeter. Fresh samples were made with constant concentrations of ct-DNA (300 μM), NaCl (20 mM) and sodium cacodylate buffer (10 mM). The concentration of metal complex was varied with the final ratios of DNA base: metal complex being between 60:1 and 8:1.

Two stock solutions were prepared; the first of metal complex and the second with a solution of double concentration DNA (DNA (600 μM), NaCl (40 mM) and sodium cacodylate buffer (20 mM)). After the addition of X μL of metal complex solution to an original 300 μM DNA solution, an equivalent addition of the second, double concentration DNA stock solution was added. This results in the concentrations of DNA, NaCl and sodium cacodylate buffer remaining unaltered throughout the titration.

2.4.3 Linear Dichroism

2.4.3.1 Principles of Linear Dichroism

This technique studies the optical anisotropy of molecules.[8] It is commonly used to probe the orientation of long molecules such as DNA and can therefore be used to probe DNA-ligand systems. Linear dichroism (LD) is defined as the difference between the absorption (A) of light linearly polarised parallel and perpendicular to an orientation axis, measured as a function of wavelength:

$$LD\ (\lambda) = A_{||}(\lambda) - A_{\perp}(\lambda)$$

Electromagnetic radiation consists of an electric and a magnetic component. These may be thought of as waves, which oscillate perpendicular to each other and to the direction of propagation of the wave, Figure 2. 6.

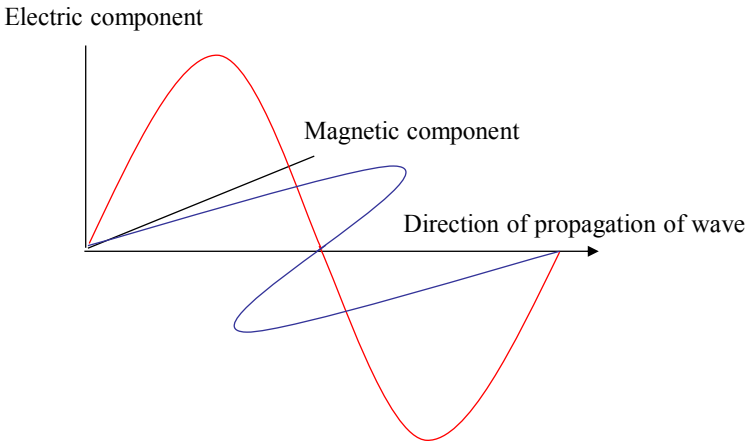

Figure 2. 6 Components of electromagnetic radiation.

Linearly polarised photons, for example, will all have their electric component oscillating in the same direction. The absorbtion of a photon of radiation causes the electron distribution in the molecule to be reorganised, with the linear, net direction of this change defining the transition polarisation. So LD may be used to give the orientation of the transitions within a molecule. Flow LD is a specific method of obtaining an LD spectrum,

used in this thesis. It is commonly used with systems which are intrinsically oriented or may be oriented during the experiment, such as DNA (min length ~250 bp). When a solution of DNA is flowed between the narrow walls of a flow couette cell, Figure 2. 7, the DNA is oriented by viscous drag. This alignment ensures that the electronic transitions normally interacting with the incident light are aligned so can interact coherently with the polarised light. The flow cell consists of a fixed outer cylinder and a rotating solid quartz inner cylinder, separated by a gap of 0.5 mm giving a total pathlength of 1 mm.

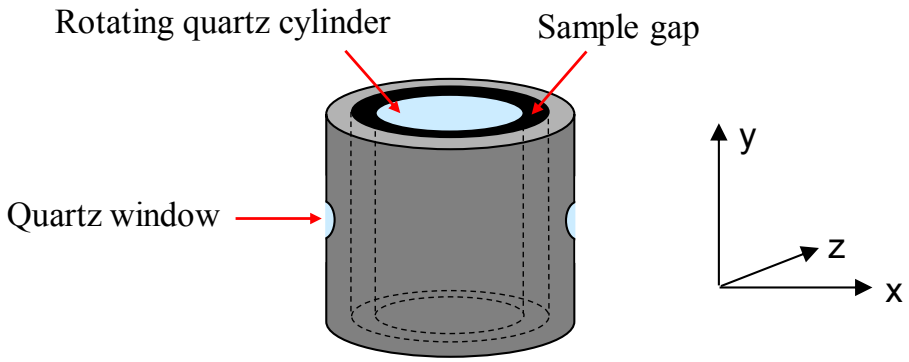

Figure 2. 7 Schematic diagram of an LD flow couette cell.[10]

A typical LD spectrum of B-DNA is shown in Figure 2. 8. The ct-DNA signal at 258 nm arises due to the orientation and electronic transitions of the DNA bases. In B-DNA these are arranged at approximately right angles (86°) to the direction of orientation, so the base π-π* signals give rise to a negative signal. The signal at 195 nm corresponds to transitions within the phosphodiester backbone.

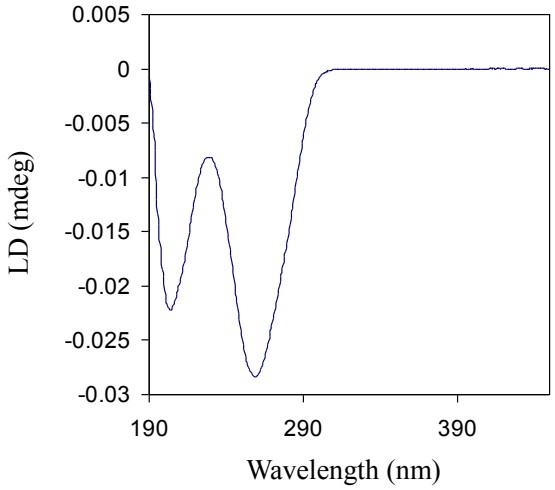

Figure 2. 8 Linear Dichroism spectrum of B-DNA

A small molecule free in solution is not large enough to be oriented so will not display an LD signal. Similarly, a molecule bound randomly to DNA will also not be oriented. A complex bound uniformly to DNA will not only possess an LD signal in its own absorption region, but it may also cause the characteristic DNA signals to be perturbed. The sign and amplitude of these signals can be used to give information about predominant binding modes such as intercalation, major/minor groove binding or covalent binding to DNA bases.

2.4.3.2 LD Experimental Procedure

Spectra were collected using a flow couette cell (Krometek) in a Jasco J-715 spectropolarimeter adapted for LD measurements. The same series of samples were prepared and analysed as for the above CD method (section 2.4.2.2).

2.4.4 Ethidium Bromide Displacement Assay

2.4.4.1 Principles of the Ethidium Bromide Displacement Assay

Ethidium bromide (EB), Figure 2. 9, binds to DNA through intercalation and displays a 20-fold increase in fluorescence upon binding.[11] For this reason EB is commonly used in fluorescence assays to assess DNA-complex interactions.[12] Fluorescence can be defined as the emission of radiation caused by a molecular transition from an excited state to a ground state. The absorption of a photon in some molecules can result in the raising of the molecule to an excited electronic state without subsequent loss of all of its energy due to radiationless decay. In the case of EB, UV radiation at 375 nm is absorbed by the dye when bound to DNA. A photon is then re-emitted at 590 nm in the red-orange region of the visible spectrum. [13] Free EB does not emit in this way due to quenching of the emission by surrounding solvent molecules.

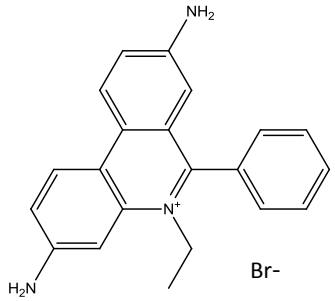

Figure 2. 9 The structure of ethidium bromide.

A method of assessing the ability of a compound to bind to DNA is to load DNA with EB and measure the fluorescence. Increasing concentrations of DNA binding complex are then added to the solution and resulting fluorescence recorded. If DNA binding of the complex is stronger than that of EB, the EB will be displaced from the DNA and thus fluorescence of the solution will decrease. This theory may be used to determine the apparent

equilibrium constant for drug binding.[14] This method can be used to detect various modes of DNA binding (not only intercalation) as, for example, complex binding in the major groove may disrupt the DNA enough to cause removal of the EB from the DNA.

2.4.4.2 Ethidium Bromide Displacement Experimental Procedure

The emission of an ethidium bromide (EB) solution (1.30 $x10^{-6}$ mol) (3.1 µl 0.1 mg/ml EB solution, 6 µl Tris base, 590 µl H_2O) was recorded as a control (Varian cary eclipse fluorescence spectrophotometer, excitation λ 540 nm, emission λ 560-750 nm). 1.5 µl ct-DNA solution (3.90 $x10^{-6}$ mol) (1.5 µl 1.55 $x10^{-3}$ ct-DNA, 3.1 µl 0.1 mg/ml EB, 6 µl 1 M Tris base, 590 µl H_2O) was then added and resulting emission measured. 1 µl metal complex (2.50 $x10^{-5}$ mol) was added to the solution, emission recorded, and this process (addition of 1 µl metal complex) repeated until emission dropped to below half of the starting value. For each emission recording the original EB emission was subtracted and results normalised. The following equation was used to calculate apparent binding constant:

$$\text{EB binding constant } (M^{-1}) \times [\text{EB}] \text{ (mol)} = K_{app} (M^{-1}) \times C_{50\%} \text{ (mol)}$$

2.4.5 DNA Emission Studies

2.4.5.1 Principles of the Emission Assay

The measurement of the emission intensity of small molecules has become a powerful analytical tool in biological sciences because of its capacity to yield information on molecular association, motion and separation. Enhancement of the fluorescence of d^6 transition metal complexes has been used for DNA and oxygen sensing as well as cell imaging purposes.[15] Enhancement of fluorescence upon DNA binding is due to the

protective environment of the DNA which reduces quenching from solvent molecules which may deactivate the excited state through hydrogen bonding. In the assay used herein, the concentration of metal complex remains constant while the concentration of DNA is increased. The fluorescence response can therefore be probed, to assess DNA-metal complex interactions.

2.4.5.2 Emission Experimental Procedure

Samples of ct-DNA ($2.00x10^{-3}$ M), NaCl (20 mM) and sodium cacodylate buffer (10 mM) were prepared. The concentration of DNA was varied with ratios of DNA base: metal complex between 1:1 and 10:1. Two stock solutions of metal complex were prepared. The first of metal complex (19.2 μM) and the second with double concentration (38.4 μM). After the addition of X μL of DNA solution to the original metal complex solution (19.2 μM), an equivalent addition of the second, double concentration metal complex stock solution was added. This results in the concentration of metal complex remaining unaltered throughout the titration. After each successive addition emission was recorded in a PTI fluorescence system, with illumination from a PTI L-201M source using a 75 W xenon arc lamp. The detection system was a Hamamatsu R928 PMT in a PTI model 814 analog/photon-counting photomultiplier (λ exc = 512 nm; λ em = 700-900 nm). UV-Visible spectra were recorded of each sample in parallel with emission.

2.4.6 DNA Photocleavage

2.4.6.1 Principles of the DNA Photocleavage Assay

A further use of small-molecule DNA binders is in the development of molecular probes for therapeutics such as photodynamic therapy. This usually depends on the complexes

ability to associate with biological molecules such as DNA.[16] Light is then used in order to activate the complex, causing damage to biological molecules and killing the target cell. For example, complexes with a long-lived, low-energy triplet excited state are capable of generating singlet oxygen, which then induces DNA damage. The assay used in this thesis probes the ability of metal complexes to cause DNA cleavage in the presence of UVA light.

2.4.6.2 DNA Photocleavage Experimental Procedure

DNA was radiolabelled with α-dATP (as per kit instructions, New England Biolabs): Linear plasmid DNA (4 µl, BS SK(-) 159 bp) was incubated with 0.4 µl dTTP (10 mM), 0.4 µl dCTP (10mM), 0.4 µl dGTP (10 mM), 2 µl 10x Ecopol buffer, 0.4 µl Klenow exo- DNA polymerase, 2.5 µl α-dATP* and 9 µl H_2O for 40 minutes at room temperature. The solution was then deprotonated and desalted using a kit (Wizard SV gel and PCR cleanup system, Promega): 25 µl DNA membrane binding solution was added to the DNA and centrifuged at 15000 x g for one minute before being transferred into a new tube and 650 µl membrane wash solution added with further centrifugation of one minute. 500 µl wash solution was then added with centrifugation for a further 5 minutes. The elution step was then followed: the filter was transferred into a new tube and 50 µl nuclease free water was added and centrifuged for one minute. This was repeated 2 x with 40 µl H_2O. This was then repeated with 50 µl H_2O, left for 5 minutes and centrifuged for one minute. The total volume was transferred into a new eppendorf and freeze-dried for future use.

Maxam gilbert solutions for DNA footprinting were then prepared for specific cleavage at guanine bases: radiolabelled DNA (~1200 CPS) (prepared as above) was incubated with

100 µl DMS buffer (50 mM sodium cacodylate, pH 8 with HCl, 1mM EDTA) to which 0.5 µl DMS was added and incubated for four minutes on ice. Following this, 25 µl DMS stop buffer (1.5 M sodium acetate pH 7, 1 M Mercapto ethanol, 100 µg/ml ct-DNA) was added. For specific cleavage at guanine and adenine bases: radiolabelled DNA (~1200 CPS) (prepared as above) was incubated with 100 µl H_2O. 25 µl formic acid was added and the solution incubated for four minutes at room temperature. Following this, 200 µl G and A stop buffer (0.3 M sodium acetate, 0.1 mM EDTA and 100 µg/ml ct-DNA) was added. DNA of both guanine cleaved and adenine and guanine cleaved samples was precipitated by the same method: 800 µl cold ethanol was added followed by incubation at -80 ºC for 30 minutes. Samples were then washed with 2 x 500 µl ethanol before being centrifuged at 184000 x g for 25 minutes, then placed in a heating block at 90 ºC to remove any remaining ethanol. Samples were then cleaved: Samples were dissolved in 90 µl H_2O followed with the addition of 10 µl piperidine, vortexed and left for 30 minutes at 90 ºC. Following this, samples were freeze dried, re-dissolved in 40 µl H_2O and further freeze dried. This was repeated 2 x. Prior to use samples were dissolved in 5 µl H_2O.

For DNA photocleavage solutions were prepared as follows; control: 0.5 µl DNA*, 3.4 µl H_2O, 0.5 µl Tris base, 0.5 µl ct-DNA (1.55 $x10^{-3}$) Metal complex solutions: 0.5 µl DNA*, 0.5 µl Tris base, 0.5 µl ct-DNA (1.55 $x10^{-3}$), metal complex (3.88 x 10^{-5} M stock solution) and H_2O to make 20:1 and 10:1 DNA base: metal complex ratio. Samples were incubated for 3.5 hrs at 90 ºC before loading, with half the sample being incubated in the dark and half under a UVA lamp.

Samples were subsequently loaded onto a denaturing gel: 13 % polyacrylamide (from 8 ml 24 % denaturing gel, 16 ml 8 % denaturing gel) (40 % denaturing gel: 38 g acrylamide, 2 g bis-acrylamide in 200 ml deionised H_2O), (24 % denaturing gel: 60 ml 40 % denaturing gel, 50 g urea, 5 ml 20 x TBE buffer in 100 ml H_2O). Gel thickness of 0.35 mm. 14 µl TEMED and 28 µl 25 % APS were added to the gel solution to set and the gel left for an hour before use. Metal complex samples as well as control and maxam gilbert reference samples were loaded onto the gel and run for three hrs at room temperature, 35 W. Gels were visualised using the BAS 2500 FUJIFILM bioimaging analyser and radioactivities associated with bands were quantified with AIDA image analyser software (Raytest, Germany).

2.4.7 DNA Three Way Junction Binding

2.4.7.1 Principles of the Three Way Junction Binding Assay

Polyacrylamide gel electrophoresis can be used to separate DNA of various length /charge/3D architecture through the application of an electric field to a gel matrix. Experiments described in this thesis were designed to mimic previous experiments,[17] using DNA oligos of 14 base pairs long. These were designed to be able to form a DNA three way junction structure in the presence of a stabilising molecule, with each arm of the 3-way junction structure being 7 base pairs in length, Figure 2. 10. This has been shown to be the minimum length of DNA needed in order to form stable structures in a polyacrylamide gel.[18]

Strand 1 – 5'CGGAACGGCACTCG

Strand 2 – 5'CGAGTGCAGCGTGG

Strand 3 – 5'CCACGCTCGTTCCG

Figure 2. 10 Oligos used in polyacrylamide gel electrophoresis experiments and the three way junction structure proposed to form.[17]

The conditions of this experiment were modified a number of times in order to find the most successful method. At 4 ºC there is formation of a three way junction structure, with a high percentage of double strand formation with all compounds tested. For this reason, gels were carried out at 25 ºC in order to suppress the formation of the double stranded species and to see more clearly three way junction stabilisation.

2.4.7.2 Three Way Junction Assay Procedure

Oligonucleotides were obtained pure.[19] DNA strand 1 was radioactively labelled at the 5' end using ^{32}P radiolabelled ATP in order for any DNA structures formed to be visualised on the gel. Samples were analysed with 15 % Polyacrylamide gel electrophoresis.

To an eppendorf (in order) the following components were added; 4 µl H_2O, 1 µl 10x PNK Buffer, 2.5 µl $3.30x10^{-6}$M ATP, 0.41 µl strand 1, 1 µl [$\gamma^{32}P$]-ATP and 1 µl kinase. The solution was incubated for 40 minutes at 37 ºC. Strand 1 was then purified by removal of

unreacted [γ^{32}P]-ATP: A 1 ml plastic syringe was packed by centrifugation with sephadex G50-fine, followed by the addition of 100 µl water to the column and further centrifugation. This procedure was repeated 3x. 90 µl water was then added to the eluent which was subsequently added back into the column, further centrifuged and collected in an eppendorf. The sample was then freeze dried and dissolved in 20 µl water before use. The Nativ Gel (15 % polyacrylamide, thickness 0.35 mm) was made as follows: 12 ml 30 % polyacrylamide (29 g acrylamide, 1 g bis-acrylamide, up to 100 ml H_2O), 1.2 ml 20x TBE, 240 µl 1 M NaCl, 10.5 ml H_2O. Directly before use 25 µl TEMED and 30 µl APS (25%) were added to the gel solution.

DNA samples were prepared by adding stoichiometric amounts of oligonucleotides (1.07 x 10^{-5} M each strand) in buffer (20mM NaCl, 2x TB). Dilutions of metal complexes were made in buffer (1x TB (50mM tris and boric acid (pH 8.3)), 10mM NaCl). Metal complex solutions were incubated with oligonucleotide solution for 15 minutes at room temperature followed by incubation on ice for 25 minutes. Loading buffer was then added and the samples loaded onto the gel. The gel was run for 1 hr at 5-7 W. Gels were visualised using the BAS 2500 FUJIFILM bioimaging analyser and radioactivities associated with bands were quantified with AIDA image analyser software (Raytest, Germany).

2.5 Cell Culture and Cell Studies

2.5.1 Cell Lines

Human breast cancer cell lines: T47D, MDA-MB-231.

Human ovarian cancer cell lines: SKOV-3, A2780-P (parental cell line), A2780-R (cisplatin resistant cell line).

Human myeloid leukaemia cell line: HL-60.

2.5.2 Cell Maintenance

All solutions and equipment used for cell maintenance were either obtained sterile or, when appropriate, autoclaved before use. Cell culture was undertaken in sterile conditions in a class 1 tissue culture hood (Aura B4, Bio Air, Italy).

All cell lines were maintained at 37 ^{o}C in a humidified chamber (5 % CO_2, 95 % air; MCO-15AC, Sanyo, Japan) in flat bottomed cell culture flasks (Falcon, UK) in continuous logarithmic culture. A2780-P, A2780-R, MDA-MB-231 and T47D cell lines were maintained in Dulbecco's Modified Eagle's Medium (DMEM) (+ 4.5 g/l glucose, Invitrogen Corporation, UK) supplemented with 10% fetal bovine serum (Invitrogen), 1 % 2 mM l-glutamine (Sigma), 1% 1 mM sodium pyruvate (Sigma), 1 % 10 mM Hepes buffer (Sigma) and antibiotics (Antibiotics Antimycotic 100× diluted to 1×, Sigma). HL-60 and SKOV-3 cell lines were maintained in RPMI-1640 medium (-L-glutamine, Invitrogen Corporation, UK) supplemented as above.

Adherent cell lines were subcultured twice weekly using a trypsin-EDTA protocol:
Media was removed and cells were washed with 5 ml phosphate buffered saline solution (PBS tablets (0.01 M phosphate buffer, 0.003 M KCl and 0.137 M NaCl, pH 7.4) Sigma, UK). PBS was then removed and replaced with 3 ml of trypsin-EDTA (10x solution (0.5% trypsin, 0.2% EDTA), diluted to 1x, Sigma, UK). The flask was then sealed and placed in the humidified chamber until all cells were detached from the surface of the flask. Following detachment, 10 ml of supplemented medium was added to the flask and the

resulting cell suspension mixed gently using a sterile pipette. Cell suspension was then transferred to a sterile 15 ml centrifuge tube (Falcon) before centrifugation at 1500 rpm for 5 minutes. Following centrifugation, supernatant was removed and the cell pellet was resuspended in 1 ml of supplemented medium. An aliquot was taken and transferred into a 75 cm^2 cell culture flask with supplemented medium, sealed, placed in the humidified chamber and allowed to grow to confluence for further use. Cell suspensions prepared in this manner were also used to seed various sized flasks, plates and/or dishes at various cell densities in preparation for experimental use (detailed information on seeding density is described for each protocol). Cell densities were determined using a haemocytometer (Neubauer improved). Non adherent cell lines were reseeded every 48hrs, by splitting 1:3 with supplemented medium.

If needed, cells were cryopreserved. Cell pellets were resuspended in 1 ml of fetal bovine serum with 10 % DMSO as a cryoprotectant. Cell suspensions were then transferred into 2 ml cryovials (Nalgene, USA). Vials were stored at -80 ^oC overnight, then removed into a liquid nitrogen storage vessel for long-term storage.

2.5.3 Cellular Uptake

2.5.3.1 Uptake into Cytosol of Cell

In order to assess the uptake and stability of metal complexes in the cytosol of the cell, cells were incubated with metal complex followed by splitting of the cells into cell membrane and cytosol extracts. A UV spectrum of the cytosol extract should show the distinctive MLCT peaks of the metal complex, if the complex has been able to enter the cell and maintain its structure throughout the experiment.

2.5.3.2 Cellular Uptake Assay Procedure

MDA-MB-231 cells were seeded at near confluence in T_{75} flat bottom culture flasks (nunc) and left for 24 hrs to adhere (37 ºC, 5 % CO_2). Medium was then removed and cells washed with 10 ml warm PBS. 9 ml metal complex (100 μM) or control (supplemented medium) was then added to the cells and incubated for a further 24 hrs (37 ºC, 5 % CO_2). Cells were then trypsinised (1 % trypsin EDTA protocol, section 2.5.2) and the resulting cell pellet washed with 1 ml cold PBS. 1 ml cold RIPA buffer (Sigma) was then added to the cell pellet and cells vortexed to resuspend, followed by incubation on ice for 10 minutes. Cells were then centrifuged, with resulting pellet being membrane extracts and the supernatant being the cytosol of the cell. A UV-Visible spectrum was recorded of the supernatant (in PBS).

2.5.4 Competitive Fluorescence Binding Studies

2.5.4.1 Principles of the Hoechst Displacement Assay

This assay is used to probe the DNA binding ability of small molecules in live cells, using the minor groove binding fluorescent DNA stain, Hoechst 33258, Figure 2. 11.

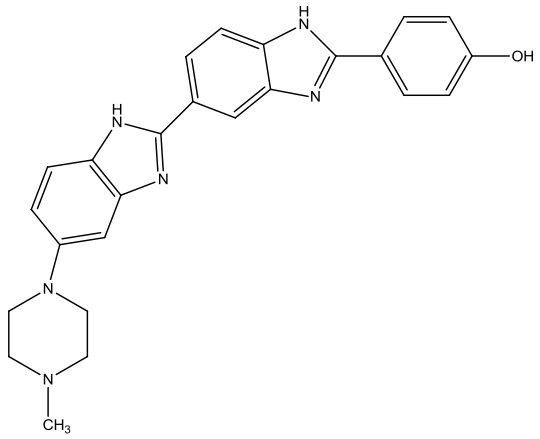

Figure 2. 11 The structure of Hoechst 33258.

This molecule stains both naked and cellular DNA and when excited at 350 nm has a distinct emission peak at 450 nm, Figure 2. 12.

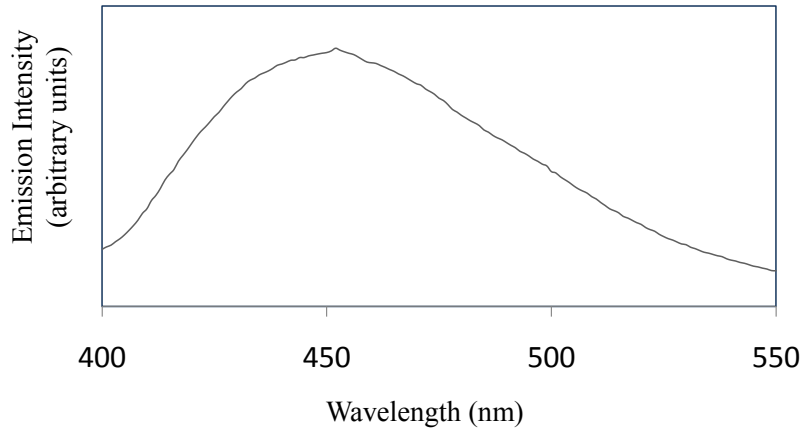

Figure 2. 12 DNA-bound Hoechst 33258 emission at 450 nm after excitation at 350 nm.

To probe cellular DNA binding of metal complexes, cells are incubated with Hoechst, followed with increasing concentrations of metal complex. If the complex binds to nuclear DNA, the Hoechst molecule may be displaced from the minor groove of the DNA and thus emission at 450 nm will decrease. The rate and extent to which the emission at 450 nm decreases with increasing compound concentration can allow the degree of DNA binding to be probed. Although the Hoechst molecule resides in the minor groove of the DNA, perturbations caused by another molecule binding to other areas of DNA can be sufficient to eject the Hoechst. Therefore this test is not only an indication of minor groove binding, but indicates more general DNA binding interactions.

2.5.4.2 Hoechst Displacement Assay Procedure

The procedure used is described by Matsuba et al.[20] HL-60 cells were preincubated with 10 μM Hoechst 33258 in 0.5 ml RPMI cell culture medium at 37 °C for 20 minutes. Metal complexes (concentrations ranging between 0 and 100 μM) were dissolved in 10 μM

Hoechst solution and added to the cell solution, followed by a further 20 minute incubation at 37 °C. Cells were then concentrated by centrifugation, washed once with chilled PBS, resuspended in chilled PBS and fluorescence measured.

Fluorescence spectra were recorded in a PTI fluorescence system with illumination from a PTI L-201M source using a 75 W xenon arc lamp. The detection system was a Shimadzu R298 PMT in a PTI model 814 analog/photon-counting photomultiplier (λ exc = 350 nm, λ emm = 400–550 nm).

2.5.5 Cell Line Testing Using the MTT Cell Viability Assay

2.5.5.1 Principles of the MTT Assay

The MTT (3-(4,5-dimethylthiazol-2-yl)-2,5-diphenyl-2H-tetrazolium bromide) colorimetric assay is used to determine the mitochondrial reductive function of cells and hence is a good indicator of cell death or inhibition of growth.[21] MTT is a water soluble dye that is able to cross cell surface membranes and is reduced to a blue, water insoluble formazan product, Figure 2. 13, by the mitochondrial enzyme succinate dehydrogenase. The formazan product, when dissolved in DMSO, has a distinct absorbance maximum at 590 nm. Absorbance at this wavelength is directly proportional to the number of viable cells within the population.[22]

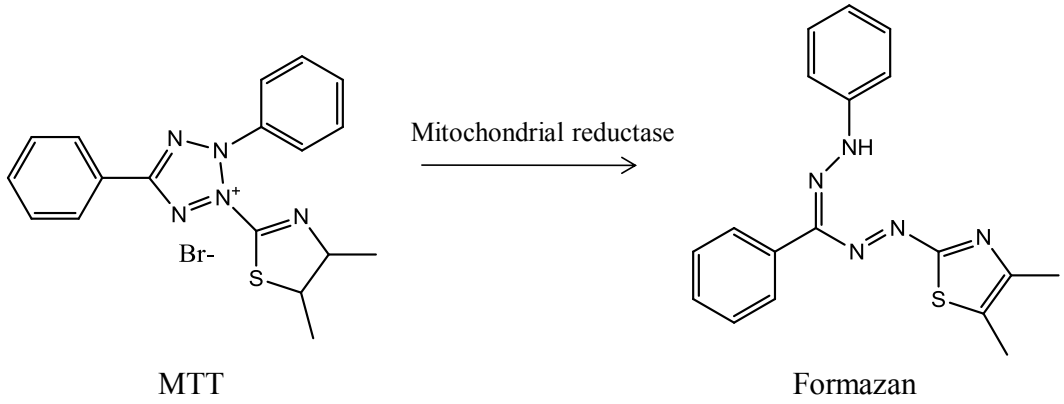

Figure 2. 13 The reduction of MTT to a formazan product in the MTT assay

After incubation of cells with a range of concentrations of metal compound the MTT assay can be used to obtain an IC_{50} value. This is the concentration of compound where 50 % of cells in a population are viable.

2.5.5.2 Cell Line Testing Procedure

Cells from confluent monolayers were removed from flasks using a 1% trypsin-EDTA protocol (see section 2.5.2). Cell viability before drug treatment was established using the trypan blue dye exclusion test, with a Neubauer hemocytometer (Hawksley Medical and Laboratory Equipment). The trypan blue exclusion assay provides a measure of membrane integrity, based on the principle that the dye is excluded from cells with an intact cytoplasmic membrane, whereas cells with damaged membranes cannot exclude the dye and are stained blue.[23] Due to differing growth rates, varying cell densities were seeded for each cell line in 100 μl of complete medium in 96-multiwell flatbottom microtiter plates (Corning Costar); A2780-P, A2780-R = 4000 cells/well; MDAMB-231 = 10000 cells/well; T47D = 25000 cells/well. Plates were incubated at 37 °C, 5% CO_2 for 24 hrs to allow cell adhesion prior to metal compound testing. Stock solutions of metal complex were freshly

prepared in complete medium with a range of concentrations between 3 and 200 μM. Each concentration was tested in quadruplicate with 100 μl of complete medium as control and plates were incubated for 72 hrs.

2.5.5.3 MTT Assay Procedure

Following incubation of cells with metal complex, 50 μl MTT solution (5mg/ml in PBS, Sigma Chemical Co, UK) was added to each well and incubated for a further two hrs. Medium was subsequently removed from wells and any resulting formazan crystals solubilised in 100 μl DMSO per well. Culture plates were rocked gently for 30 minutes before optical density was measured using a microplate reader (Bio Rad) at 590 nm against a DMSO blank (100 μl). Sample readings were blank adjusted and converted into percentage versus untreated controls.

2.5.6 Increased Molar Incubation Assay

This test was designed to probe the response of MDA-MB-231 breast cancer cells to an increased molar incubation of metal complex. The volume added was kept constant and the concentration of metal complexes was varied. 10000 cells/well were seeded in 100 μl complete medium in 96 well, flat-bottomed, microtitre plates (Corning Costar) and incubated for 24 hrs (37 ºC, 5 % CO_2) to adhere. Following this incubation, medium was removed and cells were washed with 50 μl warm PBS which was then also removed. Cells were then treated with 75 μl metal complex (in medium) of concentrations between 3.125 and 100 μM, in quadruplicate. Remaining wells were incubated with 75 μl medium as a control. This method was repeated with volumes of 100, 150 and 200 μl. Plates were

incubated for 72 hrs before cell viability was assessed via the MTT assay (see section 2.5.5.3).

2.5.7 Extended Incubation Assay

This test was intended to follow the response of MDA-MB-231 cells to metal complexes over extended time periods. 10000 cells/well were seeded in 100 µl complete medium per well of 96 well, flat-bottomed, microtitre plates (Corning Costar) and incubated for 24 hrs at 37 °C, 5 % CO_2 to adhere. Cells were then treated with 100 µl metal compound concentrations between 6.5 and 200 µM, followed by further incubation of 1-6 days. At the end of each incubation period cell viability was established using the MTT assay (see section 2.5.5.3).

2.5.8 Cellular Recovery Assay

This test was carried out in order to assess the ability of MDA-MB-231 cells to recover from incubation with metal complexes. 10000 cells/well were incubated in 100 µl medium in 96-multiwell flatbottom microtiter plates (Corning Costar) for 24 hrs to adhere (37 °C, 5 % CO_2). Cells were then treated with 100 µl of 100 µM metal complex in quadruplicate and incubated for 3 or 18 hrs. Following these incubation periods medium was removed, cells were washed with 50 µl warm PBS which was then removed and replaced with 200 µl fresh medium. Cells were then incubated for a further 1-6 days and at the end of each incubation period cell viability was established using the MTT assay (section 2.5.5.3).

2.5.9 Time Lapse Phase Contrast Microscopy

2.5.9.1 Principles of Time Lapse Microscopy

Microscopy techniques used in conjunction with a time lapse video camera are a powerful tool which can be used to record details of cells over periods of time. This allows the investigation of cellular events such as mitosis, necrosis or apoptosis during drug treatment.[24] Phenotype and morphology of cells can also be monitored. The microscope and camera are housed inside a purpose built incubator so that the cells can be filmed in the correct environment for the experiment.

2.5.9.2 Time Lapse Microscopy Experimental Procedure

$5x10^4$ cells/well were seeded in 0.5 ml complete medium per well of 24 well flatbottom plates (Corning Costar). Plates were incubated for 24 hrs (37 ºC, 5 % CO_2) for cells to adhere. Cells were then treated with metal complex concentrations of 50, 100, and 200 µM and medium as a control. Plates were incubated at 37 ºC, 5 % CO_2 in a purpose built incubator attached to a time lapse microscope (Nikon 2000, 20x, phase contrast). Images were recorded every 2 minutes for 18 hrs.

2.5.10 Fluorescent Rhodamine Phalloidin Staining of Actin Cytoskeleton

2.5.10.1 Principles of the Phalloidin Fluorescence Assay

Phalloidins are small, naturally occurring molecules that bind to the actin in cells and alter its polymerization. They are widely used to study the role of actin in biological processes.[25] In this assay, phalloidin, Figure 2. 14, a high-affinity probe which binds to actin at the junction between subunits, specific to F-actin is conjugated to the orange-fluorescent dye tetramethylrhodamine B isothiocyanate (TRITC). The fluorescence of rhodamine

phalloidin can therefore be measured showing the distribution of F-actin in permeabilised cells. F-actin is a protein which makes up part of the cellular cytoskeleton and is responsible for cellular motility, along with other biological components of the cell. The distribution of F-actin after incubation with a drug molecule can give information about disruptions to the cellular cytoskeleton caused by the drug.

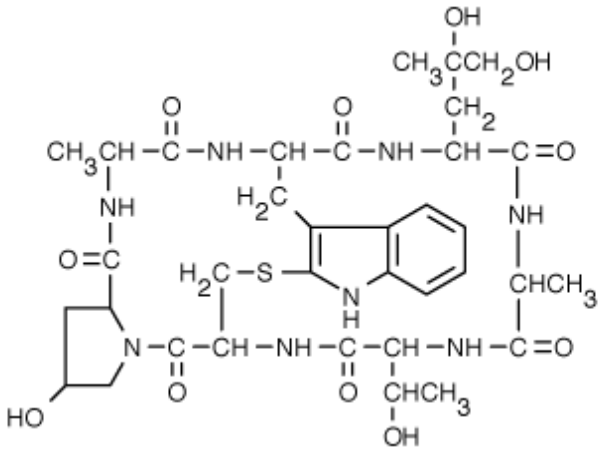

Figure 2. 14 The structure of phalloidin.

2.5.10.2 Phalloidin Fluorescence Assay Procedure

$5x10^4$ cells/well were seeded in 0.5 ml supplemented medium per well of 24 well flatbottom culture plates (Corning Costar) on top of sterile microscope coverslips. Plates were incubated for 24 hrs (37 ºC, 5 % CO_2) for cells to adhere to coverslips. Wells were then treated with metal complex concentrations of 50, 100 and 200 µM and medium as a control. Plates were incubated for a further four hrs at 37 ºC, 5 % CO_2. Following incubation media was removed from wells and cells were fixed with 500 µl 4 % paraformaldehyde, added on top of the microscope slides and incubated for 10 minutes at room temperature. Wells were then washed with 500 µl PBS x 3 (room temperature). This was followed by removal of microscope slides from wells, which were then placed cell

side down onto 100 µl drops of NH_4Cl (50 mM). These were left for 10 minutes at room temperature to neutralise the paraformaldehyde. Slides were then washed 3 x in PBS and placed (cell side down) onto 100 µl 0.1 % Triton-X in PBS. These were incubated for 4 minutes at room temperature to permeabilise cell membranes. Following this incubation slides were placed onto 100 µl drops of fluorescent rhodamine phalloidin (TRITC Phalloidin, Sigma, 4 µl 75 µM in 800 µl PBS) for 20 minutes at room temperature. Slides were then washed 3 x with PBS and 3 x with water, before being placed cell side down on microscope slides, onto 5 µl mowiol (6 ml glycerol, 2.4 g mowiol (Calbiochem), 6 ml water, 12 ml Tris-Cl pH 7.5-8.5). Slides were kept at 37 ºC for an hour before fluorescence images were recorded on a Zeiss Axiovert 135TV microscope with 63x (1.25 NA Plan NEOFLUAR Ph3) objective lens. A TRITC filter set and a mercury lamp were used for fluorescent illumination. Images were captured using a QImaging QIcam 1394 driven by Qcapture pro software.

2.5.11 Alkaline Comet Assay

2.5.11.1 Principles of the Comet Assay

The single cell gel electrophoresis or "comet" assay, originally described in 1984 by Ostling and Johanson[26] is used to assess the genotoxic potential of compounds through their ability to induce strand breaks in the DNA of eukaryotic cells. A number of modifications have been made to this assay to assess different forms of DNA damage.[27] The method used herein is the alkaline comet assay, used to assess single strand breaks in DNA.[28] After incubation of cells with metal compound, cells are embedded in agarose, lysed, electrophoresed and stained in order to image the DNA by fluorescence. During electrophoresis, intact DNA remains tightly wound in the nucleoid, or comet head. Loops

of DNA around any strand breaks migrate out towards the positively charged anode, resulting in the formation of a comet tail. The more strand breaks, the further the movement and the more intense the DNA tail. Hence, the extent of DNA damage is measured by the 'tail length' of the DNA, Figure 2. 15.

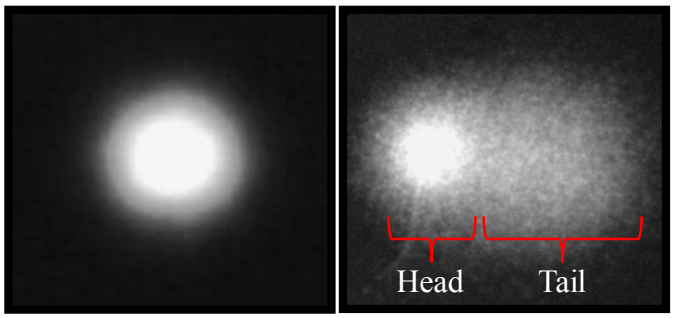

Figure 2. 15 Fluorescence microscope images of cells without (left) and with (right) DNA damage after electrophoresis.[29]

2.5.11.2 Comet Assay Procedure

The method used is based on that of Singh et al.,[28] modified by Lee et al.[30] A2780 human ovarian cancer cells were seeded at a density of 1.25 x 10^6 cells/well in 6 well flatbottom culture plates and allowed to adhere for 24 hrs (37 ºC, 5 % CO_2). Cells were then treated with three concentrations of metal compound, the top concentration being just above the calculated IC_{50} value for this cell line. Following incubation at 37 ºC for 24 hrs, cells were washed with cold PBS and gently scraped into fresh PBS (1 ml). Cells were then centrifuged (8000 x g, 5 minutes) and the resulting pellet resuspended in PBS (100 µl). An aliquot of resuspended cells (5 µl) was then placed into a sterile tube with low melting point agarose (300 µl), prewarmed to 300 ºC. This was then transferred to a glass microscope slide (150 µl per slide, VWR International) which had been pre-coated with 0.5 % normal melting point agarose. Cell solution on slides were then covered with glass coverslips (VWR International) and slides placed on a metal tray over ice for 10 minutes to

allow the agarose to solidify. Coverslips were then removed and slides incubated for 1 hr at 4 °C in cold lysis buffer (2.5 M NaCl, 0.1 M Na_2EDTA, 10 mM Tris base, 1 % sodium N - lauryl sarcosinate, 10 % DMSO and 1 % Triton X-100). Following lysis slides were placed in a horizontal electrophoresis tank containing cold electrophoresis buffer (300 mM NaOH, 1 mM Na_2EDTA) and DNA allowed to unwind without electrophoresis for 20 minutes. Slides were then subjected to electrophoresis (25 V, 0.8 Vcm^{-1}, 20 minutes) followed by washing (3 x 5 minutes) with cold neutralisation buffer (0.4 M Tris base, pH 7.5). Slides were subsequently stained by adding 50 µl Sybr gold solution (1 x solution, Invitrogen) and covered with cover slips. Slides were left in the dark at 4 ºC prior to examination. Slides were examined at 320 x magnification using a fluorescence microscope (Zeiss Axiovert 10, Germany) fitted with a 515 - 560 nm excitation filter and a barrier filter of 590 nm. A USB digital camera (Merlin, Allied Vision Technologies) received the images, which were analysed using a personal computer-based image analysis system, Comet assay IV (Perceptive instruments). Images of one hundred randomly selected nuclei were analysed per slide.

Measurement of mean percent tail intensity was chosen to assess the extent of DNA damage as this has been shown to suffer much less from inter-run variation than other comet parameters, due to its independence of electrophoresis voltage and run time.[31] Median values of three separate experiments were analysed using an ANOVA and post hoc Student's t test.[32]

2.6 Ames Bacterial Mutagenicity Assay

2.6.1 Principles of the Ames Test

The Ames bacterial reverse mutation assay is a test recognised as an initial screening process to establish the mutagenic potential of new drugs. It has been established that compounds which do not exhibit activity in the Ames test are normally found to be non-carcinogenic.[33] This short term bacterial reverse mutation assay uses specially constructed tester strains of *Salmonella typhimurium* which are unable to grow due to the absence of the amino acid histidine. This is caused by a mutation in one of the genes responsible for its biosynthesis. A mutagen incubated with these bacteria will result in many new mutations, a small proportion of which can reverse the original mutation, allowing the synthesis of histidine and the proliferation of the bacteria as discrete colonies. Potential mutagens are able to enter these strains easily as the lipopolysaccharide barrier that normally coats the surface of *Salmonella* is incomplete. Two strains were used in order to ensure a thorough investigation of mutagenic potential. Base pair or point mutations (TA100 strain) affect only a single base whereas frameshift mutations (TA98 strain) involve the insertion or deletion of a number of nucleotides.

This test can also be used to probe potential *in vivo* mutagenicity using activated rat liver S9 enzymes, a variety of mixed function oxidase enzymes.[34] Some carcinogenic compounds are biologically inactive unless metabolised into their active forms. In humans this can be carried out by cytochrome-based metabolic activation, usually in the liver. As bacterial enzymes do not have this function a mammalian exogenous source is needed. Positive controls (known mutagens and promutagens) are also incubated with the bacteria, with and without S9 in order to check the bacteria and the S9 mix. A small amount of

histidine is added to allow the bacteria to grow for a short time. After this histidine is exhausted only bacteria that have undergone a reverse mutation in their histidine production gene are able to continue to grow. Some bacteria revert spontaneously, so results are compared to a negative control. For a compound to be considered a mutagen there must be a dose-dependent increase in the number of revertant colonies, as verified by at least two independent experiments. A minimum cut-off increase between a mutagenic and non-mutagenic response is usually a 2-3 fold increase in revertants relative to negative controls.[35]

2.6.2 Ames Test Procedure

All experimental methods were carried out in sterile conditions and only one strain of *Salmonella* was used on any one day to avoid cross contamination. All reagents and equipment were sterilised before use.

16 hrs prior to the experiment master cultures of *Salmonella typhimurium* were prepared according to the method of Marron and Ames.[36] 10 ml of nutrient broth was inoculated with a loopful (10 µl) of bacteria. Light was excluded and the bacteria incubated on a rotary shaker at 37 ºC. The culture was kept on ice during the experiment. Minimal agar plates (11.5 g Agar, 700 ml water, 15 ml Vogel-Bonner salts ($MgSO_4.7H_2O$, citric acid monohydrate, K_2HPO_4, $NaNH_4PO_4.4H_2O$), 38 ml 40% glucose) were made prior to use. The bacteria were checked with positive controls of 4-nitroquinoline-N-oxide for TA98 and sodium azide for TA100 both before and during the experiment. On the day of the experiment top agar (0.6 g agar bacteriological, 0.5 g NaCl in 100 ml water) was enriched with 0.05 mM histidine and biotin (1ml per 9ml agar) and kept at 42 ºC for use. Rat liver

S9 enzymes (20 µl S9 per plate, 8 mM $MgCl_2$, 33 mM KCl, 5 mM glucose-6-phosphate, 4 mM NADP, 100 mM sodium phosphate, pH 7.4), (Tebu-Bio) were freshly prepared and kept on ice. Dilutions of metal compounds and controls (concentrations of active compounds between 0.1 and 100 µM, inactive compounds between 0.4 and 250 µM) were prepared on the day of the experiment in a sterile environment using a minimum of DMSO for water insoluble compounds and PBS for water soluble compounds. Negative controls were also prepared with DMSO and PBS to check for contamination. Compounds and controls (prepared both with and without S9) were incubated with bacteria for 20 minutes at 37 ºC then removed to an ice bath to stop bacterial growth until plated onto a minimal agar plate with molten top agar. These were incubated in the dark for 48 hrs at 37 ºC. After 24 hrs background bacterial lawn was checked and after 48 hrs resulting colonies were counted. Values reported are higher in the TA100 strain due to the naturally higher reversion frequency of this strain.[35]

2.7 References

[1] M. J. Hannon, C. L. Painting, A. Jackson, J. Hamblin and W. Errington, *Chem. Commun.*, 1997, 1807-1808.

[2] J. M. C. A. Kerckhoffs, J. C. Peberdy, I. Meistermann, L. J. Childs, C. J. Isaac, C. R. Pearmund, V. Reudegger, S. Khalid, N. W. Alcock, M. J. Hannon and A. Rodger, *Dalton Trans.*, 2007, 734-742.

[3] A. C. G. Hotze, B. M. Kariuki, and M. J. Hannon, *Angew. Chem. Int. Ed*., 2006, **45**, 4839-4842.

[4] *Drug-like Properties: Concepts, Structure Design and Methods: From ADME to Toxicity Optimization*, ed. E. Kerns and L. Di, University Press, 2008.

[5] I. P.Evans, A. Spencer and *G.* Wilkinson, *J. Chem. Soc., Dalton Trans.,* 1973, 204-209.

[6] A. Hotze, A. J. Pope and M. J. Hannon, unpublished data.

[7] I. Meistermann, PhD Thesis, University of Warwick, 2001.

[8] *Circular and Linear Dichroism*, ed. A. Rodger and B. Nordén, Oxford University Press, 1997.

[9] Source: University of Vienna, Austria: http://homepage.univie.ac.at/johannes.winkler/cd.html.

[10] M. Pascu, PhD Thesis, University of Birmigham, 2008.

[11] J. B. Lepecq and C. Paoletti, *J. Mol. Biol.*, 1967, **27**, 87-106.

[12] A. R. Morgan, J. S. Lee, D. E. Pulleyblank, N. L. Murray and D. H. Evans, *Nucleic Acid. Res.*, 1979, **7**, 547-569.

[13] *Physical Chemistry and its Biological Applications,* ed. W. S. Brey, Academic Press Inc., 1978.

[14] V. Pavlov, P. Kong, T. Lin and V. Rodilla, *Chemico-Biological Interactions*, 2001, **137**, 15-24.

[15] V. Fernandez-Moreira, F. L. Thorp-Greenwood and M. P. Coogan, *Chem. Commun*., 2010, **46**, 186-202.

[16] M. J. Clarke, *Coord. Chem. Rev.*, 2002, **232**, 69-93.

[17] J. Malina, M. J. Hannon and V. Brabec, *Chem. A Eur. J.,* 2007, **13**, 3871-3877.

[18] N. B. Leontis, W. Kwok and J. S. Newman, *Nucleic Acid. Res.,* 1991, **19**, 759-766.

[19] J. Kasparkova, O. Novakova, O. Vrana, N. Farrell and V. Brabec, *Biochemistry*, 1999, **38**, 10997-11005.

[20] Y. Matsuba, E. Edatsugi, I. Mita, A. Matsunaga and O. Nakanishi, *Cancer Chemother. Pharmacol*., 2000, **46**, 1-9.

[21] T. Mosmann, *J. Immunol. Methods*, 1983, **65**, 55-63.

[22] R. F. Hussain, A. M. E**.** Nouri and R. T. D. Oliver, *J. lmmunol. Methods,* 1993, **160**, 89-96.

[23] E. V. Komissarova, S. K. Saha and T. G. Rossman, *Tox. Appl. Pharm.,* 2005, **202**, 99-107.

[24] M. Sundaram, D. L. Guernsey, M. M. Rajarman and R. Rajaraman, C*ancer Biology and Therapy*, 2004, **3**, 207-218.

[25] J. A. Cooper, *J. Cell Biol.*, 1987, **105**, 1473-1478.

[26] O. Ostling and K. J. Johannson, *Biochem. Biophys. Res. Commun.,* 1984, **123**, 291-298.

[27] Peter Møller, *Basic & Clinical Pharmacology & Toxicology,* 2006, **98**, 336-345.

[28] N. P. Singh, M. T. McCoy, R. R. Tice and E. L. Schneider, *Exp. Cell Res.*, 1988, **175**, 184-191.

[29] S. Banwait, PhD Thesis, University of Birmingham, 2010.

[30] A. J. Lee, N. J. Hodges and J. K. Chipman, *Cancer Epidemiol. Biomarkers*, 2005, **14**, 497-505.

[31] P. L. Olive and R. E. Durand, *Cytometry Part A,* 2005, **66**, 1-8.

[32] P. Duez, G. Dehon, A. Kumps and J. Dubois, *Mutagenesis*, 2003, **18**, 159-166.

[33] *Biochemistry*, ed. J. M. Berg, J. L. Tymoczko and L. Stryer, Fifth Edition, W. H. Freeman & Company, 2002.

[34] B. M. Elliott, R. D. Combes, C. R. Elcombe, D. G. Gatehouse, G. G. Gibson, J. M. Mackay and R. C. Wolf, *Mutagenesis,* 1992, **7**, 175-177.

[35] K. Mortelmas and E. Zeiger, *Mutat. Res.,* 2000, **455**, 29-60.

[36] D. M. Maron and B. N. Ames, *Mutat. Res.*, 1983, **113**, 173-215.

Chapter 3

DNA Three-Way Junction Binding and *In Vitro* Studies of Triple Stranded Supramolecular Cylinders

Original synthesis and characterisation of $[Fe_2L_3]^{4+}$ was carried out by Dr. C. Painting, University of Warwick.

Original synthesis and characterisation of $[Fe_2L^1{}_3]^{4+}$ was carried out by Dr. L. Childs, University of Warwick.

L, L^1, $[Fe_2L_3]^{4+}$ and $[Fe_2L^1{}_3]^{4+}$ were remade for all biological testing discussed in this chapter.

Synthesis and characterisation of $[Ru_2L_3]^{4+}$ was carried out by A. Leczkowska, University of Birmingham.

Synthesis and characterisation of $[Fe_2L^p{}_3]^{4+}$ was carried out by Dr. L. Cardo, University of Birmingham.

3.1 Introduction

This chapter describes how the binding of helical complexes to DNA three-way junctions correlates with their *in vitro* anticancer activities. Complexes used were:

$[Fe_2L_3]^{4+}$ where L = $C_{25}H_{20}N_4$, Figure 3. 1;

$[Fe_2L^1{}_3]^{4+}$ where L^1 = $C_{27}H_{24}N_4$, Figure 3. 2;

$[Ru_2L_3]^{4+}$ where L = $C_{25}H_{20}N_4$, Figure 3. 3;

$[Fe_2L^p{}_3]^{4+}$, ligand shown in Figure 3. 4.

Polyacrylamide gel electrophoresis studies were carried out in order to compare the ability of these complexes to bind to and stabilise a specific DNA three-way junction structure. Cellular uptake, stability and activity against cancer cell lines of these complexes will also be discussed in order to elucidate parameters required for successful DNA binding and anticancer activity.

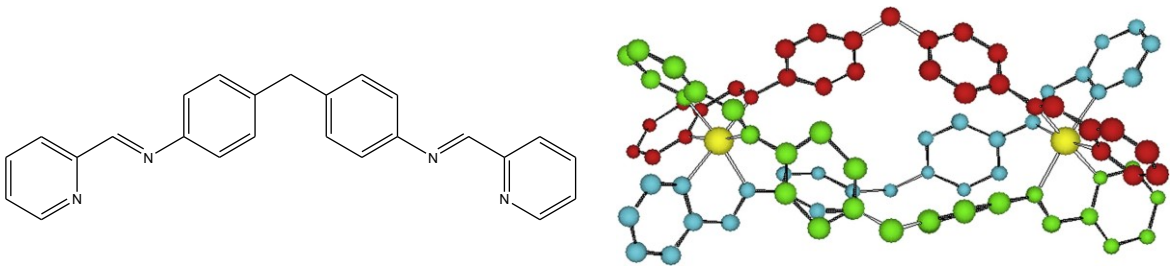

Figure 3. 1 Ligand L and X-ray crystal structure of the $[Fe_2L_3]^{4+}$ cation discussed in this chapter. Hydrogen atoms and anions have been omitted for clarity.[1]

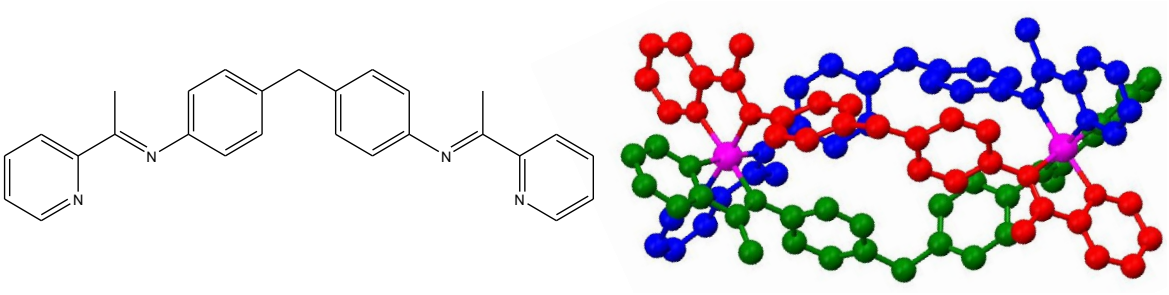

Figure 3. 2 Ligand L^1 and X-ray crystal structure of the $[Fe_2L^1{}_3]^{4+}$ cation. Hydrogen atoms and anions are omitted for clarity.[2]

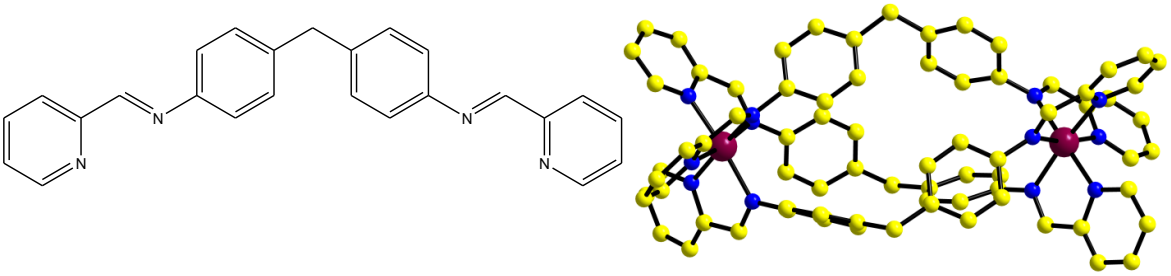

Figure 3. 3 Ligand L and X-ray crystal structure of the $[Ru_2L_3]^{4+}$ cation. Hydrogen atoms and anions have been omitted for clarity.[3]

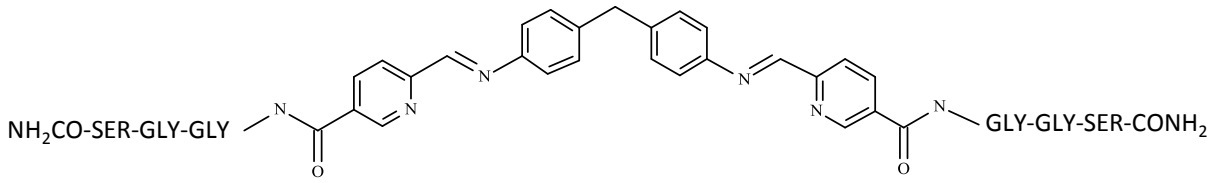

Figure 3. 4 The peptide conjugated ligand used in the synthesis of the triple stranded complex, $[Fe_2L^p{}_3]^{4+}$.[4]

3.1.1 Helical Complexes and their DNA Binding

Binding of all the helicates discussed in this chapter to double stranded DNA have been investigated previously. $[Fe_2L_3]^{4+}$ was found, through CD, LD and AFM studies to bind via a non-covalent binding mode to double stranded DNA, spanning around five base pairs and causing extensive coiling of calf thymus DNA.[5] A simulation of this binding using

computational methods can be seen in Figure 3. 5, revealing a bend of 45 ± 15 º per $[Fe_2L_3]^{4+}$.[6]

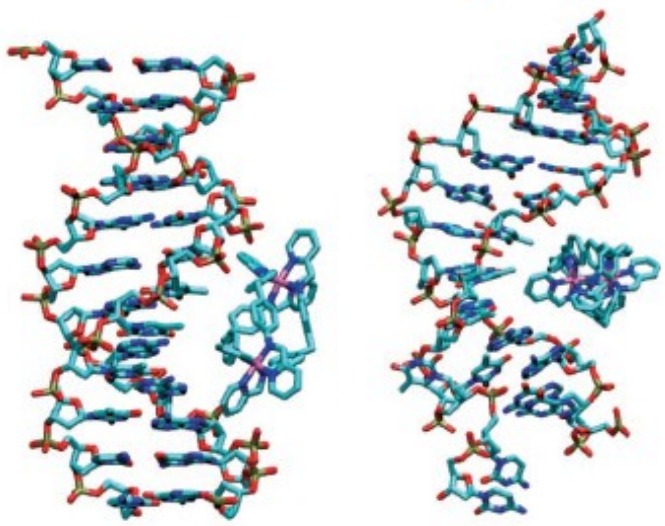

Figure 3. 5 Conformations of DNA in the presence of $[Fe_2L_3]^{4+}$ taken from the start (left) and after 2 ns (right) of MD simulations using the CHARMM22 force field.[6]

Circular dichroism studies of $[Fe_2L^1{}_3]^{4+}$ with ct-DNA show interactions indicating some binding, and retention of B-DNA conformation, with a possible binding preference for AT-DNA.[7] Linear dichroism studies show signals indicating a bending or coiling effect on double stranded DNA (though a much weaker effect than for $[Fe_2L_3]^{4+}$). Computational analysis has found $[Fe_2L^1{}_3]^{4+}$ to bind in the major groove of DNA, however, in a mode where the complex is not completely contained and instead reorients so that only one end resides within the groove.[8]

DNA binding studies of $[Ru_2L_3]^{4+}$ revealed a binding mode very similar to that of the parent $[Fe_2L_3]^{4+}$ complex, however the loss of linear dichroism signal upon DNA binding was slightly less pronounced for $[Ru_2L_3]^{4+}$ indicating slightly less of a bending/coiling effect.[9]

The peptide conjugated $[Fe_2L^p_3]^{4+}$ complex displayed the weakest DNA interactions of all the cylinders discussed in this thesis, showing no induced CD signals and only weak LD interactions.[10]

3.1.2 $[Fe_2L_3]^{4+}$ Three-Way Junction Binding

DNA junction structures are incredibly important and abundant in nature, being present whenever DNA is processed or replicates. An example of a matched three-way junction structure is shown in Figure 3. 6.

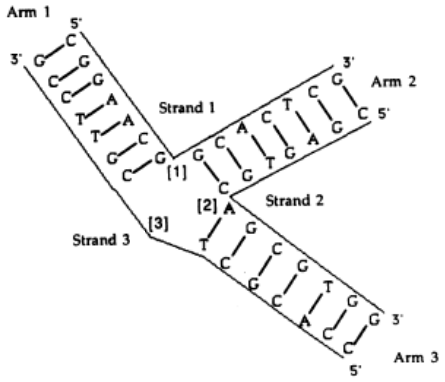

Figure 3. 6 Example of a fully matched three-way junction structure.[11]

An exciting property of the parent $[Fe_2L_3]^{4+}$ cylinder is its ability to bind in the heart of and stabilise a DNA three-way junction structure, Figure 3. 7. This binding is unique and represented the first new form of DNA recognition discovered for 40 years.[12]

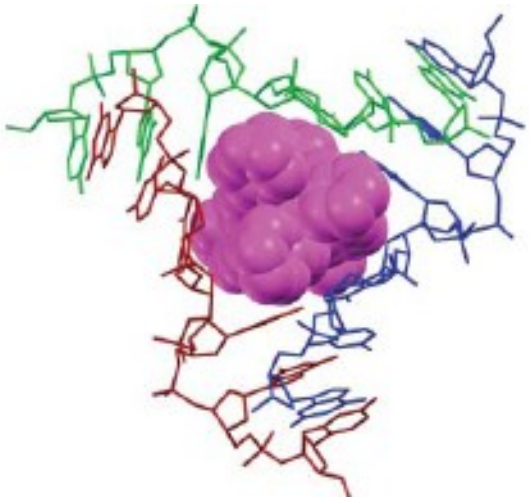

Figure 3. 7 Crystal structure of $[Fe_2L_3]^{4+}$ residing within a DNA three-way junction. $[Fe_2L_3]^{4+}$ is represented as space filling, DNA as wire frame. Hydrogen atoms and anions have been omitted for clarity. [13]

3.2 Results and Discussion

3.2.1 Three-Way Junction Binding of $[Fe_2L_3]^{4+}$ and $[Fe_2L^1{}_3]^{4+}$

It is proposed that the binding and stabilisation of the three-way junction structure caused by $[Fe_2L_3]^{4+}$ may be the foundation of its *in vitro* activity, as the formation of a three-way DNA junction structure is a major step in the DNA replication process.[14] In order to investigate this, three-way junction binding of the bulkier $[Fe_2L^1{}_3]^{4+}$ cylinder was investigated (see section 2.4.7). It was anticipated that the larger dimensions[8] of this complex due to the extra methyl groups on each ligand, will mean binding in the heart of the three-way junction is prevented due to steric hindrance between the methyl moieties and three-way junction aryl rings, Figure 3. 8.

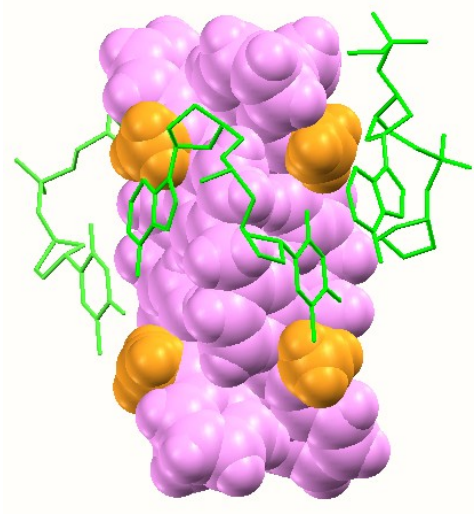

Figure 3. 8 Representation of $[Fe_2L^1{}_3]^{4+}$ (methyl groups yellow) inside a DNA three-way junction (green) showing potential hindrance between methyl groups and DNA aryl rings.

Polyacrylamide gel electrophoresis was carried out to mimic previous experiments with $[Fe_2L_3]^{4+}$. Three strands of non-palindromic DNA oligonucleotides 14 bases long were used. DNA sequences were designed in order to form a fully matched, non bulged three-way junction structure with arms 7 base-pairs in length, Figure 3. 9. Strand 1 was labelled at the 5' end with radioactive phosphorous-32 in order to visualise DNA structures on the gel. Gels were carried out at 25 ºC, as it has been shown that DNA three-way junction structures with seven base pairs per arm are not stable in a gel at 25 ºC, even in the presence of high concentrations of divalent cations.[15] Running the gel at 25 ºC therefore gives a good indication of the ability of the helicates to stabilise the three-way junction structure.

Strand 1 – 5'CGGAACGGCACTCG

Strand 2 – 5'CGAGTGCAGCGTGG

Strand 3 – 5'CCACGCTCGTTCCG

Figure 3. 9 Oligonucleotides used in gel electrophoresis studies and the three-way junction proposed to form[15]

Varying concentrations of $[Fe_2L_3]^{4+}$ and $[Fe_2L^1{}_3]^{4+}$ were incubated with the DNA oligonucleotides, with final [three-way junction (3 DNA strands): complex] ratios being 1:2, 1:1, 2:1 and 3:1. A current was applied to the gel in order to separate DNA structures formed during the incubation according to their size, charge and density. An example gel profile obtained through phosphorimaging, showing the presence of single strand, duplex and three-way junction DNA is shown in Figure 3. 10. AIDA image analyser software was used to quantify the percentage of three-way junction on the gel by profiling bands and integrating the area of peaks.

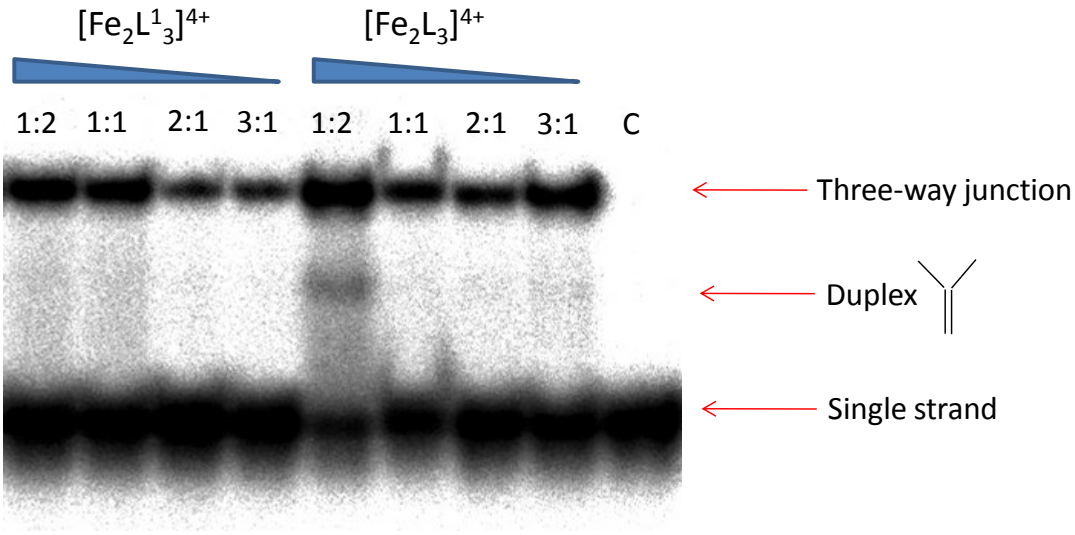

Figure 3. 10 Phosphorimaging gel profile showing three-way junction stabilisation of $[Fe_2L^1{}_3]^{4+}$ *and* $[Fe_2L_3]^{4+}$ *with control (three DNA strands and no complex).*

The percentage of three-way junction present (as a percentage of all DNA structures present in each lane on the gel) is shown in Figure 3. 11.

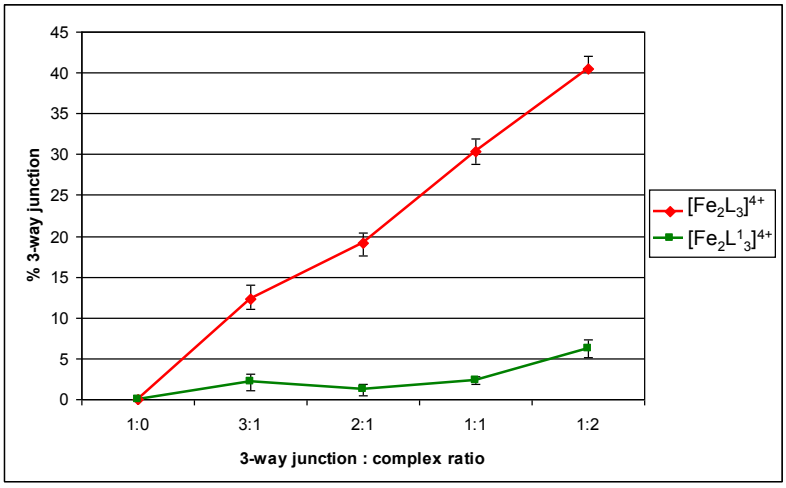

Figure 3. 11 Percentage three-way junction formed against [three-way junction: complex] ratios for $[Fe_2L_3]^{4+}$ *and* $[Fe_2L^1{}_3]^{4+}$*. Graph represents mean ± SEM from three independent experiments.*

Three-way junction stabilisation caused by $[Fe_2L^1{}_3]^{4+}$ is minimal. There is some indication of a dose response for this complex, and the percentage of three-way junction present

increases from ~ 2 % at a 3:1 three-way junction: complex ratio, to 6 % at a 1:2 three-way junction : complex ratio. It is possible that this minimal effect is due to the tetracationic charge of the complex, as polycations are known to stabilise higher order DNA structures.[16]

Stabilisation caused by $[Fe_2L_3]^{4+}$ is up to 40 %, at a 1:2 three-way junction : complex ratio, with an increase in stabilisation of the three-way junction structure with an increase in helicate concentration. This is in agreement with previous results for this complex.[15] These are very interesting results and clearly show that a very small change in dimensions in $[Fe_2L^1{}_3]^{4+}$ of 2Å[8] has a huge effect on the stabilisation of the three-way junction structure. In this case it is the exact size and shape of the parent $[Fe_2L_3]^{4+}$ which is so essential for binding and stabilisation.

It is also interesting to note the stabilisation of a DNA duplex in the gel. Bands can be seen for both $[Fe_2L_3]^{4+}$ and $[Fe_2L^1{}_3]^{4+}$, however the extent of duplex stabilisation is minimal and does not exceed 1.4 % of all DNA structures on the gel. This duplex DNA structure is not present in the control, so it may be an effect due to the tetracationic charge of the complexes causing an association of the DNA strands through the negatively charged DNA phosphate backbone. There may also be stabilisation of a Y-shaped fork of two DNA strands. At the branch point of a Y-shaped DNA junction there are four bases, rather than the 6 found at the three-way junction branch-point, nevertheless these 4 bases may form a binding site similar to that of the three-way junction.

3.2.2 Three-Way Junction Binding of $[Ru_2L_3]^{4+}$

$[Ru_2L_3]^{4+}$ has very similar dimensions to the parent $[Fe_2L_3]^{4+}$complex[3], Figure 3. 12, however it displays a number of other properties such as fluorescence upon DNA binding, DNA photocleavage and increased stability,[17] making it an attractive alternative to the parent iron complex. It is therefore important to investigate the extent of $[Ru_2L_3]^{4+}$ three-way junction binding. This will also show whether it is simply dimensions of the complex which must be correct for three-way junction binding, or if other factors, such as metal ion may play a role.

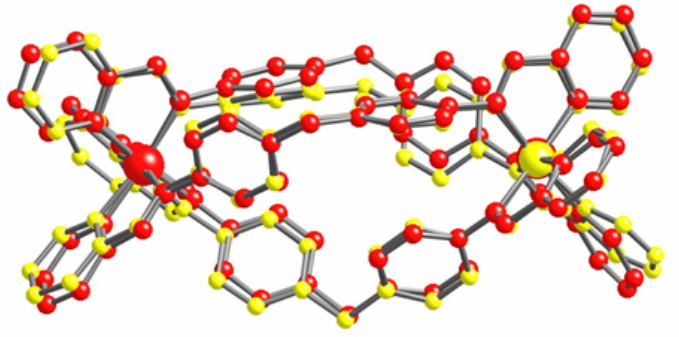

Figure 3. 12 Comparison of X-ray crystal structures of $[Ru_2L_3]^{4+}$ (yellow) and $[Fe_2L_3]^{4+}$ (red) showing analogous dimensions. Hydrogen atoms and anions have been omitted for clarity.[3]

Varying concentrations of $[Ru_2L_3]^{4+}$ were incubated with the DNA oligonucleotides before being subjected to gel electrophoresis. An example gel profile is shown in Figure 3. 13 with the relevant data for $[Fe_2L_3]^{4+}$ (previous gel, Figure 3. 10) shown as a comparison.

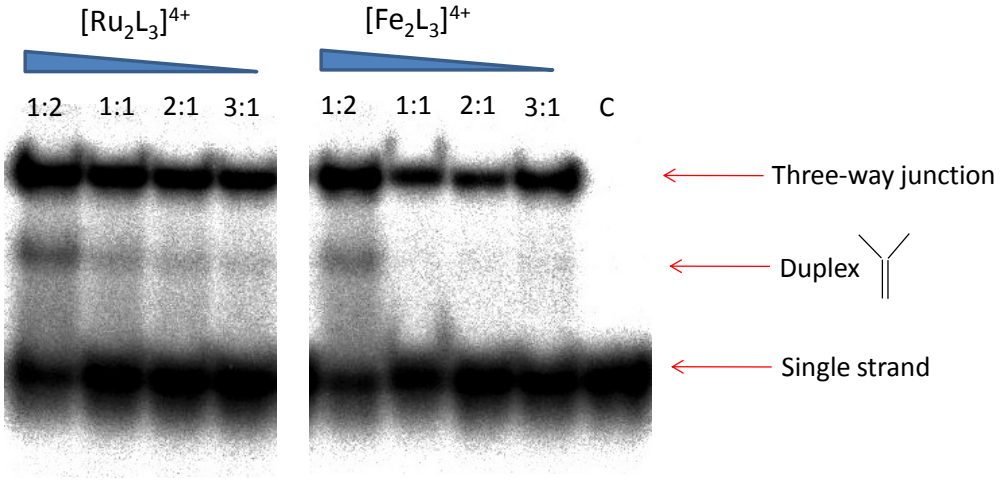

Figure 3. 13 Phosphorimaging gel profile showing three-way junction stabilisation of $[Ru_2L_3]^{4+}$ and $[Fe_2L_3]^{4+}$ with control (three DNA strands and no complex).

The amount of three-way junction present (as a percentage of all DNA structures present in each the lane on the gel) is presented in Figure 3. 14.

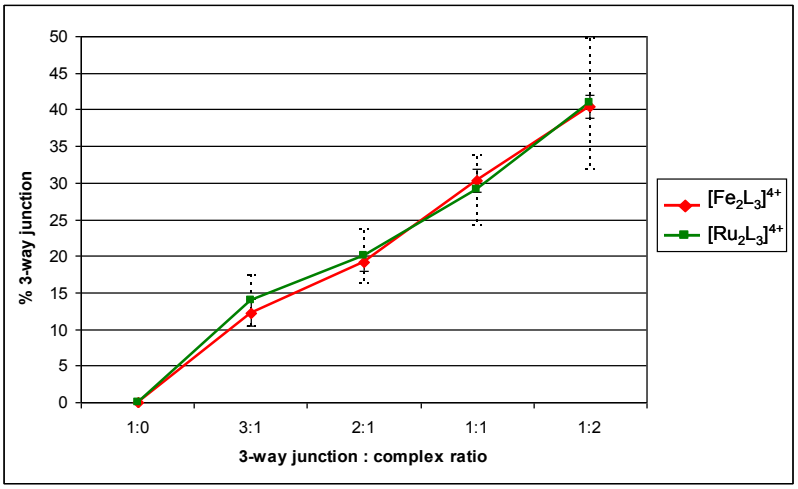

Figure 3. 14 Percentage three-way junction formed against [three-way junction: complex] ratios for $[Fe_2L_3]^{4+}$ and $[Ru_2L_3]^{4+}$. Graph represents mean ± SEM from three independent experiments. (Solid line = SEM $[Fe_2L_3]^{4+}$, Dashed line = SEM $[Ru_2L_3]^{4+}$).

Three-way junction binding of $[Ru_2L_3]^{4+}$ is almost identical to that of $[Fe_2L_3]^{4+}$, with binding increasing from ~12 % at a 3:1 three-way junction: complex ratio, to 40 % at a 1:2

three-way junction: complex ratio. This is not an unexpected result, as the charge and three dimensional shape of both complexes are very similar. Clearly these are two properties which have a large effect on three-way junction binding, and in this case the metal ion does not influence binding or stabilisation. There is also some stabilisation of the DNA duplex with $[Ru_2L_3]^{4+}$. Again, this is possibly due to the tetracationic charge of the complex.

3.2.3 Three-Way Junction Binding of $[Fe_2L^p_3]^{4+}$

A complex with larger diameter, $[Fe_2L^1_3]^{4+}$, causes a large decrease in three-way junction binding and stabilisation as compared to the parent $[Fe_2L_3]^{4+}$ complex. Therefore it is interesting to investigate the effect on three-way junction binding of a cylinder with the same core dimensions, but with appended peptides, $[Fe_2L^p_3]^{4+}$, creating a much longer structure. An example gel profile is shown in Figure 3. 15 with the relevant data for $[Fe_2L_3]^{4+}$ (previous gel, Figure 3. 10) shown as a comparison.

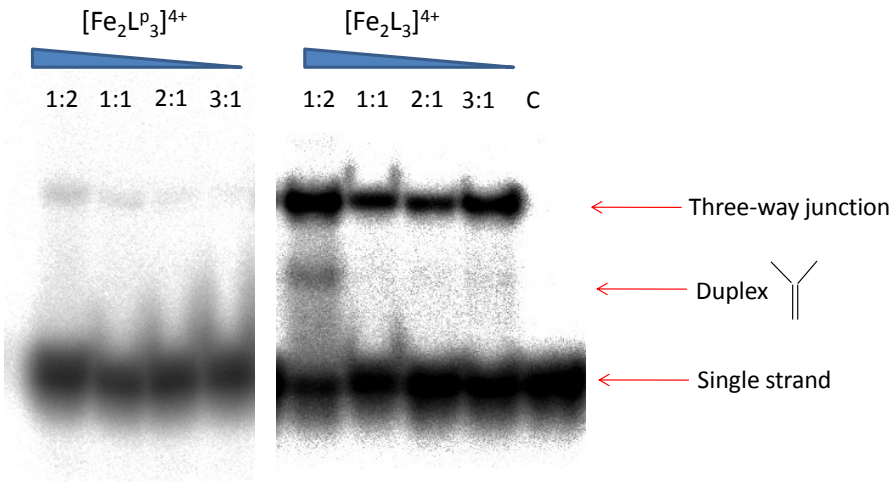

Figure 3. 15 Phosphorimaging gel profile showing three-way junction stabilisation of $[Fe_2L^p_3]^{4+}$ and $[Fe_2L_3]^{4+}$ with control (three DNA strands and no complex).

Three-way junction binding of $[Fe_2L^p_3]^{4+}$ is minimal, with stabilisation of the DNA three-way junction structure ranging from 0.02-0.45 % (as a percentage of all DNA structures

present in each lane on the gel). This minimal binding, which may simply be caused due to the charged nature of the complex, shows how important all dimensions of the complex are for successful three-way junction binding. This result might also indicate that the complexes slot into a pre-formed three-way junction structure, rather than the DNA strands assembling around them, as $[Fe_2L^p_3]^{4+}$ has the same core structure as the parent $[Fe_2L_3]^{4+}$.

3.2.4 *In Vitro* Cell Testing of $[Fe_2L_3]^{4+}$ and $[Fe_2L^1_3]^{4+}$

The range of DNA three-way junction binding and stabilisation caused by the complexes discussed herein presents a very exciting question: Does three-way junction binding correlate with anticancer activity? In order to examine this question, *in vitro* cell testing of $[Fe_2L_3]^{4+}$, $[Fe_2L^1_3]^{4+}$ and cisplatin (control) was carried out (see section 2.5.5). IC_{50} values, including those previously reported for $[Ru_2L_3]^{4+}$ [18] and $[Fe_2L^p_3]^{4+}$ [4] are shown in Table 3. 1. Cell lines chosen were the human ovarian cancer A2780-P, its cisplatin resistant analogue A2780-R and the breast cancer MDA-MB-231 cell line.

	A2780-P	A2780-R	R_f(A2780)	MDA-MB-231
$[Fe_2L_3]^{4+}$	8.7 ± 1.1	13.1 ± 2.3	1.5	34.8 ± 5.3 [i]
$[Fe_2L^1{}_3]^{4+}$	> 100[ii]	> 100[ii]	-	> 100[ii]
$[Ru_2L_3]^{4+}$ [18]	72.0 ± 3.3	152.0 ± 4.3	2.1	Not tested
$[Fe_2L^p{}_3]^{4+}$ [4]	9 ± 2	Not tested	-	34.0 ± 6
Cisplatin	4.4 ± 0.8	19.3 ± 1.8	3.6	35.2 ± 5.2

Table 3. 1 IC_{50} values (μM) in A2780-P, A2780-R and MDA-MB-231 cell lines for $[Fe_2L_3]^{4+}$, $[Fe_2L^1{}_3]^{4+}$, $[Ru_2L_3]^{4+}$, $[Fe_2L^p{}_3]^{4+}$ and cisplatin. Results represent mean ± SD of 3 separate experiments. Resistance factors are displayed for A2780 cell line; R_f = IC_{50} (A2780-R)/ IC_{50} (A2780-P).

$[Fe_2L_3]^{4+}$, which exhibits stabilisation of the DNA three-way junction structure, has an activity comparable to that of cisplatin in the MDA-MB-231 and A2780 cell lines. With an R_f factor of 1.5 for the A2780 cell line, this complex shows no cross resistance with cisplatin. These results may implicate three-way junction binding and stabilisation as a potential mode of action of this complex.

$[Fe_2L^1{}_3]^{4+}$ is inactive in all cell lines tested and causes only minimal stabilisation of the DNA three-way junction structure. This may confirm the above hypothesis that effective stabilisation of a DNA three-way junction leads to cell death, an exciting result. However,

[i] This result is discussed further in Chapter 4.

[ii] Due to comparisons being drawn with cisplatin a maximum concentration of 100 μM was tested for all compounds. Therefore above this value compounds are classed as inactive and an accurate IC_{50} value cannot be calculated.

other factors may need to be taken into consideration, for example the uptake of complexes into the cell.

$[Fe_2L^p_3]^{4+}$ has comparable activity to both $[Fe_2L_3]^{4+}$ and cisplatin in both cell lines tested, yet shows minimal three-way junction stabilisation on the gel. This may indicate that modes of cell death are different for complexes with differing supramolecular architectures, as in this case three-way junction stabilisation is not a likely mode of action.

$[Ru_2L_3]^{4+}$ is known to be less active against ovarian cancer cell lines,[18] as compared to the parent $[Fe_2L_3]^{4+}$ complex, yet these compounds show almost identical three-way junction binding. This further confirms that a number of factors, as well as supramolecular architecture need to be taken into consideration, such as the choice of metal ion. One mechanism of cytotoxicity might be three-way junction stabilisation, however, this result illustrates that modes of action may be different in different cell lines.

3.2.5 Uptake of $[Fe_2L^1_3]^{4+}$ In Live Cells

Both $[Fe_2L_3]^{4+}$ and $[Ru_2L_3]^{4+}$ are able to cross cell membranes intact and enter the cytoplasm of the cell, as shown through experiments with HL-60 cells.[18] It is important to determine at this stage if observed inactivity of $[Fe_2L^1_3]^{4+}$ is caused due to lack of DNA binding interactions or if the complex is simply not able to enter cells intact. Uptake of $[Fe_2L^1_3]^{4+}$ into the cytosol of the breast cancer cell line, MDA-MB-231 was assessed by UV-Visible spectroscopy, Figure 3. 16 (see section 2.5.3.2). Cells were treated with $[Fe_2L^1_3]^{4+}$ for 24 hours, following which, whole cell protein was extracted.

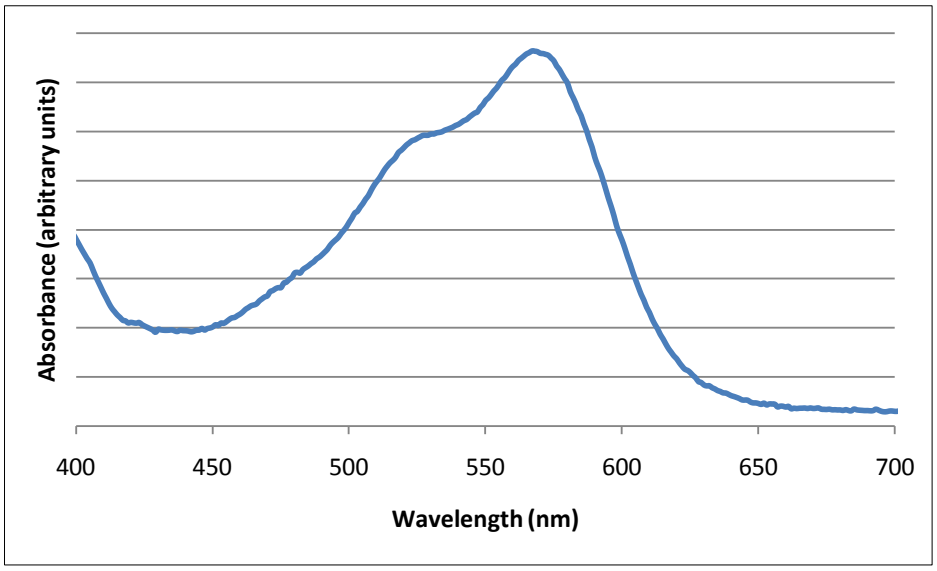

Figure 3. 16 Difference absorption spectrum of whole cell protein extract from MD-AMB-231 cells after 24 hr treatment with $[Fe_2L^1_3]^{4+}$, showing presence of compound.

The distinctive UV-Visible spectrum[7] of $[Fe_2L^1_3]^{4+}$ can be seen, indicating the presence of this complex in the protein extract. This result shows that it is possible for $[Fe_2L^1_3]^{4+}$ to cross the cell membrane and enter the cytosol of the cell intact. It should be noted, however, that although $[Fe_2L^1_3]^{4+}$ is clearly able to enter the cell, membrane extracts of MD-AMB-231 treated cells are highly coloured, shown in Figure 3. 17. This is indicative of a large amount of $[Fe_2L^1_3]^{4+}$ and to some extent the parent $[Fe_2L_3]^{4+}$ being associated with the cell membrane during the incubation period.

Figure 3. 17 MDA-MB-231 cell membrane extracts after 24 hr treatment with medium (left), $[Fe_2L_3]^{4+}$ (centre) and $[Fe_2L^1_3]^{4+}$ (right).

3.2.6 Stability of $[Fe_2L_3]^{4+}$ and $[Fe_2L^1{}_3]^{4+}$

The stability of $[Ru_2L_3]^{4+}$ in water has been assessed previously and was found to have good stability over long periods of time at room temperature.[3] The stability of $[Fe_2L^p{}_3]^{4+}$ has also been assessed[10] and was found to be stable for a period of ~ 2 hours, in aqueous buffer at 20 ºC, after which time hydrolysis of the imino bonds in the ligands causes the complex to break down. This may be a reason for this complexes inability to stabilise the three-way junction structure, or for its activity *in vitro*, however this has not been determined at this stage.

It is important to determine and compare stabilities of $[Fe_2L_3]^{4+}$ and $[Fe_2L^1{}_3]^{4+}$ in order to elucidate further reasons for differing binding and activity. The stability of $[Fe_2L_3]^{4+}$ and $[Fe_2L^1{}_3]^{4+}$ in water at 37 ºC can be seen in Figure 3. 18 and Figure 3. 19 (see section 2.4.1).

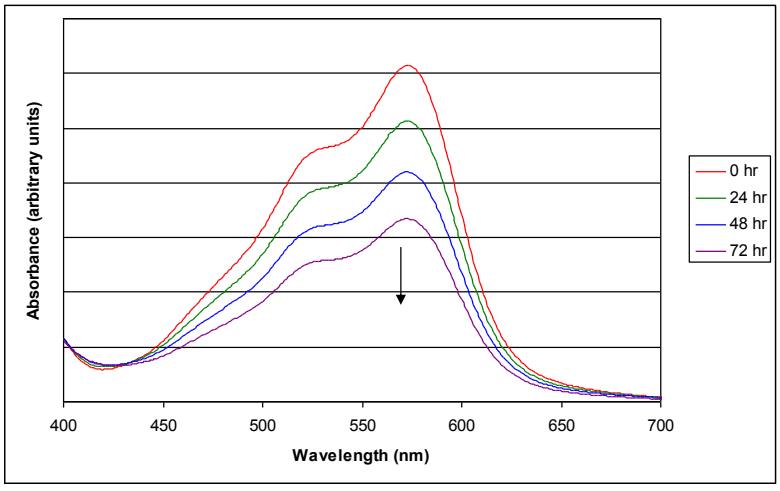

Figure 3. 18 UV-Visible spectra of $[Fe_2L_3]^{4+}$ (40 µM) in water at 37 ºC over a period of 72 hours.

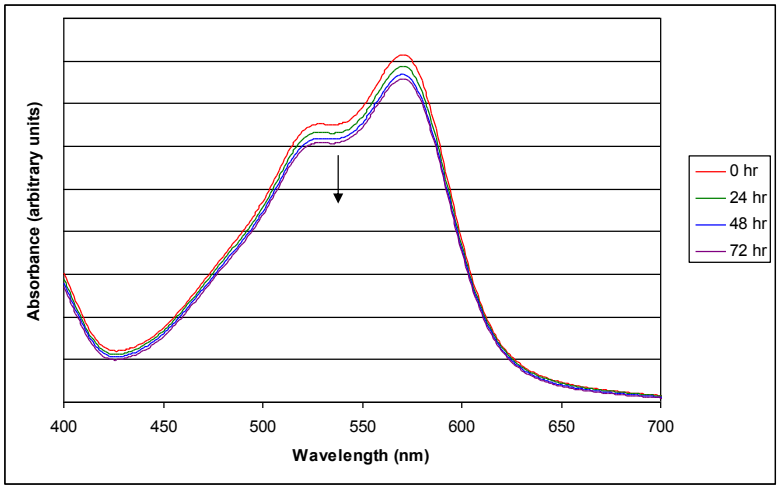

Figure 3. 19 UV-Visible spectra of $[Fe_2L^1_3]^{4+}$ (40 μM) in water at 37 ºC over a period of 72 hours.

The stability of $[Fe_2L^1_3]^{4+}$ in water is good and although there is a small decrease in intensity of the bands, peaks do not shift wavelength, showing retention of the complex in solution. The stability of $[Fe_2L_3]^{4+}$ is not as good, and there is a reduction of ~50 % in intensity of the bands over this time period. There is, however, no wavelength shift so the complex that remains in solution is $[Fe_2L_3]^{4+}$.

The constituents (ligand, $FeCl_2$) of the parent $[Fe_2L_3]^{4+}$ have been assessed for anticancer activity[18] and were found to be inactive. This should rule out activity caused simply through instability of the complex, and furthermore it is known that the time period it takes for $[Fe_2L_3]^{4+}$ to enter the cell nucleus is less than 20 minutes,[19] during which time the complex is stable. Therefore, it can be concluded that the stabilities of $[Fe_2L_3]^{4+}$ and $[Fe_2L^1_3]^{4+}$ are not directly responsible for their differing *in vitro* anticancer activities.

3.3 Conclusions and Further Work

The specific three dimensional shape of complexes appears to be important for the stabilisation of a DNA three-way junction structure under the conditions used herein. Changing the diameter of the parent $[Fe_2L_3]^{4+}$ complex by as little as 2Å in $[Fe_2L^1{}_3]^{4+}$ [8] reduces this stabilisation dramatically. A change in metal ion does not appear to be as important, with $[Ru_2L_3]^{4+}$ binding being analogous to that of $[Fe_2L_3]^{4+}$. When it comes to anticancer activity, however, it has been shown that there are other factors which need to be taken into consideration. For breast cancer cell lines, where both $[Fe_2L_3]^{4+}$ and $[Ru_2L_3]^{4+}$ display a good activity, with $[Fe_2L^1{}_3]^{4+}$ being inactive, it would appear that three-way junction binding is playing a major role in cytotoxicity, an exciting result. Activity of $[Fe_2L^p{}_3]^{4+}$ in this cell line may be due to stability issues, this being the least stable of all the complexes. For ovarian cancer cell lines where only $[Fe_2L_3]^{4+}$ and $[Fe_2L^p{}_3]^{4+}$ display good activity, it would appear that there are factors other than three-way junction binding to consider. This may range from the choice of metal ion to interaction with other cellular targets not previously considered. This needs to be the subject of further investigation.

To date, it has not been possible to separate the enantiomers of $[Fe_2L^1{}_3]^{4+}$.[20] It is unlikely that either enantiomer will convey a significantly higher anticancer activity however it may be the case that one enantiomer has slightly differing DNA binding, as is the case for the parent $[Fe_2L_3]^{4+}$. Synthesis of the ruthenium analogue of $[Fe_2L^1{}_3]^{4+}$ and investigation of anticancer activity would be beneficial in order to understand the role of the metal ion in this complex.

3.4 References

[1] M. J. Hannon, *Chem. Soc. Rev*., 2007, **36**, 280-295.

[2] L. Childs, Masters Thesis, University of Warwick, 1999.

[3] G. Pascu, PhD Thesis, Univeristy of Birmingham, 2008.

[4] L. Cardo, PhD Thesis, Univeristy of Birmingham, 2010.

[5] M. J. Hannon, V. Moreno, M. J. Prieto, E. Molderheim, E. Sletten, I. Meistermann, C. J. Isaac, K. J. Sanders and A. Rodger, *Angew. Chem., Intl. Ed.*, 2001, **40**, 879-884.

[6] S. Khalid, M. J. Hannon, A. Rodger, and M. Rodger, *Chem. Eur. J.,* 2006, **12**, 3493-3506.

[7] I. Meistermann, PhD Thesis, University of Warwick, 2001.

[8] S. Khalid, M. J. Hannon, A. Rodger and M. Rodger, *J. Molecular Graphics and Modelling*, 2007, **25**, 794-800.

[9] G. I. Pascu, A. C. G. Hotze, C. Sanchez-Cano, B. M. Kariuki, and M. J. Hannon, *Angew. Chem. Int. Ed*., 2007, **46**, 4374-4378.

[10] L. Cardo and M. J. Hannon, *Inorg. Chim. Acta.*, 2009, **362**, 784-792.

[11] J. L. Kadrmas, A. J. Ravin and N. B. Leontis, *Nucleic Acid. Res.*, 1995, **23**, 2212-2222.

[12] A. Oleksy, A. G. Blanco, R. Boer, I. Usón, J. Aymami, A. Rodger, M. J. Hannon and M. Coll, *Angew. Chem., Intl. Ed.*, 2006, **45**, 1227-1231.

[13] M. J. Hannon, *Pure Appl. Chem*., 2007, **79**, 2243-2261.

[14] *Molecular Biology of the Cell,* ed. B. Alberts, A. Johnson, J. Lewis, M. Raff, K. Roberts and P. Walter, Garland Science, Taylor & Francis group, 2008.

[15] J. Malina, M. J. Hannon and V. Brabec, *Chem. Eur. J*., 2007, **13**, 3871-3877.

[16] N. B. Leontis, W. Kwok and J. S. Newman, *Nucleic Acid. Res.,* 1991, **19**, 759-766.

[17] J. Malina, M. J. Hannon and V. Brabec, *Chem. Eur. J*., 2008, **14**, 10408-10414.

[18] C. Sanchez-Cano, PhD Thesis, University of Birmingham, 2009.

[19] A. C. G. Hotze, N. J. Hodges, R. E. Hayden, C. Sanchez-Cano, C. Paines, N. Male, M-K. Tse, C. M. Bunce, J. K. Chipman and M. J. Hannon, *Chemistry & Biology*, 2008, **15**, 1258-1267.

[20] J. M. C. A. Kerckhoffs, J. C. Peberdy, I. Meistermann, L. J. Childs, C. J. Isaac, C. R. Pearmund, V. Reudegger, S. Khalid, N. W. Alcock, M. J. Hannon and Alison Rodger, *Dalton Trans.*, 2007, 734-742.

Chapter 4

In Vitro Studies of an Iron Triple Stranded Supramolecular Cylinder

Original synthesis and characterisation of $[Fe_2L_3]^{4+}$ *was carried out by Dr. C. Painting, University of Warwick.*

L and $[Fe_2L_3]^{4+}$ *were remade for all biological testing discussed in this chapter.*

4.1 Introduction

This chapter details *in vitro* biological studies of the triple stranded iron cylinder, $[Fe_2L_3]^{4+}$ where L = $C_{25}H_{20}N_4$, Figure 4. 1.

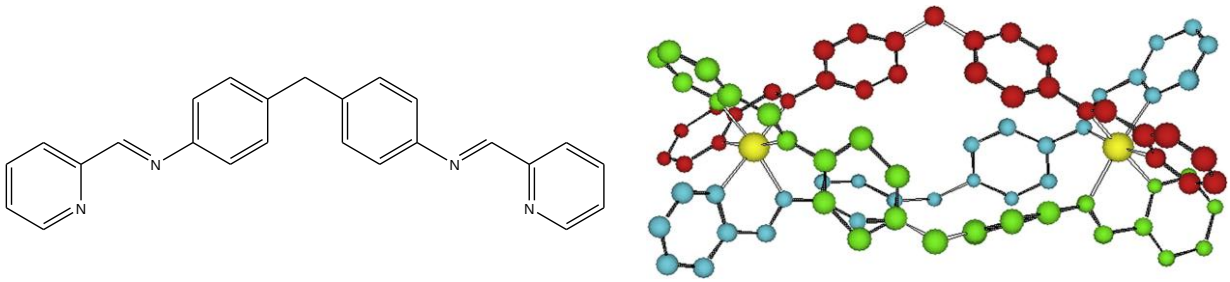

Figure 4. 1 Ligand L and X-ray crystal structure of the $[Fe_2L_3]^{4+}$ cation discussed in this chapter. Hydrogen atoms and anions have been omitted for clarity.[1]

In order for this promising drug compound to progress further towards the clinic its effects on human cell lines and mode of action must be investigated. It is anticipated that a highly charged compound of this nature will interact with many biological molecules en-route to nuclear DNA, causing various effects. In this chapter, studies are carried out on the highly dedifferentiated, invasive, hormone independent, breast cancer cell line MDA-MB-231.[2] These studies are designed in order to probe the response of the cells to incubation with the $[Fe_2L_3]^{4+}$ cylinder, including changes in cell morphology and the cells' potential for recovery. How these effects differ from those of the traditional alkylating agent cisplatin (a clinical agent that binds in a covalent manner to DNA causing direct mutation and cell death),[3] will be discussed.

The impact of this work is not only in elucidating the mechanism of action and increasing understanding of the drug in the current study, but also in assessing the suitability of methods currently used for initial *in vitro* drug screening of novel compounds with unknown modes of action.

4.1.1 The Supramolecular $[Fe_2L_3]^{4+}$ Cylinder and its Biological Action

DNA binding interactions of the $[Fe_2L_3]^{4+}$ helicate were discussed in chapters 1 and 3. DNA binding in whole, live cells has also been assessed, via a Hoechst (a minor groove binding dye) displacement assay.[4] Quenching of the Hoechst emission confirmed that $[Fe_2L_3]^{4+}$ is able to enter the nucleus of live cells and interact with nuclear DNA, Figure 4. 2.

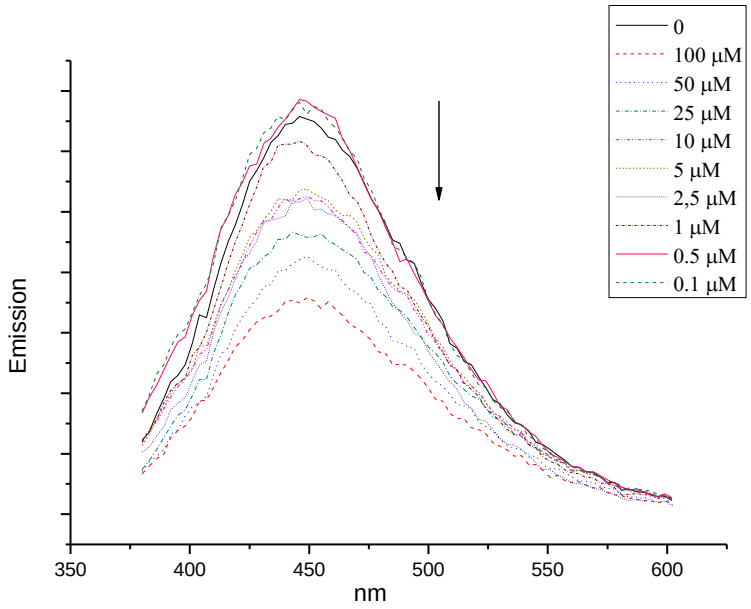

Figure 4. 2 Quenching of Hoechst emission by $[Fe_2L_3]^{4+}$ in HL-60 cells. Concentration of $[Fe_2L_3]^{4+}$ indicated in top left corner.[4]

$[Fe_2L_3]^{4+}$ displays cytotoxicity in all cell lines tested, including MRC-5, a non-tumour cell line,[5] Table 4. 1.

Cell Line	HBL100	T47D	SKOV-3	HL-60	MRC-5
$[Fe_2L_3]^{4+}$	27 ± 5	52 ± 10	35 ± 5	18 ± 3	19 ± 3
Cisplatin	4.9 ± 0.3	28.0 ± 1.7	6.0 ± 0.3	7 ± 1	< 3

Table 4. 1 Cytotoxicities (IC_{50} in μM) of $[Fe_2L_3]^{4+}$ and cisplatin, after 72 hour continuous treatment of a panel of tumour cell lines, as assessed by the MTT assay. Results represent mean of three separate experiments ± SD.[5]

Crucially, $[Fe_2L_3]^{4+}$ does not exhibit any genotoxicity or mutagenicity, a huge drawback of many current anticancer agents, and the reason for the emergence of secondary cancers caused by their use as treatment.[6] These biological tests have been presented in a recent paper.[5]

4.2 Results and Discussion

4.2.1 *In Vitro* Cell Testing of $[Fe_2L_3]^{4+}$

Cell line testing was carried out on the breast cancer cell line, MDA-MB-231, as $[Fe_2L_3]^{4+}$ had not been previously tested against this cell line. The MTT assay (See section 2.5.5) was used to assess toxicity, with calculation of an IC_{50} value after 72 hours continuous incubation with $[Fe_2L_3]^{4+}$, Table 4. 2.

Cell Line	MDA-MB-231
$[Fe_2L_3]^{4+}$	34.8 ± 5.3
Cisplatin	35.2 ± 5.2

Table 4. 2 Cytotoxicities (IC_{50} in μM) of $[Fe_2L_3]^{4+}$ and cisplatin, after 72 hour continuous treatment of MDA-MB-231, as assessed by the MTT assay. [i] *Results represent mean of three separate experiments ± SD.*

These results confirm this cell line as a good choice for further investigation, as both $[Fe_2L_3]^{4+}$ and cisplatin have very similar IC_{50} values.

4.2.2 *In Vitro* Effect of Increased Molar Incubation of $[Fe_2L_3]^{4+}$

It was noted during routine dose range-finding experiments[ii], that cellular toxicity appeared to be not only related to the concentration of $[Fe_2L_3]^{4+}$ incubated with the cells, but that when a higher volume was incubated (higher number of moles $[Fe_2L_3]^{4+}$) more cell death was observed, Figure 4. 3.

[i] Parallel experiments with $[Fe_2L_3]^{4+}$, medium and MTT showed no interactions, confirming the MTT assay as a suitable method for assessing cell viability.
[ii] Experiments carried out in the lab of Dr. Boris Kysela, University of Birmingham Medical School

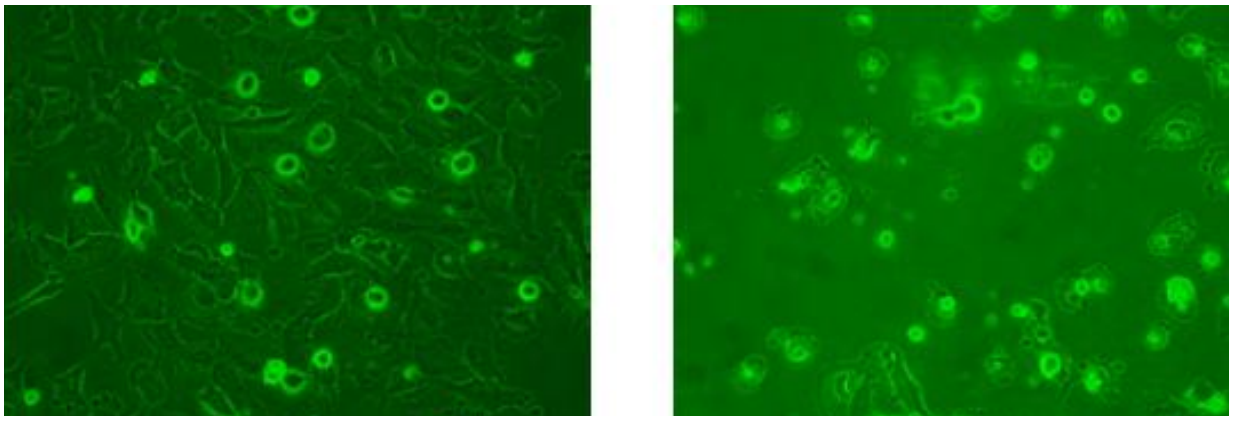

75 µM $[Fe_2L_3]^{4+}$, 1 ml media *75 µM $[Fe_2L_3]^{4+}$, 3 ml media*

Figure 4. 3 Standard light-microscopy photographs of MRC-5 VA cells treated with varying volumes of $[Fe_2L_3]^{4+}$, illustrating reduced number of cells with increased molar incubation.[iii]

In order to investigate this observed effect, MDA-MB-231 cells were treated with varying volumes of $[Fe_2L_3]^{4+}$, keeping concentrations constant and therefore changing the number of moles $[Fe_2L_3]^{4+}$ incubated with cells. Cell viability was assessed via the MTT assay and IC_{50} calculated using a range of concentrations (see section 2.5.6). Figure 4. 4 shows IC_{50} values obtained for $[Fe_2L_3]^{4+}$ and cisplatin against incubation volume.

[iii] Pictures created in the lab of Dr. Boris Kysela, University of Birmingham Medical School

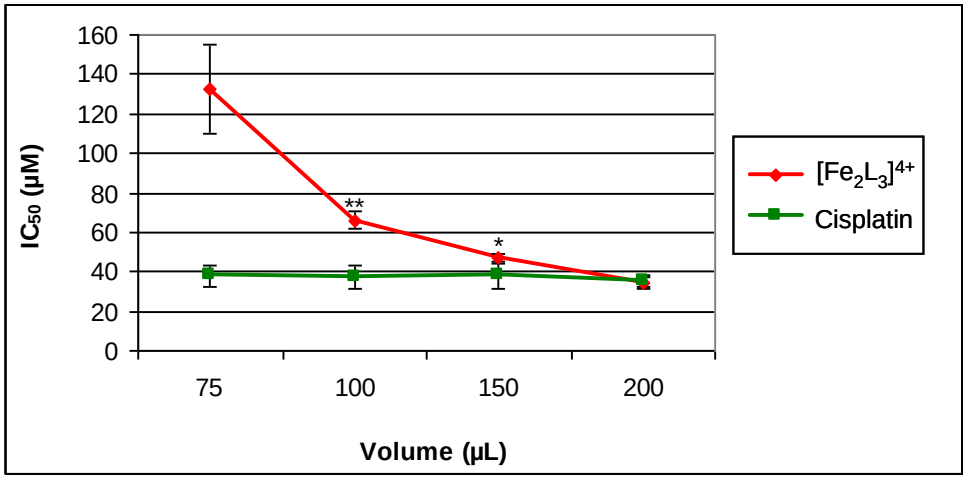

Figure 4. 4 Activity against the breast cancer cell line MDA-MB-231 of $[Fe_2L_3]^{4+}$ and cisplatin following 72 hour incubation with varying volumes of compound, as assessed using the MTT assay. Data are reported as IC_{50} versus volume. Graph represents mean ± SEM from three independent experiments.

It is clear that as the incubation volume of $[Fe_2L_3]^{4+}$ is increased the IC_{50} value decreases dramatically (increase in toxicity). This was unexpected and from the literature appears unprecedented. As seen for cisplatin, where a change in incubation volume has no effect on observed IC_{50} value, it is usually concentration that is important for determining cell stasis or death. In this case a one way ANOVA returned a p value of > 0.05 (0.98) showing no statistical significance of an increase in incubation volume on IC_{50} value for cisplatin. For $[Fe_2L_3]^{4+}$, a one way ANOVA returned a p value of < 0.05 (0.046) showing that the increase in incubation volume on IC_{50} value is statistically significant and an increase in number of moles incubated causes an increase in toxicity.

These results may imply a mechanism of action of $[Fe_2L_3]^{4+}$ where the maximum uptake is not dependent upon concentration, as is the case with cisplatin, but that the cell takes up and concentrates $[Fe_2L_3]^{4+}$ within it. There are a number of explanations for this observed effect; that $[Fe_2L_3]^{4+}$ can enter the cell passively and/or actively but that the DNA binding constant is sufficiently strong that most is bound to biomolecular targets; alternatively, the observed concentration of $[Fe_2L_3]^{4+}$ in the cells could be caused by an active uptake mechanism which is not balanced by efflux (active or passive).

4.2.3 Impact of $[Fe_2L_3]^{4+}$ on Cellular Morphology

It was also noted that cells treated with $[Fe_2L_3]^{4+}$ displayed an altered cellular phenotype when compared to both those treated with cisplatin and negative controls. Figure 4. 5.

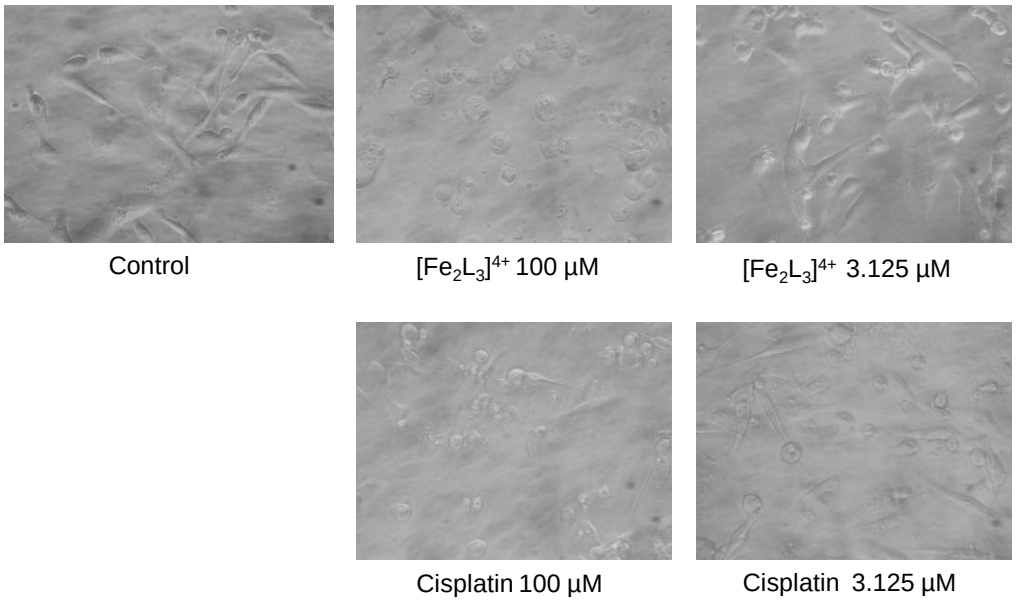

Figure 4. 5 Standard light microscopy photos showing MDA-MB-231 cells after 24 hour continuous treatment with $[Fe_2L_3]^{4+}$ and cisplatin, with medium as control.

The difference in cellular phenotype of cells treated with $[Fe_2L_3]^{4+}$, cisplatin and medium is clear and this phenotype persists for the remainder of the 72 hour incubation. $[Fe_2L_3]^{4+}$ treated cells have rounded up and lack any lamellipodia. It would appear on first sight that the cells in this state are dead, however there is no visual evidence of apoptosis or necrosis and as will be seen, mitochondrial function is retained and the cells are able to recover from this state (see section 4.2.8). This altered cellular phenotype may be evidence of a previously unexplored mode of action for $[Fe_2L_3]^{4+}$.

4.2.4 *In Vitro* Time Lapse, Phase Contrast Imaging with $[Fe_2L_3]^{4+}$

From the standard light microscope photos discussed above it is not clear exactly what morphological changes have occurred to the cell, as the altered phenotype is present at the first time point of 24 hours. The next step was therefore to investigate the progression of morphological events throughout the first 24 hours of the incubation. This was achieved through time-lapse video microscopy, a technique often used to monitor cells over continuous periods.[7] (See section 2.5.9). Images were recorded every two minutes for a period of 18 hours. Figure 4. 6- Figure 4. 12 show video stills from incubations with varying concentrations of $[Fe_2L_3]^{4+}$, cisplatin and control (medium). Also see attached video CD (video speed = 50ms/frame or 25 frames/second).

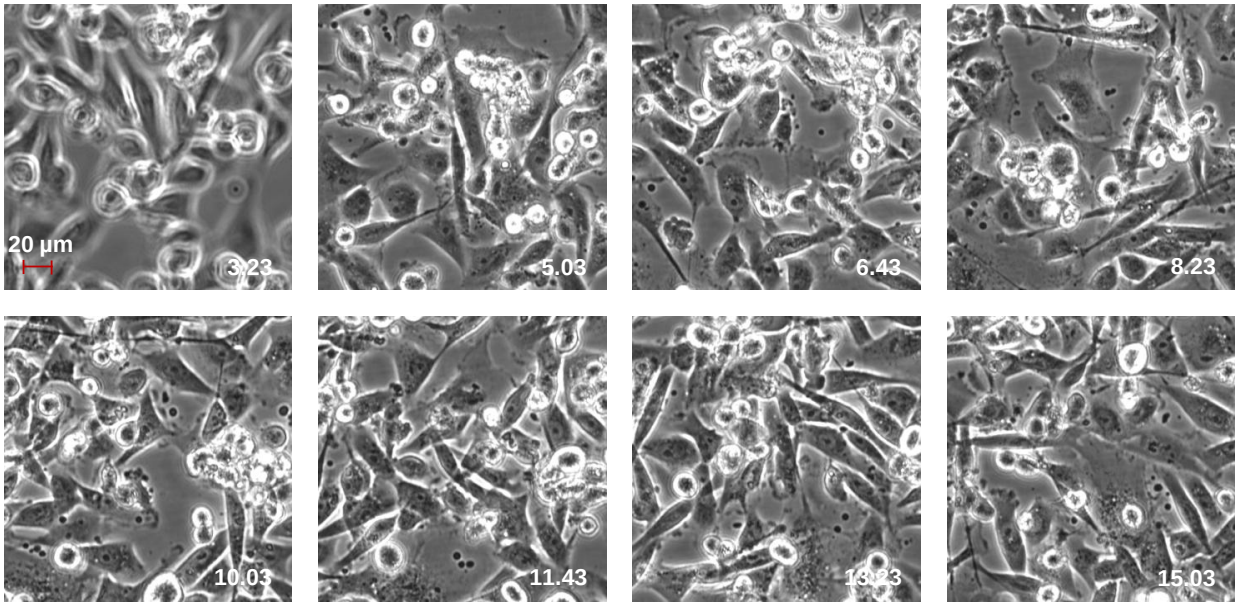

Figure 4. 6 Video stills (time indicated in right hand corner in hours) taken during continuous treatment of MDA-MB-231 cells with medium (control). 20x.

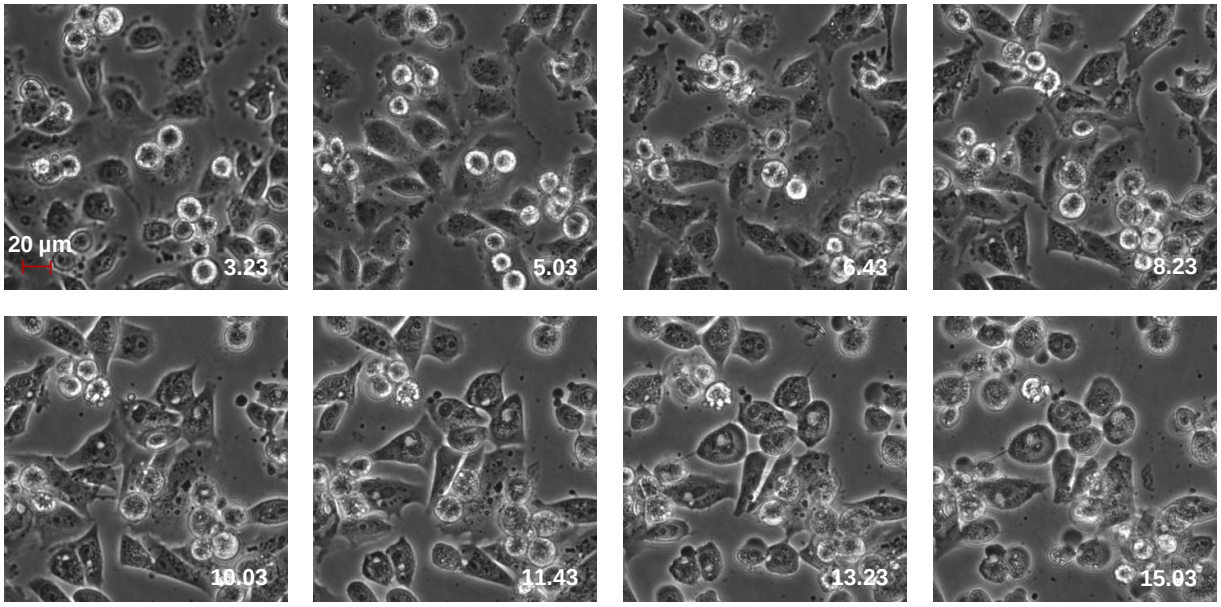

Figure 4. 7 Video stills (time indicated in right hand corner in hours) taken during continuous treatment of MDA-MB-231 cells with 200 µM $[Fe_2L_3]^{4+}$. 20x.

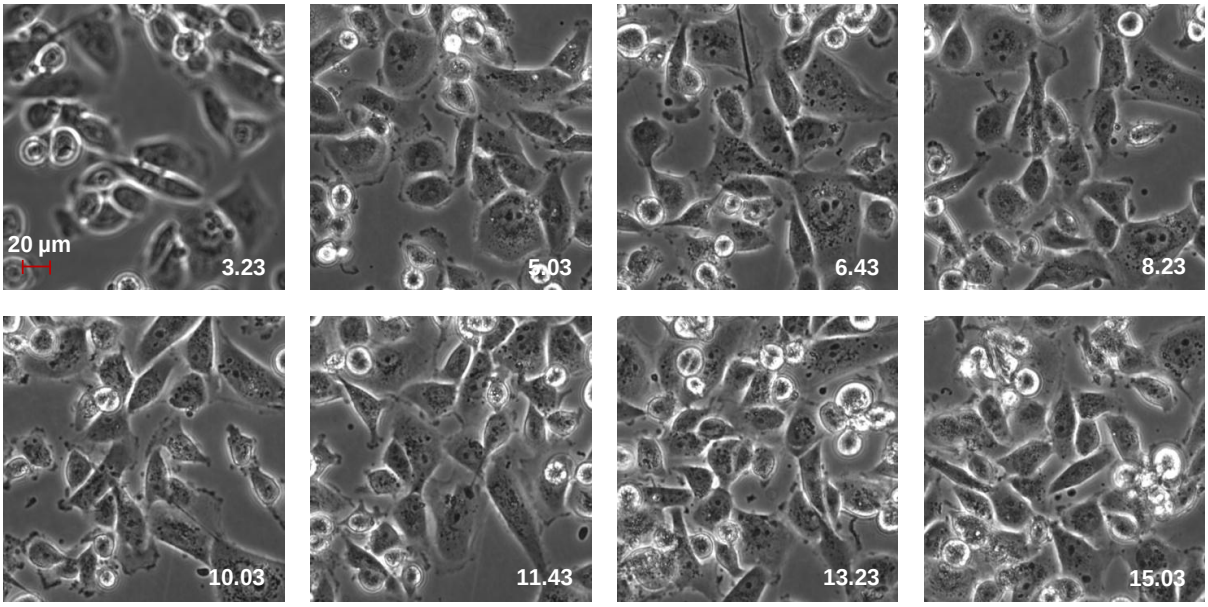

Figure 4. 8 Video stills (time indicated in right hand corner in hours) taken during continuous treatment of MDA-MB-231 cells with 100 µM $[Fe_2L_3]^{4+}$. 20x.

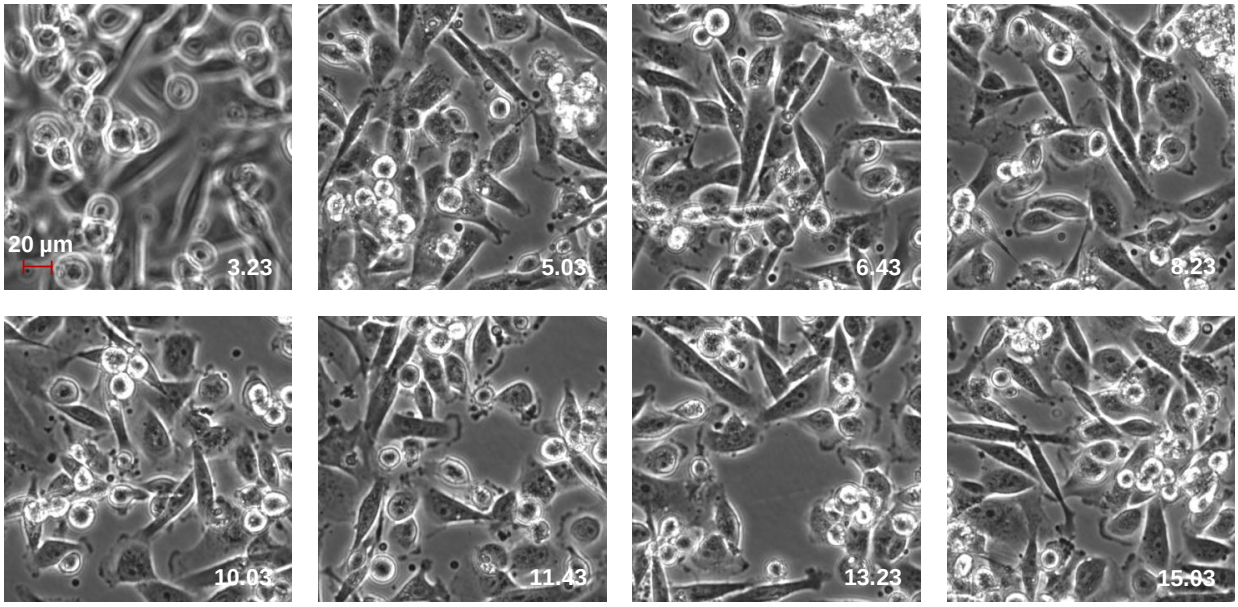

Figure 4. 9 Video stills (time indicated in right hand corner in hours) taken during continuous treatment of MDA-MB-231 cells with 50 µM $[Fe_2L_3]^{4+}$. 20x.

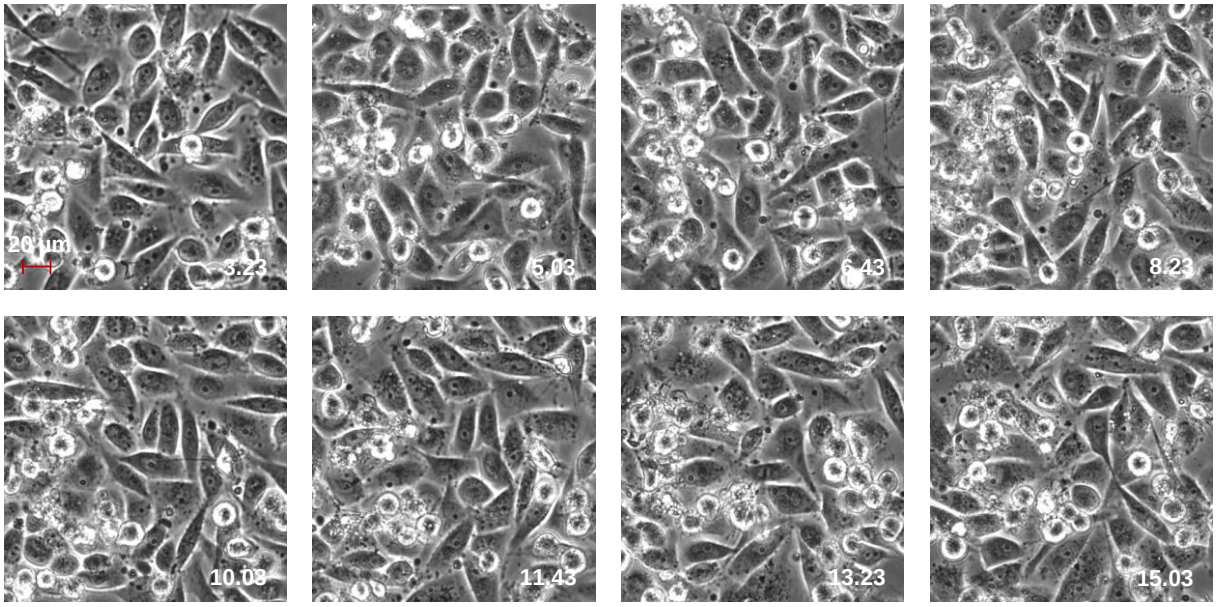

Figure 4. 10 Video stills (time indicated in right hand corner in hours) taken during continuous treatment of MDA-MB-231 cells with 200 µM cisplatin. 20x.

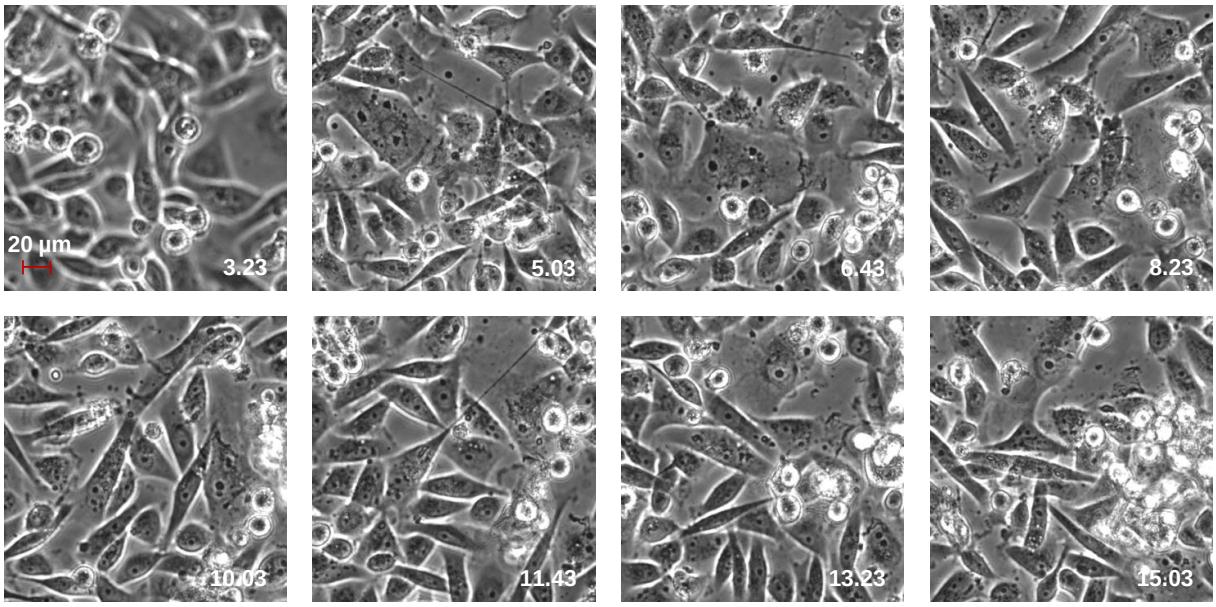

Figure 4. 11 Video stills (time indicated in right hand corner in hours) taken during continuous treatment of MDA-MB-231 cells with 100 µM cisplatin. 20x.

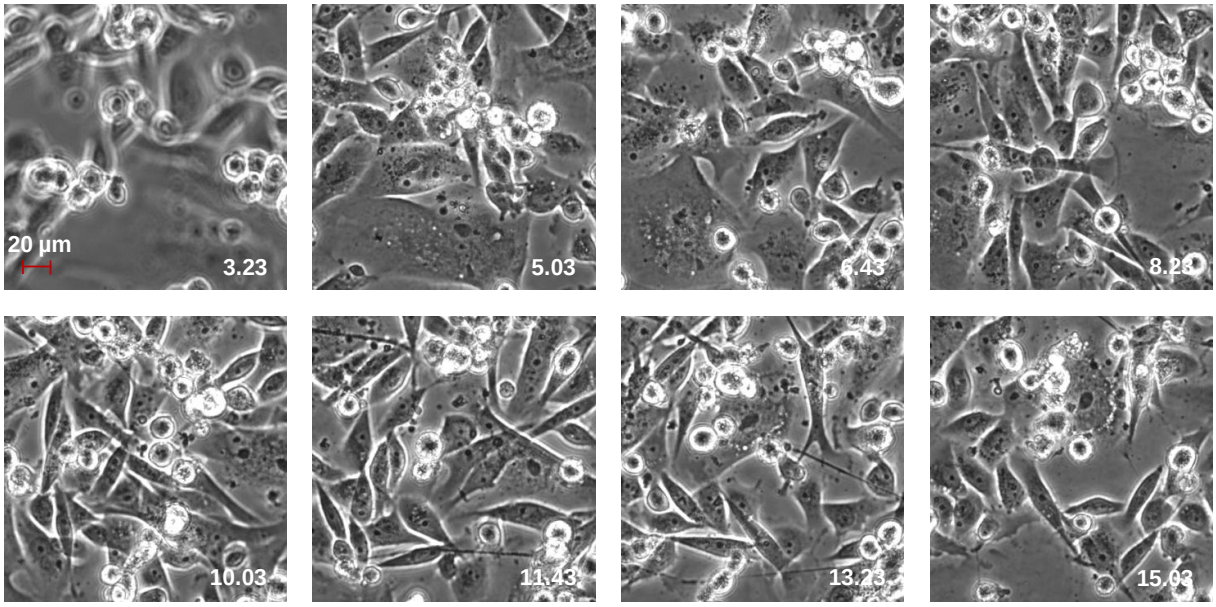

Figure 4. 12 Video stills (time indicated in right hand corner in hours) taken during continuous treatment of MDA-MB-231 cells with 50 µM cisplatin. 20x.

Cells in control wells displayed normal cellular behaviour; extensive movement of cells accompanied by some lamellipodia extensions at leading edges and limited membrane ruffling.[8] Widespread cell division can also be seen and hence cell number increases throughout the incubation. Incubation with cisplatin does not change the morphology or mobility of the cells, however, in agreement with the literature a lack of cell division is evident (aberrant mitosis followed by apoptosis).[9]

A clear dose response can be seen for $[Fe_2L_3]^{4+}$ treated cells. Extensive membrane ruffling (protrusions on the dorsal surface of cells) is present after a period of ~three hours. This is unusual behaviour for this cell line, implicating the disruption of a number of cell signalling processes affecting one or more of the actin cytoskeleton, integrin production,

lamellipodia/filopodia and cell movement. It is also evident that cell division has ceased. After a period of ~8 hours membrane ruffling is no longer evident and cell mobility stops altogether, although the cells maintain their adhesion to the culture surface. After a period of ~11 hours, the cells appear to lose some of this adhesion and round up, losing contact with neighbouring cells. There is, however, no evidence of necrosis, nor are cellular fragmentation or budding observed, as would be expected with apoptosis.[10] It is likely, therefore (when coupled with previous evidence of $[Fe_2L_3]^{4+}$ causing cell cycle arrest and induction of apoptosis)[5] that the cells are in an early-apoptotic state.

This effect is not observed with most metal based drugs, however, a similar cell rounding, or 'ballooning' effect, coupled with loss of contact with neighbouring cells has been documented in a photo-activatable platinum pro-drug, Figure 4. 13, *after* exposure to UV irradiation.[11]

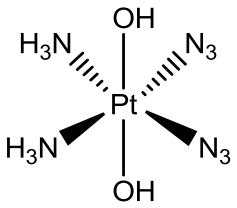

Figure 4. 13 A platinum diazide complex which exhibits cell ballooning and light activated destruction of cancer cell nuclei.[11]

Diverse cell surface receptors control structural rearrangements in the actin cytoskeleton in response to external stimuli. It is not unreasonable to assume that the presence of $[Fe_2L_3]^{4+}$ could disrupt any number of these signals. All signals eventually converge inside the cell on a family of GTPases-the Rho protein family (Ras superfamily), often implicated in cancers.[12] Indeed signalling pathways are an attractive target for anticancer drug development.[13]

Disruption of the cellular cytoskeleton would cause all the events observed, however there are so many different pathways involved with cytoskeleton maintenance that it is not possible to know at this stage which of these are being disrupted. However, it would appear from this evidence that DNA binding may not be the only mechanism of action of $[Fe_2L_3]^{4+}$, or that the downstream effects of such DNA binding have been underestimated.

4.2.5 Actin labelling of Cellular Cytoskeleton after Incubation with $[Fe_2L_3]^{4+}$

A change in actin dynamics and cytoskeleton structure is observed for both NAMI-A[14] and RAPTA,[15] both potent antimetastatic agents. Taking into account the unusual membrane ruffling activity of cells when treated with $[Fe_2L_3]^{4+}$, it seemed pertinent to assess if there is any disruption to the actin cytoskeleton. This was achieved by staining $[Fe_2L_3]^{4+}$ treated MDA-MB-231 cells with the fluorescent dye rhodamine phalloidin which detects F-actin filaments (see section 2.5.10). This test was carried out after a four hour incubation period in order to assess the extent of actin disruption during the membrane ruffling phase. Phalloidin stained actin filaments after incubation with varying concentrations of $[Fe_2L_3]^{4+}$ and medium (control) can be seen in Figure 4. 14 to Figure 4. 15.

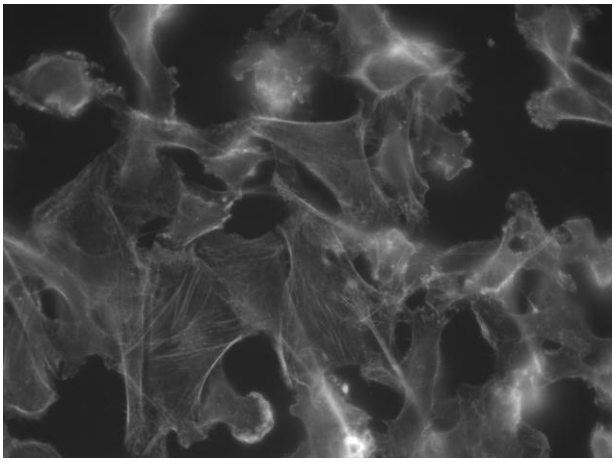

Figure 4. 14 Phalloidin stained actin filaments of MDA-MB-231 cells after four hour continuous incubation with medium (control).

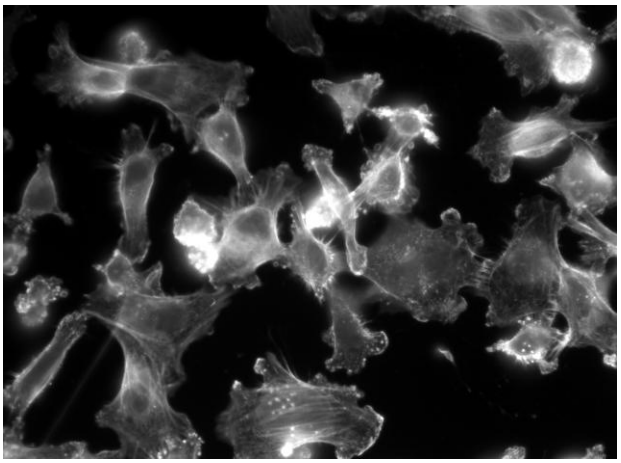

Figure 4. 15 Phalloidin stained actin filaments of MDA-MB-231 cells after four hour continuous incubation with 200 µM $[Fe_2L_3]^{4+}$.

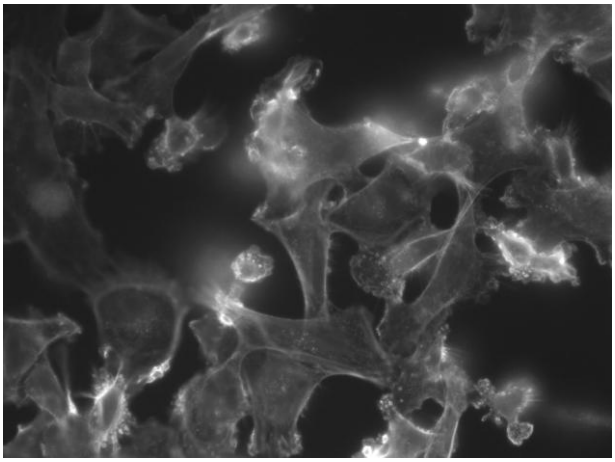

Figure 4. 16 Phalloidin stained actin filaments of MDA-MB-231 cells after four hour continuous incubation with 100 µM $[Fe_2L_3]^{4+}$.

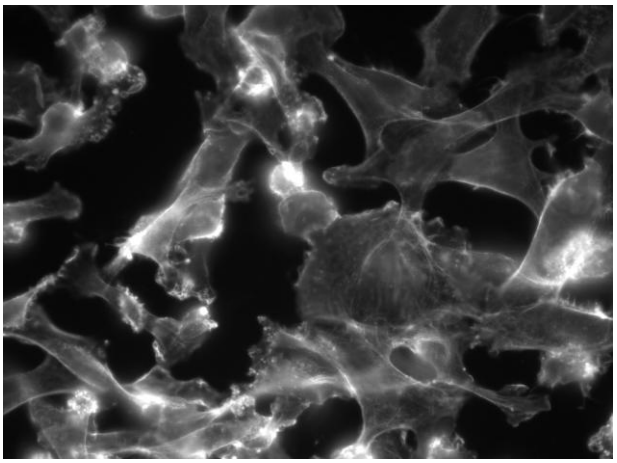

Figure 4. 17 Phalloidin stained F-actin filaments of MDA-MB-231 cells after four hour continuous incubation with 50 µM $[Fe_2L_3]^{4+}$.

A clear dose response can be seen with increasing concentrations of $[Fe_2L_3]^{4+}$. Stress fibres (thin fibres throughout the body of the cells) are present in both control and $[Fe_2L_3]^{4+}$ treated cells, however the normal triangular shape of cells in the control is perturbed in $[Fe_2L_3]^{4+}$ treated cells. Furthermore, the edges of $[Fe_2L_3]^{4+}$ treated cells are irregular and there are a greater number of broad, rounded lamellipodia extrusions from the cells along with a number

of ‘blobs’ of actin, correlating with membrane ruffling seen at this time point. This result confirms that the irregular membrane activity seen in time-lapse microscopy experiments may be caused, at least in part, to a disruption in actin polymerisation and architecture. However, it cannot be confirmed at this stage the exact binding modes or interactions causing this disruption, only that disruption of actin polymerisation may be involved.

4.2.6 *In Vitro* Extended Incubation of Cells with $[Fe_2L_3]^{4+}$

The effects of $[Fe_2L_3]^{4+}$ on cells have, thus far, been investigated over a maximum time period of 72 hours. With these experiments showing unexpected results, differing substantially to those of cisplatin, it is interesting to examine the fate of the cells over a longer period of time. An IC_{50} test is most commonly carried out at 24-72 hour time periods. However, it has been suggested that such short incubations may not correlate with *in vivo* activity.[16] To assess the activity of $[Fe_2L_3]^{4+}$ and cisplatin over an extended period, cell viability over a range of concentrations and hence IC_{50} values were determined for periods of up to six days, Figure 4. 18 (see section 2.5.7).

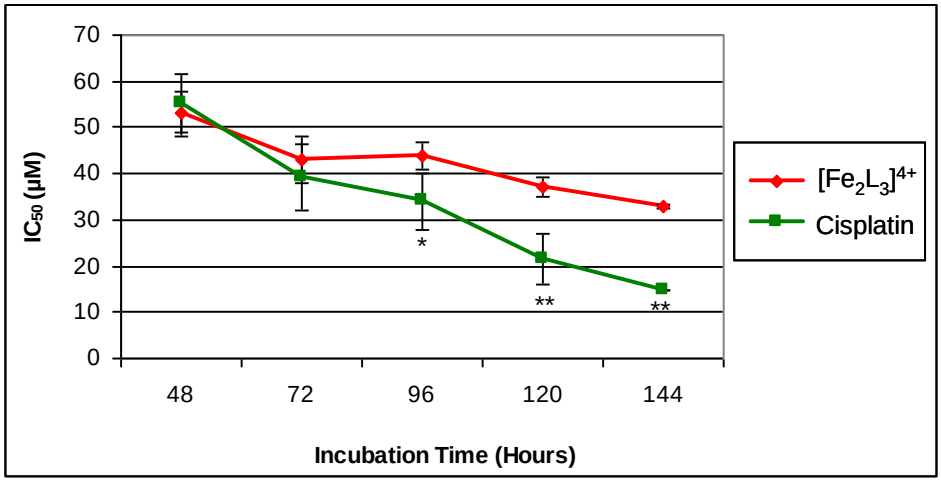

Figure 4. 18 Activity against the breast cancer cell line MDA-MB-231 with $[Fe_2L_3]^{4+}$ and cisplatin following 48, 72, 96, 120 and 144 hour continuous incubations, as assessed using the MTT assay. Data are reported as IC_{50} versus time. Graph represents mean ± SEM from three independent experiments.

At the 24 hour time period both $[Fe_2L_3]^{4+}$ and cisplatin showed activities of > 500 µM, so it is assumed that although these compounds may have entered the cell and potentially bound to nuclear DNA, their action has not yet been sufficient to cause any cell death. At the 48 and 72 hour time points both $[Fe_2L_3]^{4+}$ and cisplatin display similar IC_{50} values. However, over a longer time period it is clear that the cellular toxicity of $[Fe_2L_3]^{4+}$ does not continue to increase as dramatically as that of cisplatin, with the total reduction in IC_{50} being 38 % for $[Fe_2L_3]^{4+}$ (one-way ANOVA returning a value of > 0.05 (0.2) showing no statistical significance). This is compared to 73 % reduction in IC_{50} for cisplatin (one-way ANOVA returning a value of < 0.001 (9.09×10^{-5}) showing high statistical significance in reduction of IC_{50} over the 2-6 day period). The final IC_{50} value of $[Fe_2L_3]^{4+}$ is more than twice that of cisplatin.

4.2.7 Recovery of Cells After Three Hour Incubation with $[Fe_2L_3]^{4+}$

It is interesting to determine if cells are able to recover from the membrane ruffling phenotype induced though incubation with $[Fe_2L_3]^{4+}$. For comparison, cell density (as optical density measurement after application of the MTT assay) with $[Fe_2L_3]^{4+}$ (100 µM), cisplatin (100 µM) and control (medium) was plotted for periods of up to six days of continuous treatment. Figure 4. 19 (see section 2.5.7).

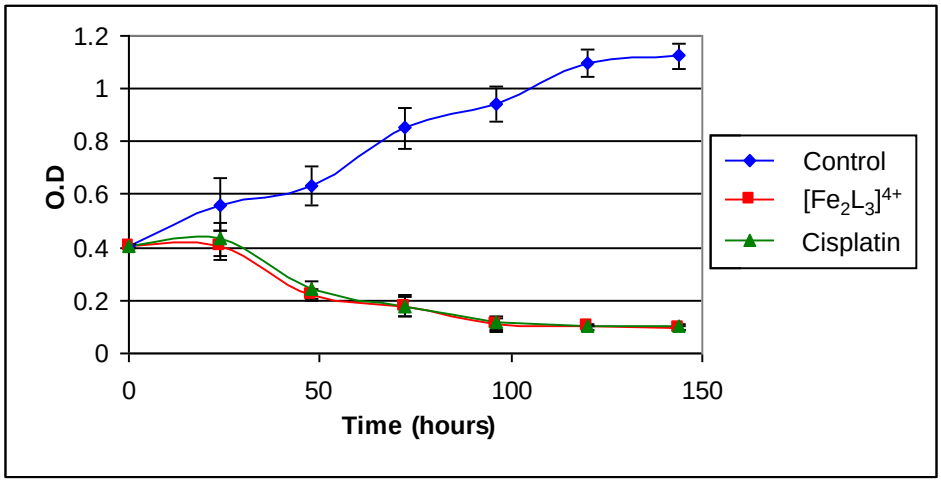

Figure 4. 19 Continuous treatment of MDA-MB-231 cells with $[Fe_2L_3]^{4+}$ and cisplatin (100 µM) over periods of 1-6 days. Optical density from the MTT assay is plotted against time with medium as control. Results represent mean of three separate experiments ± SEM.

With continuous treatment it would appear that $[Fe_2L_3]^{4+}$ and cisplatin have a very similar effect on the cells, causing their numbers to remain constant for approximately 24 hours, then to decrease rapidly, followed by a plateau in cell density at ~ 96 hours. The control shows a steady increase in cell number over the time period of the incubation.

Figure 4. 20 shows the dramatic change seen after three hours incubation with $[Fe_2L_3]^{4+}$ (100 µM) or cisplatin (100 µM), followed by incubation with medium only for a further 1-6 days (see section 2.5.8).

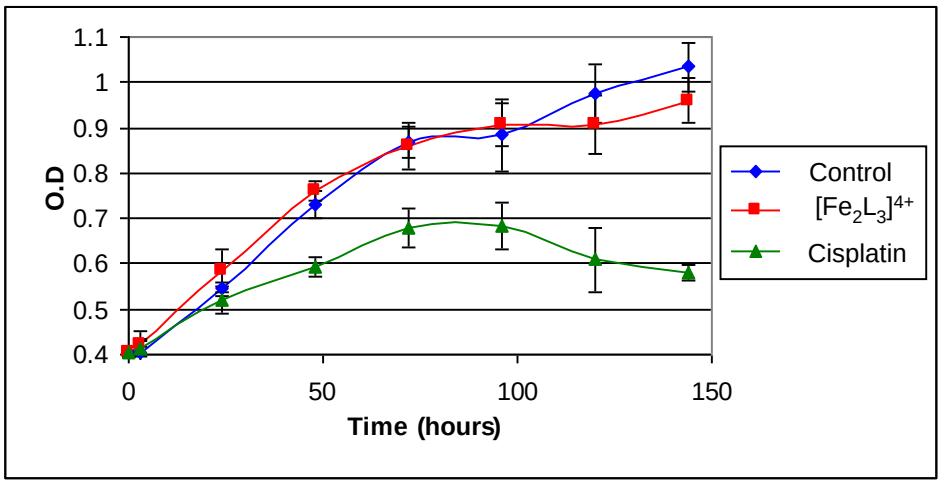

Figure 4. 20 Treatment of MDA-MB-231 cells with $[Fe_2L_3]^{4+}$ and cisplatin (100 µM) over a period of three hours, followed by incubation with medium only for a period of 1-6 days. Optical density from the MTT assay is plotted against time with medium as control. Results represent mean of three separate experiments ± SEM.

$[Fe_2L_3]^{4+}$ treated cells recover to almost equal density of the control, showing that the change in morphology seen previously is not permanent, that $[Fe_2L_3]^{4+}$ must be present in order to exert an effect and can be washed from the cell. Recovery to a normal cellular phenotype is also observed under a light microscope. Cisplatin treated cells are able to recover to some extent, however cell density declines again after ~96 hours.

4.2.8 Recovery of Cells after 18 Hour Incubation with $[Fe_2L_3]^{4+}$

With recovery from the three hour, membrane ruffling phase clearly possible, the question remains as to whether cells are able to recover from the 18 hour time point, Figure 4. 21 (see section 2.5.8). At this stage the cells are no longer dividing, balled up and completely stationary. (This phenotype persists throughout the remainder of the continuous incubation experiments).

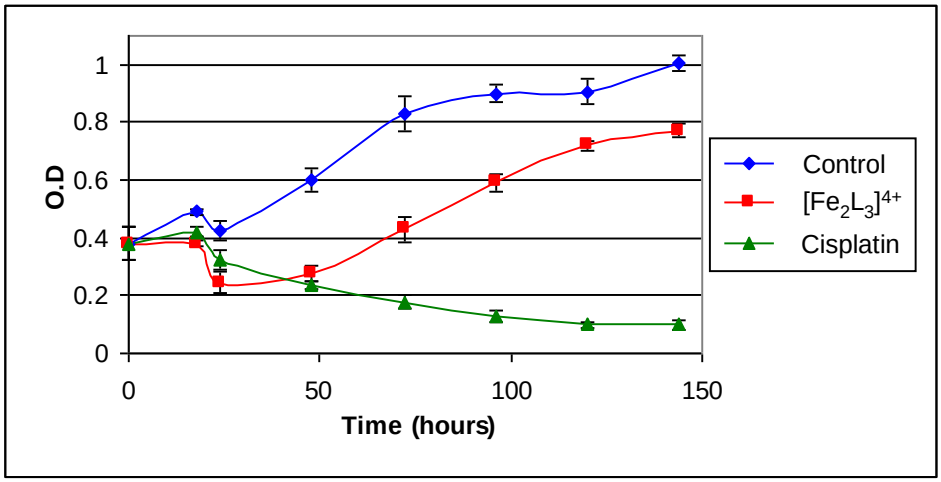

Figure 4. 21 Treatment of MDA-MB-231 cells with $[Fe_2L_3]^{4+}$ and cisplatin (100 µM) over a period of 18 hours, followed by incubation with medium only for a period of 1-6 days. Optical density from the MTT assay is plotted against time with medium as control. Results represent mean of three separate experiments ± SEM.

It is clear that cells incubated with $[Fe_2L_3]^{4+}$ are able to recover, and continue to replicate at a similar rate to control cells, however, some cells were clearly killed during the incubation period and cell density never reaches that of the control. Recovery to a normal cellular phenotype can also be seen under a light microscope. Cisplatin treated cell density declines throughout.

These results give further indication that $[Fe_2L_3]^{4+}$ activity may be caused via disruption of a number of cell signalling processes and a continuous presence of the drug is needed in order to block signalling pathways. This does not, however, rule out DNA binding as a mode of action, but more likely confirms that there is more than one mode of action, and that $[Fe_2L_3]^{4+}$ can be easily washed from the cell.

4.3 Conclusions and Further Work

In this study, the effects on the breast cancer cell line, MDA-MB-231 of the cylindrical, di-iron tetracationic drug candidate, $[Fe_2L_3]^{4+}$, were investigated. A toxicity study, using IC_{50} value, showed that observed cellular toxicity relates to the overall amount of compound (number of moles) rather than the concentration. This is an exciting result, and this phenomenon has not previously been documented.

Further differences between $[Fe_2L_3]^{4+}$ and cisplatin are documented through changes to morphology and phenotype of cells, as well as the ability of cells to recover with removal of $[Fe_2L_3]^{4+}$. This can give clues about potential modes of action, in this case relating to cell signalling and the actin cytoskeleton.

Time course experiments show that $[Fe_2L_3]^{4+}$ enters the cell and exerts its activity over the first 72 h, but thereafter its activity declines. This may be useful in the clinic as it could allow same-dose readministration.

The mechanism of entry and exact mode of action of $[Fe_2L_3]^{4+}$ needs to be investigated further. It would be beneficial to carry out the experiments described in this chapter with the analogous ruthenium cylinder $[Ru_2L_3]^{4+}$, as this drug compound has a different spectrum of activity yet very similar DNA binding interactions to $[Fe_2L_3]^{4+}$.

4.3.1 Impact on *In Vitro* drug assays

Significantly, these results demonstrate that methods currently employed to assess toxicity of new drug candidates may not be appropriate for non-covalent binding drugs or drugs with an unknown mode of action, unless careful consideration is paid to incubation time and volume. Promising non-covalent drug activity may be missed if the time point and volume selected for an IC_{50} assay are inadvertently inappropriate for that compound. Another example of this is that of the phase (II) clinical trial drug NAMI-A, which exhibits selective metastases inhibition *in vivo* and *in vitro* invasion inhibition, both unrelated to cellular cytotoxicity.[17] The results presented here have implications for the way *in vitro* toxicity testing is used to assess novel non-covalent DNA-binding drugs.[18]

4.4 References

[1] M. J. Hannon, V. Moreno, M. J. Prieto, E. Molderheim, E. Sletten, I. Meistermann, C. J. Isaac, K. J. Sanders and A. Rodger, *Angew. Chem., Intl. Ed.*, 2001, **40**, 879-884.

[2] R. M. Korah, V. Sysounthone, Y. Golowa and R. Wieder, *Cancer Res.*, 2000, **60**, 733-740.

[3] Y. Uno and M. Morita, *Mutat. Res*., 1993, **4**, 269-75.

[4] C. Sanchez-Cano, PhD Thesis, University of Birmingham, 2009.

[5] A. C. G. Hotze, N. J. Hodges, R. E. Hayden, C. Sanchez-Cano, C. Paines, N. Male, M-K. Tse, C. M. Bunce, J. K. Chipman and M. J. Hannon, *Chemistry & Biology*, 2008, **15**, 1258-1267.

[6] *Cisplatin Chemistry and Biochemistry of a Leading Anticancer Drug*, ed. B. Lippert, Wiley-VCH, 1999.

[7] G. V. Kalayda, B. A. J. Jansen, C. Molenaar, P. Wielaard, H. J. Tanke and J. Reedijk, *J. Biol. Inorg. Chem*., 2004, **9**, 414-422.

[8] *Molecular Biology of the Cell*, ed. B. Alberts, A. Johnson, J. Lewis, M. Raff, K. Roberts and P. Walter, Garland Science, Taylor & Francis group, 2008.

[9] D. Wang and S. J. Lippard, *Nat. Rev. Drug Discov.*, 2005, **4**, 307-320.

[10] G. Majno and I. Joris, *Am. J. Pathol*., 1995, **146**, 3-15.

[11] P. J. Bednarski, R. Grunert, M. Zielzki, A. Wellner, F. S. Mackay and P. J. Sadler, *Chemistry & Biology*, 2006, **13**, 61–67.

[12] *The Molecular Biology of Cancer*, ed. S. Pelengaris and M. Khan, Blackwell, 2006.

[13] G. Powis, *Pharmacology and Therapeutics*, 1994, **62**, 57-9.

[14] G. Sava, F. Frausin, M. Cocchietto, F. Vita, E. Podda, P. Spessotto, A. Furlani, V. Scarcia and G. Zabucchi, *Eur. J. Cancer*, 2004, **40**, 1383-1396.

[15] A. Bergamo, A. Masi, P. J. Dyson and G. Sava, *Int. J. Oncology*, 2008, **33**, 1281-1289.

[16] J. M. Brown, *Oncol. Res.*, 1997, **9**, 213-215.

[17]A. Bergamo, B. Gava, E. Alessio, G. Mestroni, B. Serli, M. Cocchietto, S. Zorzet, G. Sava, *Int. J. Oncology*, 2002, **21**, 1331-1338.

[18] A. J. Pope, C. Bruce, B. Kysela and M. J. Hannon, *Dalton Trans.*, 2010, **39**, 2772-2774.

Chapter 5

In Vitro Studies of Double Stranded Ruthenium Supramolecular Cylinders

Original synthesis and characterisation of the range of complexes discussed in this chapter was carried out by Dr A. Hotze, University of Birmingham.

Ligands and metal complexes were remade for all biological testing discussed in this chapter.

5.1 Introduction

This chapter details mutagenicity, toxicological and cellular studies of the unsaturated ruthenium(II) isomeric complexes; ββ-, γγ-$[Ru_2L^2{}_2Cl_2]$ and ββ-$[Ru_2L^2{}_2(NO_3)_2]$, where L^2 is the bis pyridyl azo ligand $C_{23}H_{18}N_6$, Figure 5. 1. Due to the wide range of cytotoxicities and the promising anticancer activity of a number of these complexes[1] further biological studies are warranted. With a cisplatin style of coordinative DNA interaction combined with the supramolecular size and helical nature of the ruthenium triple stranded $[Ru_2L_3]^{4+}$ complex (discussed in chapter 3) the unsaturated ruthenium complexes discussed herein bridge the fields of supramolecular architecture and anticancer drug design.

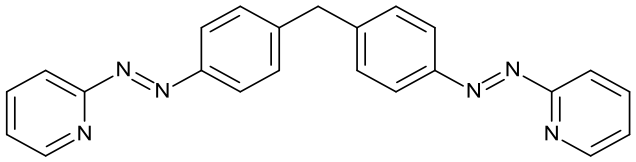

Figure 5. 1 The bis pyridyl azo ligand, L^2 used in the synthesis of ruthenium complexes. Hydrogen atoms have been omitted for clarity.

An optimised route to the synthesis of ligand L^2 will be discussed, as this is a complex synthesis involving a number of steps. Also, some studies into the thermodynamics of isomerisation of these complexes will be detailed.

5.1.1 Mononuclear Ruthenium Azopyridine Complexes

Ruthenium is well suited to medicinal applications due to its low rate of ligand exchange, easily accessible oxidation states (Ru(II), (III) and (IV)) and its ability to mimic iron when binding to certain biological molecules.[2] For these reasons a number of ruthenium drug complexes have been synthesised to date. Most relevant to this chapter are the

ruthenium(II) isomeric complexes of the form $[RuL^{(azpy)}{}_2Cl_2]$ where $L^{(azpy)} = C_{11}H_9N_3$, Figure 5. 2, synthesised in the lab of Reedijk.

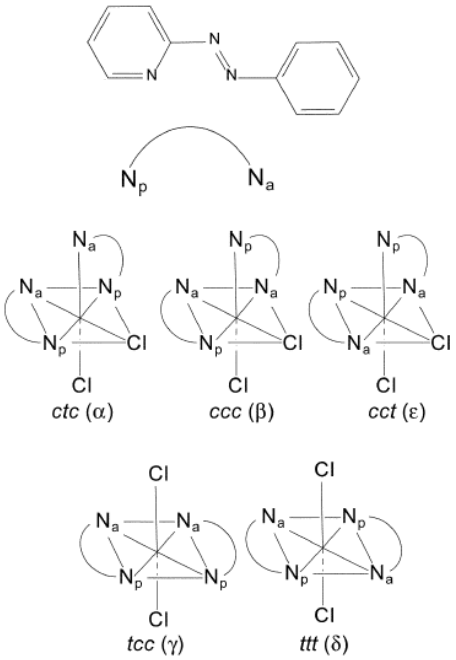

Figure 5. 2 Schematic diagram of ligand $L^{(azpy)}$ and the five theoretically possible isomers of the $[RuL^{(azpy)}{}_2Cl_2]$ complexes. The letters indicate Cl ligands, pyridine nitrogen atoms (N_p) and azo nitrogen atoms (N_a) respectively. [3]

There exist five possible geometric isomers labelled according to literature,[3] with the structure of the α, β, γ and δ isomers having been confirmed by X-ray crystallography and NMR. The final isomer (ε) was found to be unstable.[3] The anticancer properties of the α, β and γ isomers have been evaluated, with several displaying higher activity than cisplatin. Furthermore, it was determined that contrary to traditional belief, it is not necessary for these complexes to have the chloride ligands in a *cis* position in order for them to display anticancer activity. This is demonstrated by the γ isomer displaying higher cytotoxicity in all cell lines tested, Table 5. 1. This was an important structure activity relationship discovery for this range of complexes, the molecular reasons for which are still under investigation.[4]

	A498	EVSA-T	H226	IGROV	M19	MCF-7	WIDR
α-[$RuL^{(azpy)}_2Cl_2$]	0.27	0.063	0.48	0.27	0.064	0.27	0.27
β-[$RuL^{(azpy)}_2Cl_2$]	8.8	0.96	13.3	3.4	0.75	6.23	11.4
γ-[$RuL^{(azpy)}_2Cl_2$]	0.20	0.019	0.17	0.041	0.017	0.052	0.065
Cisplatin	7.5	1.4	10.9	0.6	1.9	2.3	3.2

Table 5. 1 IC_{50} values (μM) of several isomers of [$RuL^{(azpy)}_2Cl_2$] and cisplatin against a panel of tumour cell lines.[4]

5.1.2 Unsaturated Dinuclear Ruthenium Helicates

Five dinuclear isomers of the complex [$Ru_2L^2_2Cl_2$], Figure 5. 3 have been previously synthesised in the Hannon group. It was anticipated, based on the mononuclear counterparts and steric constraints that only the α, β and γ isomers could exist. Indeed the dinuclear γγ, γα, γβ, αα and ββ, isomers have been synthesised.[1,5]

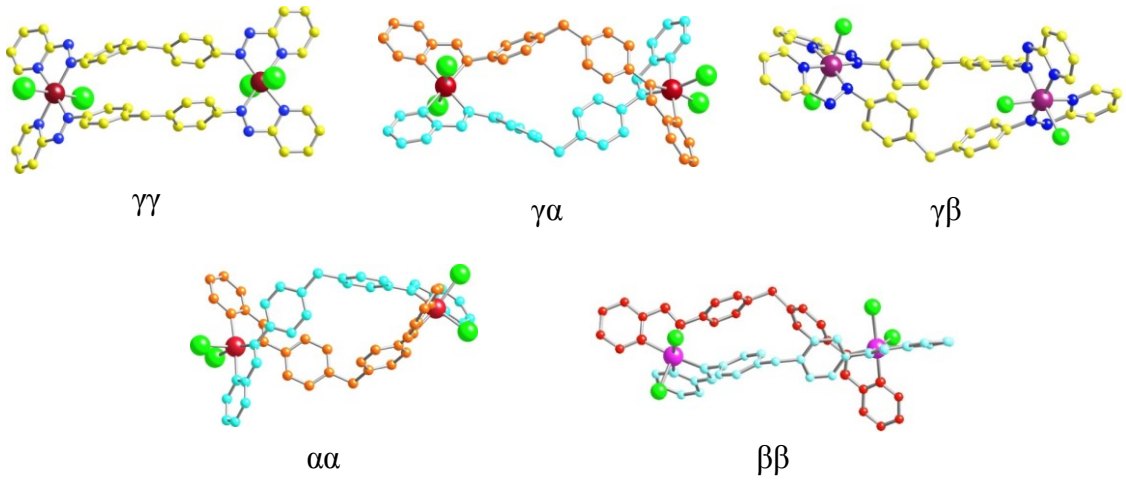

Figure 5. 3 Crystal structures of [$Ru_2L^2_2Cl_2$] isomers synthesised in the Hannon group. Hydrogen atoms have been omitted for clarity.

The γγ complex is not helical, but shows a metallo-cyclophane structure.[1] The remaining four complexes are double-helicates, with the γα and γβ complexes being a new class of helix where the chiral twist is induced by only one of the metal centres (the α/β centre). The αα isomer is a more typical helix, with both metals displaying the same chirality. Finally, the crystal structure of the ββ complex shows an asymmetrical double helical structure. This may be an artefact of crystal packing as a solvent molecule resides near the phenyl rings.[5]

The poor solubility of the above complexes led to the synthesis of the water soluble ββ-$[Ru_2L^2_2(NO_3)_2]$ analogue, Figure 5. 4, through replacement of the chloride ions.

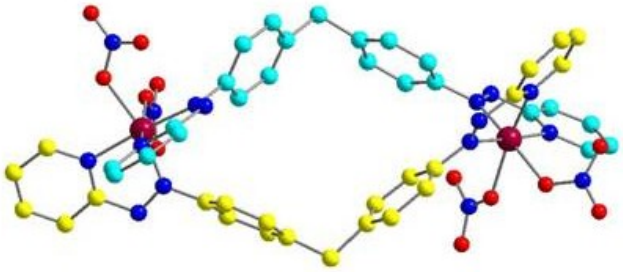

Figure 5. 4 Crystal structure of the ββ-$[Ru_2L^2_2(NO_3)_2]$ complex. Hydrogen atoms are omitted for clarity.[5]

In this structure both ligands have a roof type arrangement and there is monodentate coordination of the NO_3 moieties through an oxygen atom. The chloride to nitrate ligand exchange was only carried out with the ββ isomer, reasons for which will be discussed later in this chapter.

5.1.2.1 Biological Studies of Unsaturated Dinuclear Ruthenium Helicates

Due to the low water solubility and neutral charge of the chloride complexes, no DNA binding interactions were observed. However, CD and LD DNA binding studies were

possible with the water soluble ββ-[$Ru_2L^2_2(NO_3)_2$] complex, revealing weak CD interactions with a decrease in both DNA bands, similar to those observed for transplatin[6] (but less severe). LD interactions indicated some binding and bending/coiling of the DNA strand. B-DNA conformation was retained throughout both CD and LD titrations.[5] ββ-[$Ru_2L^2_2(NO_3)_2$] was incubated with the model base 9-ethylguanine followed by ESI mass spectrometry analysis. This revealed the formation of the mono-adducts ββ-[(9-Etgua$_{-H}$)$Ru_2L^2_2$], ββ-[(9-Etgua)$Ru_2L^2_2(H_2O)_2$] and the bis-adduct ββ-[$(9\text{-Etgua})_2Ru_2L^2_2$].[5] It is assumed that the bis-adduct is due to the coordination of one model base per ruthenium atom, as in the mononuclear case coordination of only one model base is possible due to steric constraints.[4] All these studies suggest binding of ββ-[$Ru_2L^2_2(NO_3)_2$] in the major groove of DNA along with some coordinative binding.

The cytotoxicities of the dinuclear ruthenium complexes along with their mononuclear counterparts are shown in Table 5. 2 against the ovarian cancer cell line A2780-P and the cisplatin resistant cell line, A2780-R.

	A2780-P (μM)	A2780-R (μM)	R_f
γγ-$[Ru_2L^2{}_2Cl_4]$	0.08	0.07	0.88
γα-$[Ru_2L^2{}_2Cl_4]$	0.36	4.9	13.6
γβ-$[Ru_2L^2{}_2Cl_4]$	2.07	3.9	1.9
ββ-$[Ru_2L^2{}_2Cl_4]$	Not active	Not active	-
ββ-$[Ru_2L^2{}_2(NO_3)_4]$	1.2	8.2	6.8
α-$[RuL^{(azpy)}{}_2Cl_2]$	0.85	0.98	1.2
β-$[RuL^{(azpy)}{}_2Cl_2]$	1.9	8.9	4.7
β-$[RuL^{(azpy)}{}_2(NO_3)_2]$	9.7	12.1	1.2
cisplatin	2.9	20	6.9

Table 5. 2 IC_{50} values (μM) of γγ-, γα-, γβ-, ββ-$[Ru_2L^2{}_2Cl_4]$ and ββ-$[Ru_2L^2{}_2(NO_3)_4]$ with mononuclear counterparts and cisplatin as reference compounds in the A2780-P/R ovarian cancer cell lines with resistance factors (R_f = IC_{50} A2780-R/ IC_{50} A2780-P). [4, 5, 7]

The cytotoxicities of the γγ and γα complexes are very high and all complexes, excluding the ββ-Cl_4 complex, show lower IC_{50} values (higher activity) than cisplatin. It is also interesting to note that the γγ- and γβ- compounds have an R_f factor of less than 2, indicating these complexes may not be susceptible to the resistance mechanisms present in the A2780-R cell line. The spectrum of activities of the dinuclear compounds are very similar to those of the mononuclear counterparts.[7] The only notable difference is the ββ-Cl_4 complex, where the mononuclear isomer shows good activity, although being a factor of 10 less active than the other mononuclear compounds.[4]

5.2 Results and Discussion

5.2.1 Synthesis and Isomerisation Studies

The synthesis of the bispyridyl azo ligand was carried out according to published methods (see section 2.3.1) and purified via an optimised isocratic HPLC method with a 10 % water, 90 % methanol solvent system.

An attempt was made to remove the chloride ligands from the γγ-$[Ru_2L^2{}_2Cl_4]$ isomer however this was not possible at temperatures lower than ~ 40 °C. It is hypothesised that this is due to the *trans* orientation of the chlorides which has also been documented for the mononuclear counterparts.[8] Above this temperature a change of colour is observed from green to blue. This was further investigated to see if it was an isomerisation process. It was found that 100 % isomerisation to the ββ isomer had occurred. This isomerisation process can be carried out at 40 ºC for a number of days or through reflux in a high boiling point solvent for a few hours. In the mononuclear case isomerisation to a β isomer is also observed above 40 ºC.[9] This shows that in this case the ββ-$[Ru_2L^2{}_2Cl_4]$ isomer is the thermodynamically favoured product.

The only reported isolation of the αα-$[Ru_2L^2{}_2Cl_4]$ isomer was on a single occasion after standing the γα-$[Ru_2L^2{}_2Cl_4]$ isomer in an NMR tube at room temperature. In order to investigate this isomerisation process further, the reaction of a 40 μM sample was followed by UV-Visible spectroscopy. At room temperature no change was observed however at 50 °C a colour change and a hypsochromic shift (to shorter wavelength) occurred. No isosbestic points were present in the spectrum, however, showing it is unlikely that full isomerisation to the αα-$[Ru_2L^2{}_2Cl_4]$ isomer has occurred, Figure 5. 5.

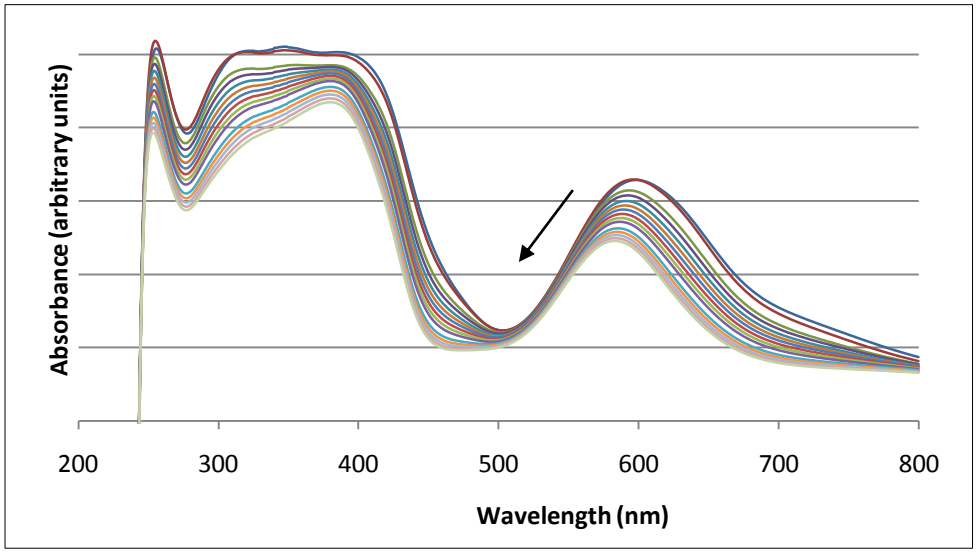

Figure 5. 5 UV-Visible spectra of 40 μM γα-[$Ru_2L^2{}_2Cl_4$] in deuterated chloroform every hour over 18 hours at 50 °C.

Unfortunately, when this reaction was scaled up in order to obtain enough sample for NMR characterisation, no change in compound was seen. Thus the αα-[$Ru_2L^2{}_2Cl_4$] isomer may only be stable under certain conditions.

5.2.2 *In Vitro* DNA Binding Studies of ββ-[$Ru_2L^2{}_2(NO_3)_4$]

It is clear from previous CD, LD and model base studies that the ββ-[$Ru_2L^2{}_2(NO_3)_4$] complex binds to naked DNA in a covalent manner[5], therefore the next step is to consider the DNA binding in live cells. This could clarify DNA binding as a potential mode of anticancer activity. A whole-cell Hoechst displacement assay (see section 2.5.4) was used to assess if ββ-[$Ru_2L^2{}_2(NO_3)_4$] was able to enter live cells and bind to nuclear DNA, Figure 5. 6.

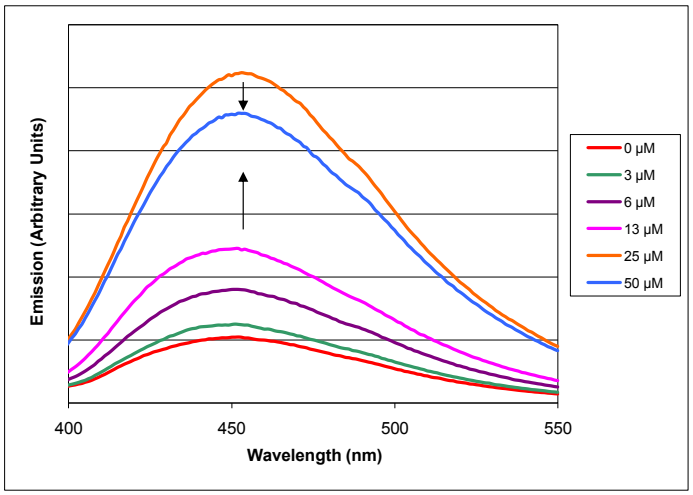

Figure 5. 6 Emission of 10 µM Hoechst- 33258 with HL-60 cells when treated with varying concentrations of ββ-[$Ru_2L^2_2(NO_3)_4$]. λ exc. = 350 nm.

This test involved the preloading of HL-60, a human myeloid leukaemia cancer cell line, selected as it can be grown in suspension rather than as an adherent cell line, with 10 µM Hoechst- 33258, a minor groove DNA binder. Following this incubation, varying concentrations of ββ-[$Ru_2L^2_2(NO_3)_4$] were added and the resulting Hoechst fluorescence measured. After excitation at 350 nm, an emission centred at 450 nm is expected for Hoechst bound to DNA. If the Hoechst molecule is ejected from DNA through competitive binding of another agent, the resulting emission at 450 nm will decrease. It would therefore be expected that the more ββ-[$Ru_2L^2_2(NO_3)_4$] that binds to DNA, the more Hoechst will be ejected and the resulting emission at 450 nm will decrease. Figure 5. 6 clearly indicates that increasing the concentration of ββ-[$Ru_2L^2_2(NO_3)_4$] incubated with the cells causes an increase in Hoechst emission. This increase is seen up to a ββ-[$Ru_2L^2_2(NO_3)_4$] concentration of 25 µM, the opposite response to that expected. At 50 µM ββ-[$Ru_2L^2_2(NO_3)_4$] the emission is lowered. It should be noted, however, that ruthenium absorbs in the excitation region of this assay, which may affect the results observed.

In order to test the interaction between ββ-$[Ru_2L^2_2(NO_3)_4]$ and Hoechst, without the presence of DNA, a 10 μM solution of Hoechst was incubated with increasing concentrations of ββ-$[Ru_2L^2_2(NO_3)_4]$, Figure 5. 7.

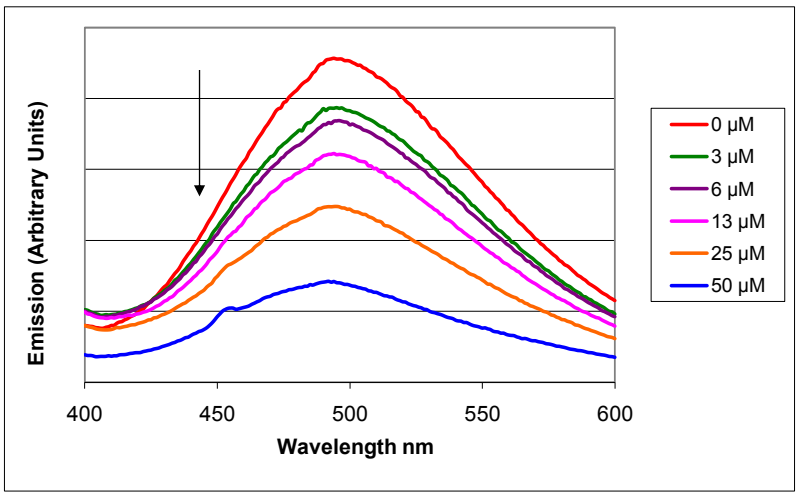

Figure 5. 7 Emission of 10 μM Hoechst with varying concentrations of ββ-$[Ru_2L^2_2(NO_3)_4]$. λ exc. = 350 nm.

500 nm is the emission wavelength expected for free Hoechst, and it was found that increasing concentrations of ββ-$[Ru_2L^2_2(NO_3)_4]$ quenches the Hoechst emission.

It appears that ββ-$[Ru_2L^2_2(NO_3)_4]$ is increasing the amount of Hoechst bound to nuclear DNA within the HL-60 cells. The exact mechanism of this interaction is still under investigation, however one hypothesis is that the ββ-$[Ru_2L^2_2(NO_3)_4]$ may be disrupting the cell membrane, allowing more Hoechst to enter the cell from solution and bind to nuclear DNA. At a ββ-$[Ru_2L^2_2(NO_3)_4]$ concentration of 50 μM the decrease in emission intensity may be caused by complete disruption of the cell membrane, allowing Hoechst to be displaced from the DNA by ββ-$[Ru_2L_2(NO_3)_4]$ in solution.

5.2.3 Mutagenicity Studies of γγ-, ββ-$[Ru_2L^2{}_2Cl_4]$ and ββ-$[Ru_2L^2{}_2(NO_3)_4]$

The γγ-, ββ-$[Ru_2L^2{}_2Cl_4]$ and ββ-$[Ru_2L^2{}_2(NO_3)_4]$ isomers were tested for compound related mutagenicity using the Ames bacterial reverse mutation assay (see section 2.6). This range of complexes, representing the most and least cytotoxic as well as the water soluble derivative are important to investigate to confirm that activity is not accompanied by mutagenicity. In order to ensure a thorough investigation of mutagenic potential two *Salmonella* strains were used to test for frameshift (TA98 strain) and base pair/point mutations (TA100 strain). These bacterial strains carry a mutation which makes them unable to synthesise the amino acid histidine, which is essential for bacterial growth. Incubation with a mutagenic compound will reverse this inherent mutation, leading to the bacteria being able to synthesise histidine and hence grow (these bacteria are termed revertants). The test is extended to probe mutagenicity of potential *in vivo* products of metabolism by repeating experiments with an incubation step including activated rat liver S9 enzymes, a variety of mixed function oxidase enzymes.[10] The number of revertant bacterial colonies present after a 48 hour incubation period are counted and compared to both positive and negative controls. A mutagenic response is usually defined as a 2-3 fold increase in revertants relative to negative controls.[11]

Figure 5. 8 to Figure 5. 10 show the number of bacterial revertants after incubation with the three complexes for the salmonella typhimurium TA98 strain.

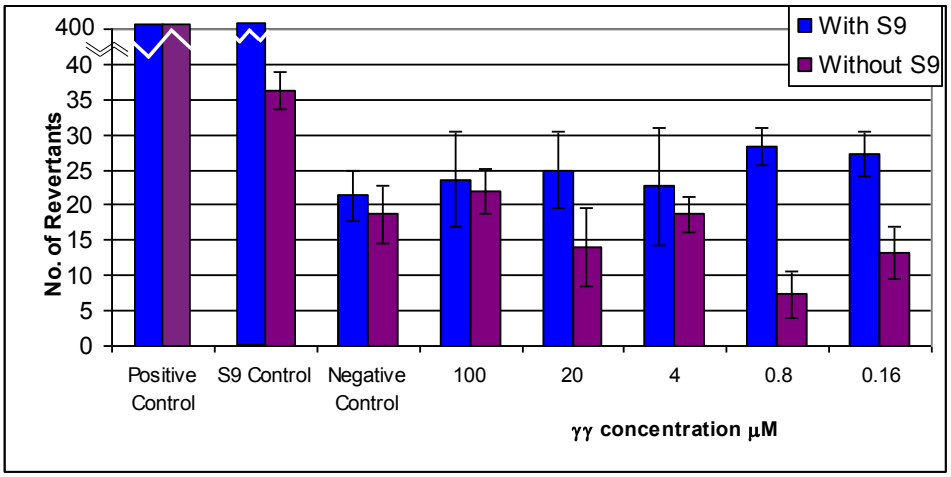

Figure 5. 8 Number of bacterial revertants of Salmonella typhimurium TA98 after incubation with varying concentrations of γγ-[$Ru_2L^2{}_2Cl_4$]. Results represent mean ± SEM. Positive control/Mutagen: 4-nitroquinoline-N-oxide. S9 control/Promutagen: chrysoidine Y. Negative control: PBS.

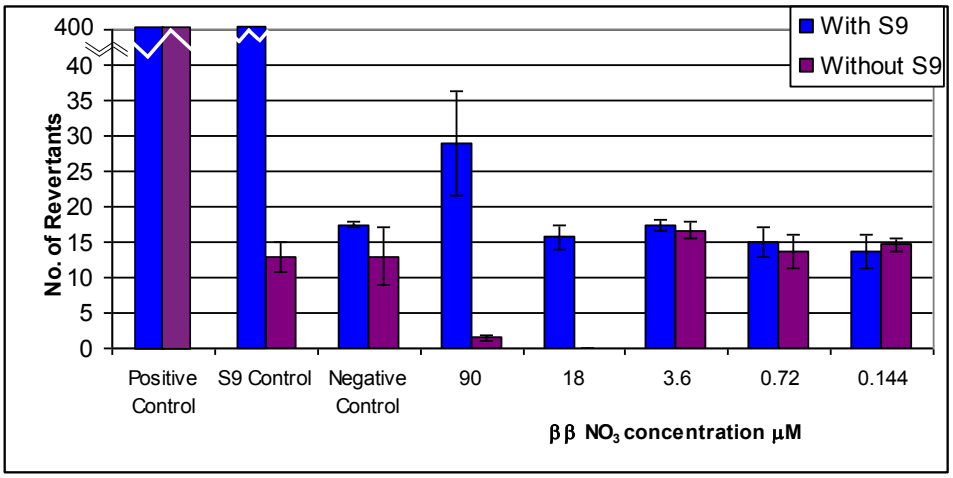

Figure 5. 9 Number of bacterial revertants of Salmonella typhimurium TA98 after incubation with varying concentrations of ββ-[$Ru_2L^2{}_2(NO_3)_4$]. Results represent mean ± SEM. Positive control/Mutagen: 4-nitroquinoline-N-oxide. S9 control/Promutagen: chrysoidine Y. Negative control: PBS.

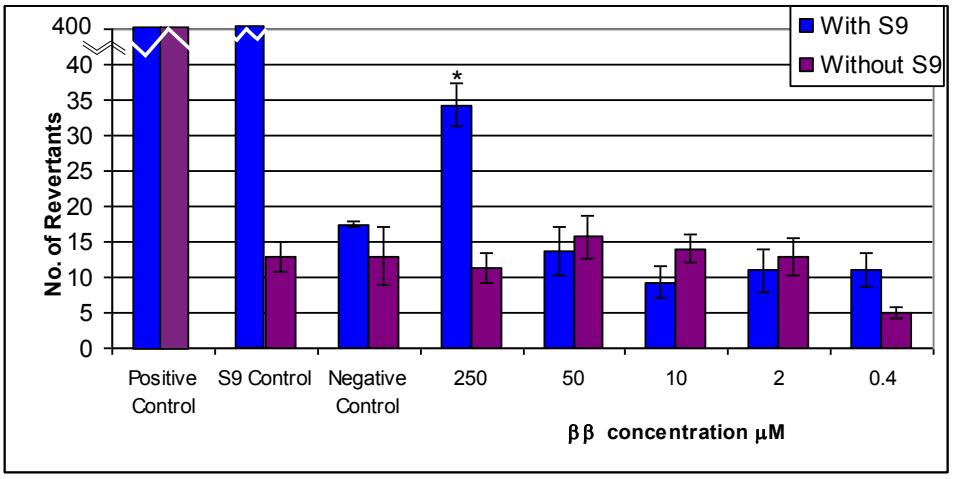

Figure 5. 10 Number of bacterial revertants of Salmonella typhimurium TA98 after incubation with varying concentrations of ββ-[$Ru_2L^2{}_2Cl_4$]. Results represent mean ± SEM. Positive control/Mutagen: 4-nitroquinoline-N-oxide. S9 control/Promutagen: chrysoidine Y. Negative control: PBS.

It is clear from all positive controls that the bacteria and S9 liver enzyme mix are functioning correctly with >400 revertants in each case. In conjunction with statistical ANOVA results to assess the significance of the data, mutagenicity of the complexes can be determined. Figure 5. 8 shows that γγ -[$Ru_2L^2{}_2Cl_4$] does not cause significantly more mutations than negative controls both with or without S9 activation, with p values of 0.93 and 0.24 respectively (when $p > 0.05$ shows no statistical significance). There is no dose response confirming that this compound is not a mutagen under these conditions.

From Figure 5. 9 it can be seen that ββ-[$Ru_2L^2{}_2(NO_3)_4$] (without S9 enzymes) is toxic (most/all bacteria are killed) at high doses. This is not the case in the presence of S9 enzymes and it is therefore probable that the complex binds to proteins/bio-molecules within the mixture or is chemically modified by the enzymes, so is unable to exert its

toxic effect on the bacteria. Again, with S9 a p value of 0.082 indicates no significance.

There is a small increase in mutagenicity in the presence of S9 enzymes for the highest dose of ββ-[$Ru_2L^2{}_2Cl_4$], Figure 5. 10, however a post-hoc students t-test showed this to be the only statistically significantly data point. Without S9 p = 0.966 confirming no dose response. It should be noted that the concentrations used were very high, and for the active compounds the dose incubated with the bacteria was far higher than the IC_{50} values of the complexes.

Figure 5. 11 to Figure 5. 13 show the number of bacterial revertants for the salmonella typhimurium TA100 strain. Values reported are higher than with the TA98 strain due to the naturally higher reversion frequency of the TA100 strain.[11]

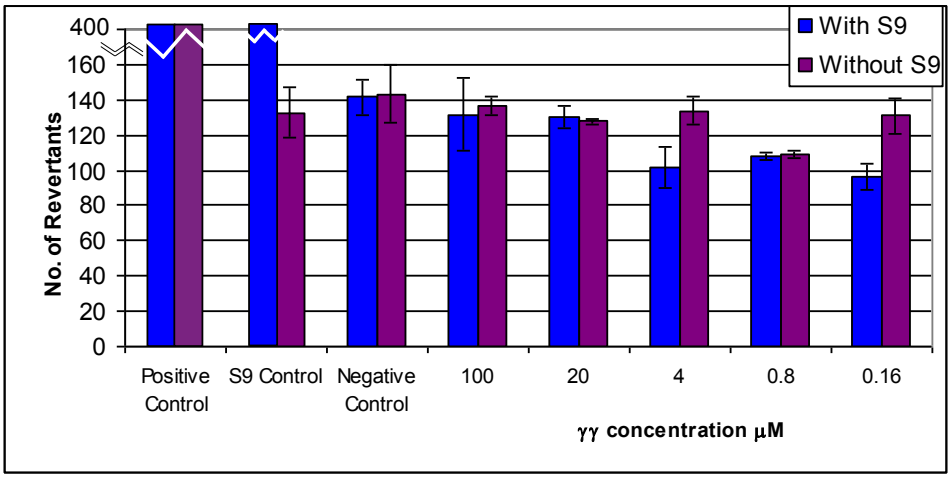

Figure 5. 11 Number of bacterial revertants of Salmonella typhimurium TA100 after incubation with varying concentrations of γγ-[$Ru_2L^2{}_2Cl_4$]. Results represent mean ± SEM. Positive control/Mutagen: Sodium Azide. S9 control/Promutagen: chrysoidine Y. Negative control: PBS.

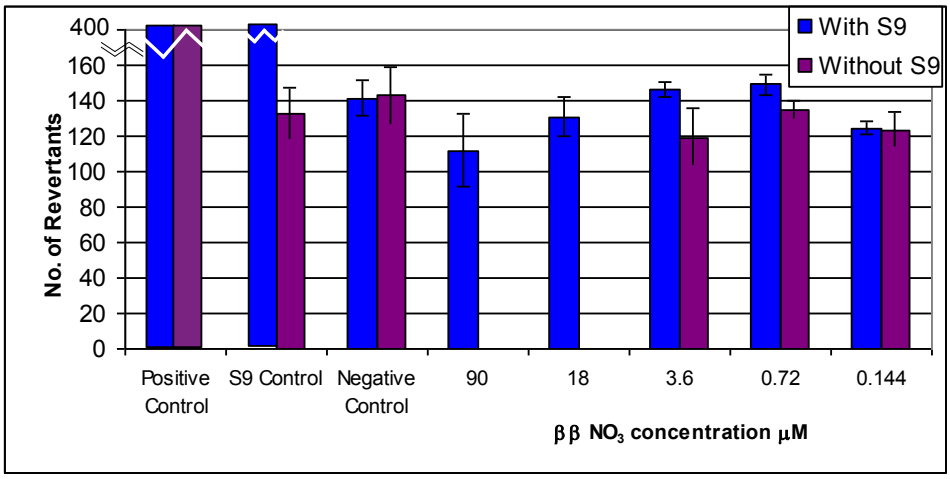

Figure 5. 12 Number of bacterial revertants of Salmonella typhimurium TA100 after incubation with varying concentrations of ββ-[$Ru_2L^2{}_2(NO_3)_4$]. Results represent mean ± SEM. Positive control/Mutagen: Sodium Azide. S9 control/Promutagen: chrysoidine Y. Negative control: PBS.

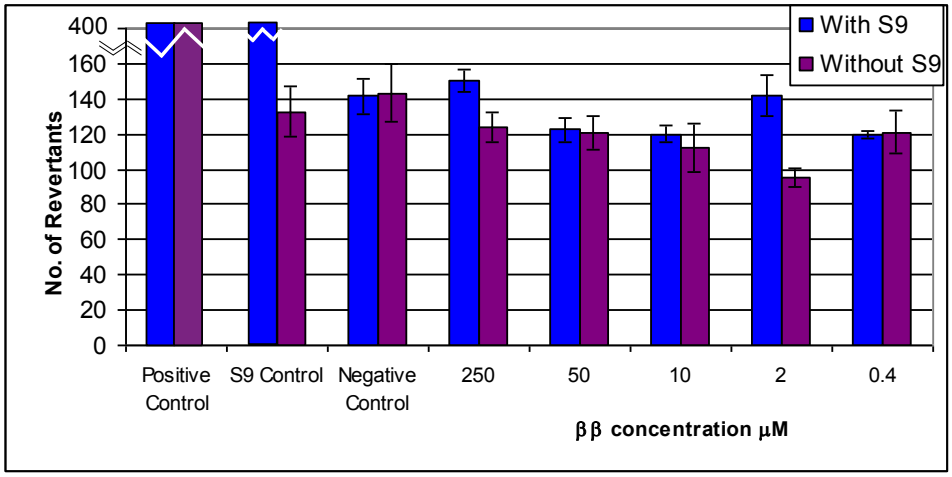

Figure 5. 13 Number of bacterial revertants of Salmonella typhimurium TA100 after incubation with varying concentrations of ββ-[$Ru_2L^2{}_2Cl_4$]. Results represent mean ± SEM. Positive control/Mutagen: Sodium Azide. S9 control/Promutagen: chrysoidine Y. Negative control: PBS.

As is the case for the TA98 strain, none of the complexes showed mutagenicity with or without S9 activation. For γγ-[$Ru_2L^2{}_2Cl_4$], p = 0.11 (with S9), 0.19 (without S9) and for ββ-[$Ru_2L^2{}_2(NO_3)_4$], p = 0.22 (with S9). Again, this complex was toxic to the

bacteria at the highest doses without S9. It is also interesting to note that with both bacterial strains, the only complex which indicated any likelihood of being mutagenic was the inactive ββ-$[Ru_2L^2_2Cl_4]$ compound in the presence of S9 where p = 0.045 (with S9), 0.19 (without S9).

From this data we can conclude that none of the active compounds cause point or frameshift mutations under these conditions. It has been established that compounds which do not exhibit activity in the Ames test are normally found to be non-carcinogenic[12] so this is an important result, as mutagenic potential is a huge clinical drawback of other covalent DNA binders such as cisplatin.

5.2.4 Genotoxicity Studies of γγ-$[Ru_2L^2_2Cl_4]$ and ββ-$[Ru_2L^2_2(NO_3)_4]$

Genotoxic potential (causing DNA strand breaks) is a major drawback of many current anticancer agents such as cisplatin. In order to assess the genotoxic potential of γγ-$[Ru_2L^2_2Cl_4]$ and ββ-$[Ru_2L^2_2(NO_3)_4]$, the alkaline comet assay was used to detect DNA single strand breaks in the human ovarian cancer cell line A2780 (see section 2.5.11). In this test, cells are incubated with compound, followed by cell lysis, DNA staining and electrophoresis. The larger the DNA 'comet' resulting from electrophoresis, the more DNA strand breaks are present. Figure 5. 14 and Figure 5. 15 show mean % tail intensity from comets for the compounds γγ-$[Ru_2L^2_2Cl_4]$ and ββ-$[Ru_2L^2_2(NO_3)_4]$.

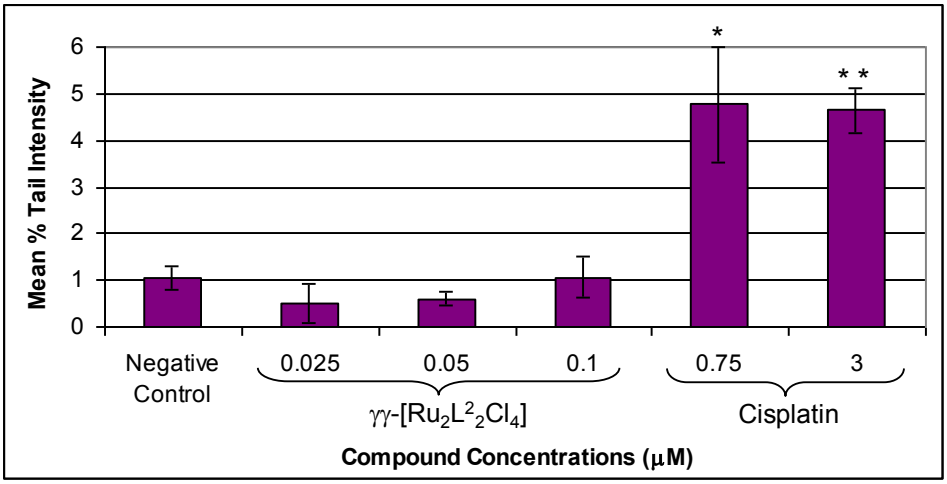

Figure 5. 14 Mean % tail intensity of comets from incubation of A2780 cells with γγ-[$Ru_2L^2{}_2Cl_4$] and cisplatin. Data represents mean of three independent experiments ± SEM. Negative control: DMEM medium.

Concentrations tested were up to the IC_{50} value of the complex. A one-way ANOVA to assess the significance of the dose response for γγ-[$Ru_2L^2{}_2Cl_4$] returned a p value of 0.53 and it is clear from Figure 5. 14 that mean % tail intensity is not significantly higher for γγ-[$Ru_2L^2{}_2Cl_4$] than for the negative control, indicating that treatment does not cause DNA single-strand breaks in this cell line. The negative control displayed is that of medium, but statistical tests were also repeated with DMSO (γγ-[$Ru_2L^2{}_2Cl_4$] solvent), showing no significance. The results displayed for cisplatin are the highest and lowest doses tested, and a p value of 0.017 indicates that this data is significant, with cisplatin causing a high number of DNA strand breaks in this cell line.

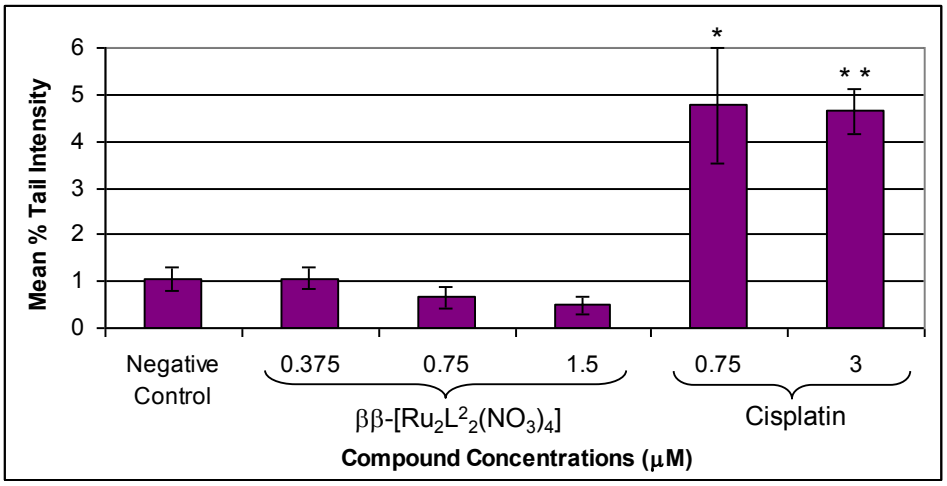

Figure 5. 15 Mean % tail intensity of comets from incubation of A2780 cells with ββ-[$Ru_2L^2_2(NO_3)_4$] and cisplatin. Data represents mean of three independent experiments ± SEM. Negative control: DMEM medium.

In the case of ββ-[$Ru_2L^2_2(NO_3)_4$] there is also no indication of direct DNA damage, with a one-way ANOVA p value of 0.28 indicating no significant dose response.

Negative activity in this test for both these cytotoxic compounds is another important result, as the potent genotoxicity of drugs in current clinical use is often responsible for the formation of secondary cancers (especially leukaemias).[13]

5.3 Conclusions and Further Work

Some of the synthetic strategies used to make this intriguing set of dinuclear ruthenium double stranded isomers have been investigated and it has been confirmed that, like the mononuclear counterparts, the ββ isomer is thermodynamically favoured over the γγ isomer.

Some very interesting results have been obtained with the water soluble, ββ-[$Ru_2L^2_2(NO_3)_4$] complex, a derivative of the original chloride compound. Results

show that the mechanism of action may be different to that initially expected, of covalent DNA binding. Results presented here may indicate that this compound is interacting with the cell membrane; however it is not known at this stage whether or not this is a contributing factor to cell death.

Furthermore, and possibly most importantly, mutagenicity and genotoxicity studies have shown that the highly anticancer active γγ-$[Ru_2L^2_2Cl_4]$ and ββ-$[Ru_2L^2_2(NO_3)_4]$ compounds are not mutagenic and do not cause DNA single strand breaks. These anticancer agents have been compared throughout to those of cisplatin, which although a successful agent in the clinic, does possess all these undesirable properties.

This range of ruthenium compounds, combining both a covalent cisplatin style of DNA binding with a supramolecular structure have not only improved anticancer activity in the cell lines tested, but have eliminated other negative effects responsible for a number of side effects in the clinic. This work is clearly an important step forward in the field of supramolecular anticancer drug design.

It is anticipated that further cell membrane studies with the ββ-$[Ru_2L^2_2(NO_3)_4]$ complex will generate interesting and important results. It is also necessary to compare these results to those of the original chloride complexes, to elucidate possible modes of action, as the interaction of ββ-$[Ru_2L^2_2(NO_3)_4]$ with Hoechst in live cells is a very interesting and unusual finding. It may also be beneficial to extend work carried out into mutagenicity of the ββ-$[Ru_2L^2_2(NO_3)_4]$ compound. This compound is toxic to the bacteria at the highest doses, however in the presence of S9 liver enzymes this is not the case, and the bacteria continue to grow at a background level. It would

be interesting to compare this result with cellular cytotoxicity of the compound after incubation with S9 enzymes to confirm whether cytotoxicity is also affected.

5.4 References

[1] A. C. G. Hotze, B. M. Kariuki, and M. J. Hannon, *Angew. Chem. Int. Ed*., 2006, **45**, 4839 –4842.

[2] C. S. Allardyce and P. J. Dyson, *Platinum Metals Rev.*, 2001, **45**, 62–69.

[3] A. H. Velders, K. van der Schilden, A. C. G. Hotze, J. Reedijk, H. Kooijman and A. L. Spek, *Dalton Trans.,* 2004, 448-455.

[4] A. C. G. Hotze, PhD Thesis, University of Leiden, 2003.

[5] A. C. G. Hotze , A. J. Pope, B. M. Kariuki and M. J. Hannon, unpublished work.

[6] J. P. Macquet and J. L. Butour, *Eur. J . Biochem.,* 1978, **83**, 375-387.

[7] A. C. G. Hotze, M. Bacac, A. H. Velders, B. A. J. Jansen, H. Kooijman, A. L. Spek, J. G. Haasnoot and J. Reedijk, *J. Med. Chem.,* 2003, **46**, 1743-1750.

[8] R. A. Krause and K. Krause, *Inorg. Chem.,* 1982, **21**, 1714-1720.

[9] A. C. G. Hotze, A. H. Velders, F. Ugozzoli, M. Biagini-Cingi, A. M. Manotti-Lanfredi, J. G. Haasnoot and J. Reedijk, *Inorg. Chem*., 2000, **39**, 3838-3844.

[10] B. M. Elliott, R. D. Combes, C. R. Elcombe, D. G. Gatehouse, G. G. Gibson, J. M. Mackay and R. C. Wolf, *Mutagenesis,* 1992, **7**, 175 -177.

[11] K. Mortelmas and E. Zeiger, *Mutat. Res.,* 2000, **455**, 29-60.

[12] *Biochemistry, Fifth Edition*, ed. J. M. Berg, J. L. Tymoczko and L. Stryer, W. H. Freeman & Company, 2002.

[13] *Cisplatin Chemistry and biochemistry of a leading anticancer drug*, ed. B. Lippert, Wiley-VCH, 1999.

Chapter 6

Design, Synthesis and Biological Studies of a Novel Ruthenium Supramolecular Cylinder

6.1 Introduction

This chapter details the molecular design, synthesis, characterisation, biophysical and *in vitro* studies of a dinuclear, helical ruthenium(II) complex containing bis-pyridyl-azo and bipyridine ligands; $[Ru_2L^2_2(bpy)_2]^{4+}$, where $L^2 = C_{23}H_{18}N_6$ and bpy = $C_{10}H_6N_2$, Figure 6. 1. This complex was designed to exhibit non-covalent DNA binding interactions and was synthesised via an optimised route from the biologically active unsaturated ruthenium(II) double stranded complex ββ-$[Ru_2L^2_2(NO_3)_4]$ (discussed in chapter 5).

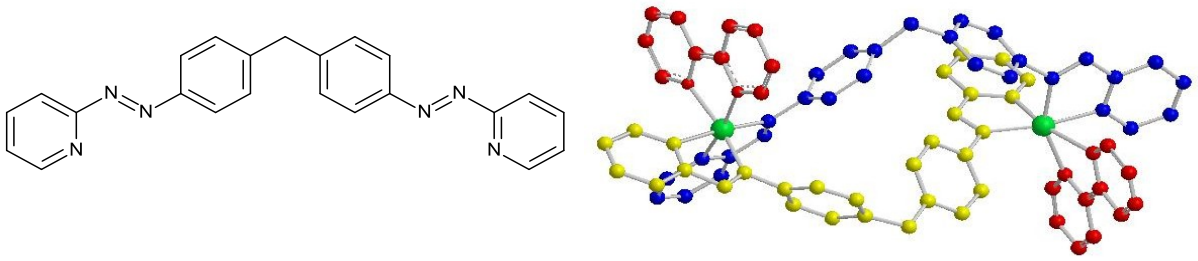

Figure 6. 1 Ligand L^2 and representation of the $[Ru_2L^2_2(bpy)_2]^{4+}$ cation discussed in this chapter.

Ruthenium compounds have been used in varied applications and have attracted much attention due to their diverse chemical and physical properties. There is a large amount of evidence to indicate cytotoxicity correlates with DNA binding[1,2,3,4] and in order to improve the performance of ruthenium drugs a number of ligand modifications have been made with the intention of changing the physical or biological properties. These include the attachment of carboxylato groups or extended aromatic surfaces[5] in order to, for example, change ligand exchange kinetics or solvation properties. Modifying the ligand surface of a known drug molecule in order to change its physical and biological properties is the approach used in this chapter.

6.1.1 Mononuclear Ruthenium Complexes

The mononuclear ruthenium(II) azpy complexes, $[Ru_2L^{(azpy)}{}_2Cl_2]$ Figure 6. 2 (also discussed in section 5.1.1), are a good example of how altering ligand surface can change important properties of the molecule. This range of compounds is also structurally related to the dinuclear compound discussed in this chapter. All mononuclear azpy complexes isolated displayed potent cytotoxicities.[6]

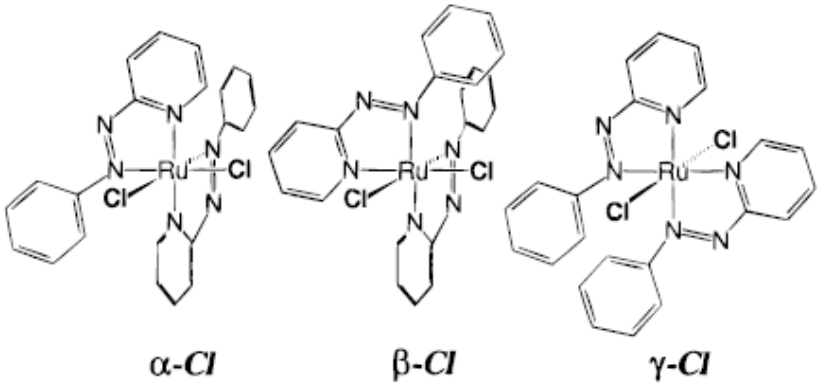

Figure 6. 2 Structures of the Δ enantiomers of α-, β- and γ-$[RuL^{(azpy)}{}_2Cl_2]$.[6]

The α isomer, with the Cl, N-pyridine and N-azo elements being *cis*, *trans* and *cis* respectively, (see nomenclature from chapter 5) is the most active complex, with cytotoxicities in the range 0.063-0.98 μM. The β isomer (Cl, N-pyridine and N-azo elements all *cis*) is the least active (0.75-11.4 μM) against the panel of tumour cell lines tested.[7] As is the case for the structurally similar complex *cis*-$[Ru(bpy)_2Cl_2]$,[8] steric constraints mean the coordination of only one guanine residue to each azpy complex is possible. Model-base adducts with α-$[RuL^{(azpy)}{}_2Cl_2]$ are kinetically more stable than with β-$[RuL^{(azpy)}{}_2Cl_2]$, suggesting that differing DNA binding abilities due to specific ligand orientations are a potential explanation as to why α is the most, and β the least active isomer.[9]

It has been shown with the mononuclear azpy complexes that exchanging the chloride ligands for other mono- or bidentate ligands can be used as a way of tailoring properties and refining structure activity relationships. In all cases the replacement of the chloride ligands caused an increase in IC_{50} value (decrease in cytotoxicity) of the complex, Table 6. 1. This can be useful in order to define the important features required for DNA binding and hence activity of complexes.

	A2780	A498
α-$[RuL^{(azpy)}_2Cl_2]$	0.85	0.27
α-$[RuL^{(azpy)}_2(NO_3)_2]$	8.5	-
α-$[RuL^{(azpy)}_2(ox)]$	6.3	-
α-$[RuL^{(azpy)}_2(mal)]$	7.9	-
α-$[RuL^{(azpy)}_2(bpy)]$	-	89.8
β-$[RuL^{(azpy)}_2Cl_2]$	1.9	8.8
β-$[RuL^{(azpy)}_2(NO_3)_2]$	9.7	-
β-$[RuL^{(azpy)}_2(bpy)]$	-	92.0
$[RuL^{(azpy)}_3]$	-	55.4
$[RuL^{(azpy)}(bpy)_2]$	-	77.8
Cisplatin	2.3	7.5

Table 6. 1 IC_{50} values (μM) of mononuclear ruthenium(II) complexes with cisplatin as reference in the A2780-P ovarian and A498 renal carcinoma cell lines. (ox = oxalate, mal = malonate, bpy = 2, 2-bipyridine) (-) indicates complex not tested in this cell line.[7]

In the ovarian cell line A2780-P, the cytotoxicity of the α isomer was reduced from 0.85 μM to 8.5 μM with the addition of two nitrate moieties, to 6.3 μM with the addition of an

oxalate anion and to 7.9 μM with the addition of a malonate. The β isomer similarly showed a reduction in cytotoxicity from 1.9 μM for the parent chloride complex to 9.7 μM for the nitrate complex.[7] It should also be noted, however, that removing the chloride ligands also dramatically increases the solubility of these compounds in aqueous media-a desirable property.

A further example utilising the bipyridine ligand is that of the mononuclear mer-$[RuL^{(azpy)}_3]$. The IC_{50} of this complex is 55.4 μM in the A498 cell line. This is increased to 77.8 μM for the complex $[RuL^{(azpy)}(bpy)_2]$ and further to 89.8 μM for the complex α-$[RuL^{(azpy)}_2(bpy)]$. β-$[RuL^{(azpy)}_2(bpy)]$ has the highest IC_{50} of this range of complexes at 92.0 μM[7]

6.1.2 Ruthenium Helicates

There have been a limited number of ruthenium helicates synthesised to date, the most relevant of which are those published by the Hannon group.[1] The single stranded Ru(II) complex, $[Ru_2L(bpy)_4]^{4+}$ [10]where L = $C_{25}H_{20}N_4$, Figure 6. 3, has two bipyridine moieties on each ruthenium centre.

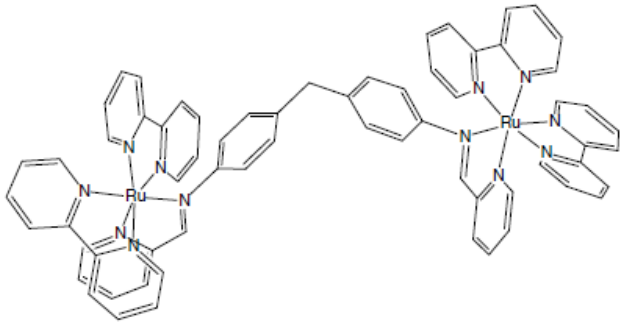

Figure 6. 3 Representation of the $[Ru_2L(bpy)_4]^{4+}$ cation. Hydrogen atoms and anions are omitted for clarity.[10]

The DNA binding of the enantiomers of this complex were investigated using circular dichroism and fluorescent displacement assays. Results showed that the complex has a bending effect (possibly through electrostatic binding outside of the grooves) which causes the DNA to coil.[10] This compound is inactive against cancer cell lines, an interesting result which will be discussed later in this chapter.

A further supramolecular, helical complex is the triple stranded, di-ruthenium(II) complex; $[Ru_2L_3]^{4+}$ [11] where L = $C_{25}H_{20}N_4$, Figure 6. 4 (also discussed in chapters 1 and 3).

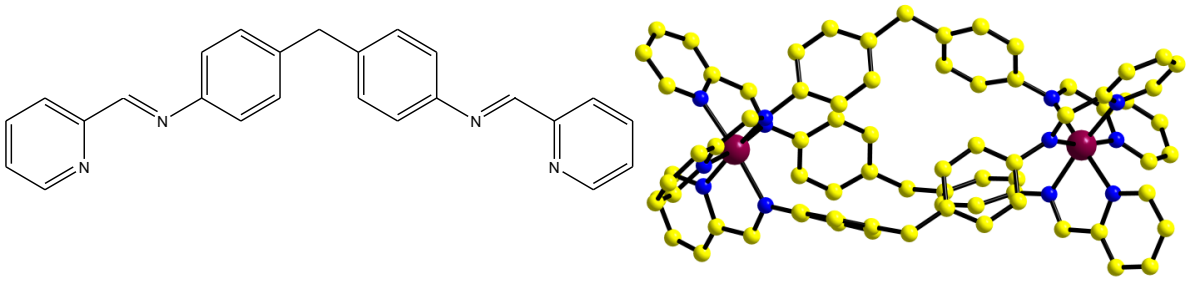

Figure 6. 4 Ligand L and X-Ray crystal structure of the $[Ru_2L_3]^{4+}$ cation. Hydrogen atoms and anions are omitted for clarity.[12]

This cylinder is based on the parent iron(II) triple stranded complex, $[Fe_2L_3]^{4+}$ (also discussed in chapters 1, 3 and 4) and indeed the structures are almost identical, Figure 6. 5. The central iron(II) atoms were replaced with ruthenium(II) in order to benefit from the extra stability and photophysical properties of these metal centres.

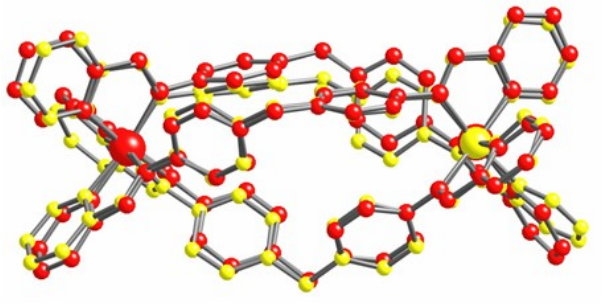

Figure 6. 5 Comparison of X-ray crystal structures of ruthenium (yellow) and iron (red) supramolecular cylinders.[12]

$[Ru_2L_3]^{4+}$ displays very strong DNA binding and DNA coiling as well as a fluorescence response upon DNA binding.[12] It also displays some anticancer activities within the range of cisplatin.[11] Interestingly however its anticancer activity is restricted to breast cancer cell lines and the complex shows limited activity in any of the ovarian cancer cell lines tested.[13]

6.2 Results and Discussion

6.2.1 Molecular Design Approach

The target complex lies (in design) between the single and triple stranded dinuclear ruthenium(II) complexes discussed above. It is a dinuclear double stranded complex with additional blocking ligands completing the coordination sphere of each ruthenium(II) centre, Figure 6. 6.

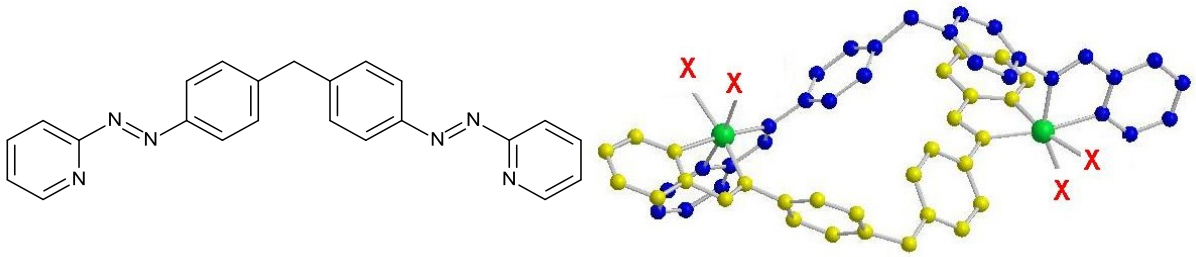

Figure 6. 6 Ligand L^2 and representation of the desired structure, $[Ru_2L^2{}_2(X)_4]$. Ligand X may be any mono- or bidentate ligand.

It is hoped that this complex will improve upon the single stranded design, having a reduced flexibility but not all the structural features of the triple stranded cylinder. Some of the important structural and design characteristics needed for non-covalent DNA recognition, binding and anticancer activity might hence be elucidated. The synthetic procedure developed was designed so that a range of different ligands may be added to the original design in order to create a compound with a tunable ligand surface. Properties may therefore be tailored for different chemical or biological interactions and to study the effect of different DNA binding on anticancer properties. Herein the bipyridine complex, Figure 6. 1, is presented as the first complex in this series.

6.2.2 Synthesis of ββ -$[Ru_2L^2_2(bpy)_2]^{4+}$

The synthesis of this compound from ββ-$[Ru_2L^2_2(NO_3)_4]$ is presented in Figure 6. 7, with the starting material being the unsaturated ββ-$[Ru_2L^2_2(Cl)_4]$ compound discussed in chapter 5. This isomer was initially chosen as the chloride ligands can be easily removed, with retention of the ββ- configuration. This is also the only isomer of this range of compounds that is not active against cancer cell lines and it would therefore be attractive to see if a change in binding mode to a non-covalent interaction would confer some activity.

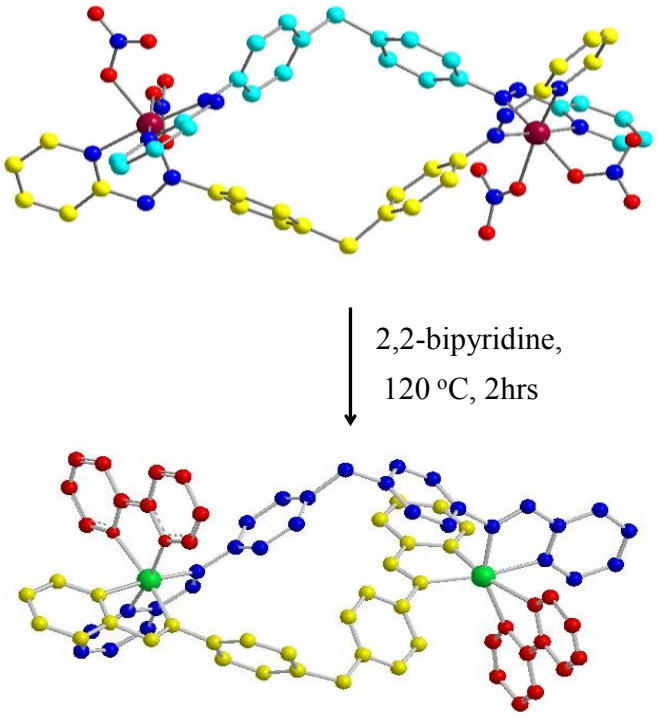

Figure 6. 7 Schematic of reaction procedure from the neutral, unsaturated ββ-[$Ru_2L^2{}_2(NO_3)_4$] complex to the desired ββ -[$Ru_2L^2{}_2(bpy)_2$]$^{4+}$ complex.

Initially, the ββ-[$Ru_2L^2{}_2(NO_3)_4$] complex was synthesised as described in chapter 2 (section 2.3.2). From this structure the bipyridine complex was synthesised via replacement of the NO_3 ligands with 2, 2-bipyridine. The bipyridine complex synthesised has a 4+ charge, unlike the unsaturated chloride/nitrate compounds which are neutral molecules. This greatly improves the water solubility and has also been shown to aid interaction with biomolecules and cellular uptake.[14]

The ^{1}H NMR spectrum, Figure 6. 8, shows that this is indeed the ββ isomer as expected.

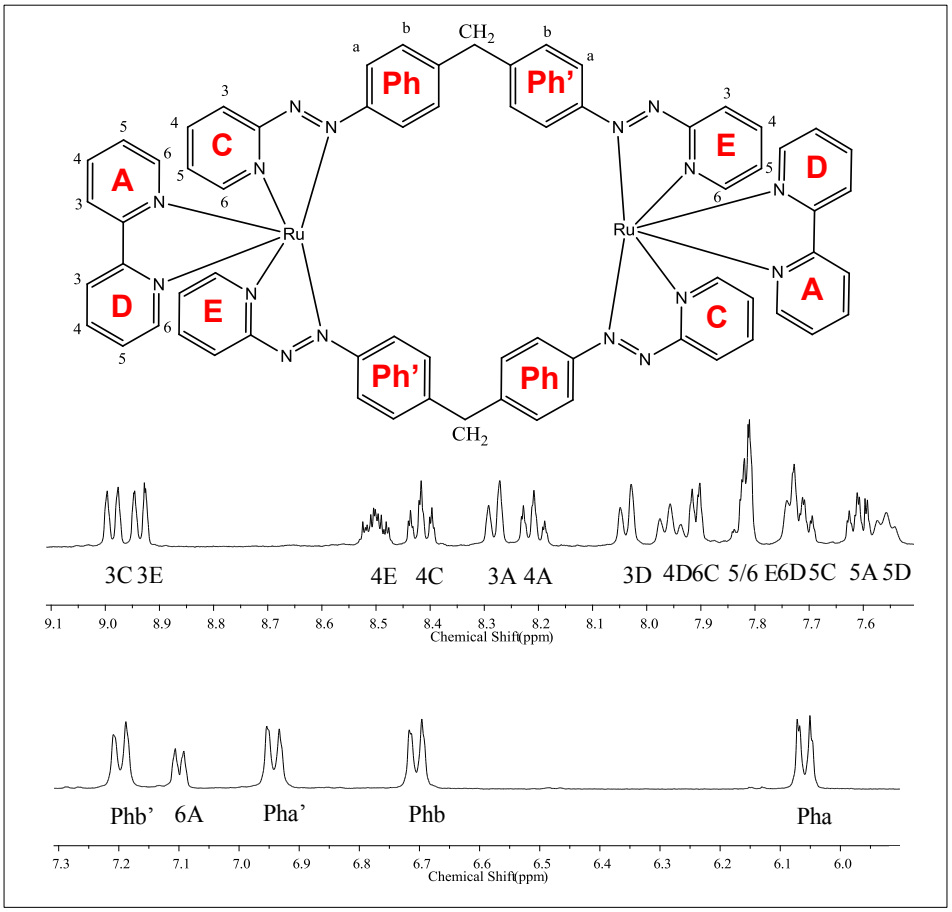

Figure 6. 8 Representation of structure of ββ-[$Ru_2L^2{}_2(bpy)_2$]$(NO_3)_4$[i] with numbering scheme and aromatic region of ^1H NMR spectrum (CD_3CN).

It is notable that the spectrum contains six distinct rings: four pyridyl and two phenyl.

nOe interactions between 3A-3D, 3A-4D and 4A-3D demonstrate that two of the pyridine rings are linked: ie. the bipyridine is non-symmetrical, but that only one bipyridine environment is present (not two distinct bipyridines). Peaks between 6A-6C and 6A-5/6E confirm the A ring of the bipyridine is the one close to the pyridine of the ligand strand and

[i] Structure is shown in 2D not 3D, for ease of visualisation and is the ββ- isomer, not αα- as might be implied from this 2D representation.

peaks between Pha / Pha'-6D confirm that the D ring is the one close to the phenyl rings of the ligand strand.

The remaining rings (two pyridine and two phenyl) are therefore on the ligand (L^2) strand. Long range nOe coupling between Pha' and 3E was used to confirm that phenyl ring Ph' is attached to pyridine ring E and phenyl ring Ph is attached to pyridine ring C. There are two possibilities: that one ligand strand contains C and Ph and the other Ph' and E and the two strands are non-equivalent: or that C, Ph, Ph' and E are the four rings in each strand and the two strands are identical. The former would imply two CH_2 singlet peaks (or one singlet if they overlap exactly). The latter would lead to two distinct coupled protons on the CH_2 (diastereotopic protons) because of the helical chirality. Examination of the CH_2 reveals that it is two coupled doublets at almost identical chemical shift, confirming the second situation, Figure 6. 9.

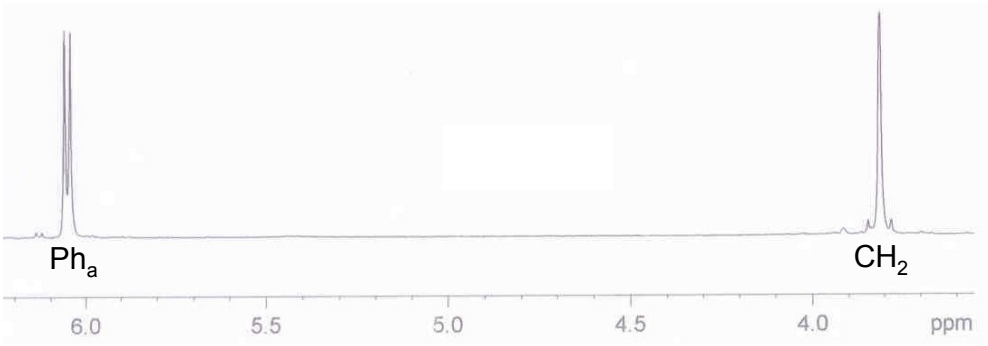

Figure 6. 9 Area of ββ-$[Ru_2L^2{}_2(bpy)_2]^{4+}$ NMR spectrum (CD_3CN) showing two coupled doublets in the CH_2 peak.

There are also some Ph-Ph' nOe interactions showing possible π-stacking in the structure. This would also explain why the Pha peak is at a much lower chemical shift than Pha'/Phb' peaks (if it is involved in pi-stacking).

The crystal structure of the ββ-$[Ru_2L^2_2(NO_3)_4]$ starting material, Figure 6. 10 shows that the two pyridine rings at either end of the ligand L^2 strand are non-equivalent (one is *trans* to an azo nitrogen and the other is *trans* to a nitrate). The ββ-$[Ru_2L^2_2(bpy)_2]^{4+}$ NMR implies the structure is very similar to that of ββ-$[Ru_2L^2_2(NO_3)_4]$ which is only consistent with a ββ- configuration.

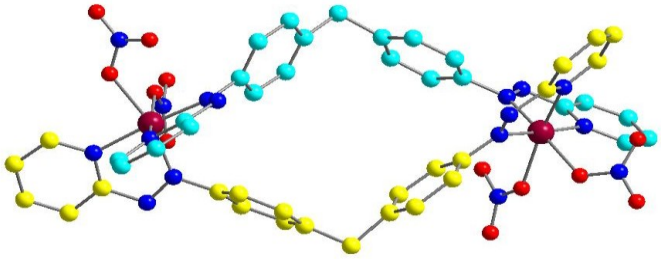

Figure 6. 10 Crystal structure of ββ-$[Ru_2L^2_2(NO_3)_4]$ showing non-equivalence of pyridine rings at each end of ligand L^2 strand.

The ESI mass spectrum of $[Ru_2L^2_2(bpy)_2]^{4+}$ in acetonitrile shows peaks corresponding to $[Ru_2L^2_2(bpy)_2]^{4+}$ (*m/z* 318), $[Ru_2L^2_2(bpy)_2]^{3+}$ (*m/z* 424) and $[Ru_2L^2_2(bpy)_2]^{2+}$ (*m/z* 636) with a correct isotopic distribution confirming a dinuclear double stranded conformation is retained in solution. Electrochemical reduction can take place during ESI mass spectrometry and the ruthenium ion is able to retain its octahedral geometry with a change in oxidation state. This explains the retention of structure with a change in charge of the mass spectrometry fragments.

6.2.3 DNA Binding Studies of ββ-$[Ru_2L^2_2(bpy)_2]^{4+}$

In order to probe DNA binding of this compound, a number of techniques have been used; CD, LD, emission and photocleavage studies. A comparison between this compound and the related $[Fe_2L_3]^{4+}$, $[Ru_2L_3]^{4+}$ and $[Ru_2L(bpy)_4]^{4+}$ complexes will be discussed, as it is

important to view these results in context in order to gain information about how specific structure relates to DNA binding interactions and cytotoxic activity.

6.2.3.1 Circular Dichroism

Circular dichroism (see section 2.4.2) was used to probe any changes in ct-DNA structure as the concentration of ββ-$[Ru_2L^2{}_2(bpy)_2]^{4+}$ was increased. This can give information on binding interactions and changes to the ct-DNA conformation. The concentration of ct-DNA was kept constant throughout the experiment and the resulting spectrum is shown in Figure 6. 11.

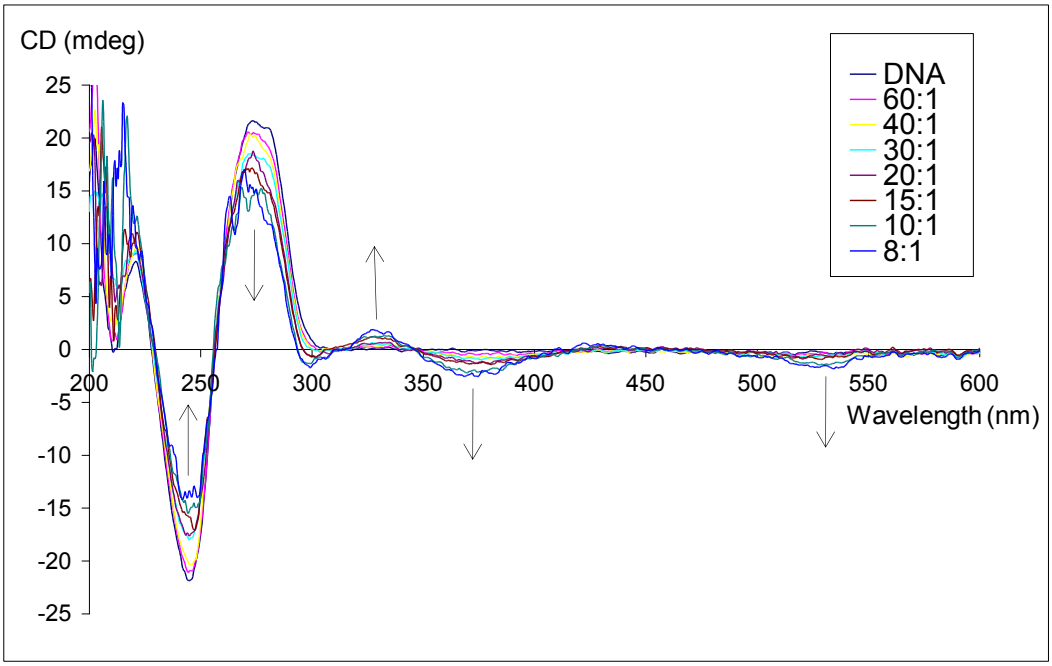

Figure 6. 11 CD spectra of ct-DNA (300 μM) in the presence of varying concentrations of ββ- $[Ru_2L^2{}_2(bpy)_2]^{4+}$. Mixing ratios are indicated as DNA bases to complex.

ββ- $[Ru_2L^2{}_2(bpy)_2]^{4+}$ shows a strong interaction with ct-DNA, with addition resulting in strong induced metal to ligand charge transfer (MLCT) signals in the 300-550 nm region, indicating complex-DNA interactions. The characteristic DNA band at 270 nm decreases

in intensity while the DNA band at 248 nm increases in intensity (becomes less negative). The change in CD value for these bands is due to the contribution to the DNA signal of the 'in ligand' transitions of the cylinder. These small structural DNA modifications are expected upon binding of the complex, confirming that ββ-$[Ru_2L^2_2(bpy)_2]^{4+}$ is indeed binding to the DNA. Importantly, the characteristic B-DNA CD signal is retained throughout the titration, confirming retention of this form of DNA throughout.

The nature of the DNA binding can be investigated by examining a specific area of the CD spectrum and plotting induced CD signal (ICD) versus ββ-$[Ru_2L^2_2(bpy)_2]^{4+}$ concentration at one wavelength, Figure 6. 12.

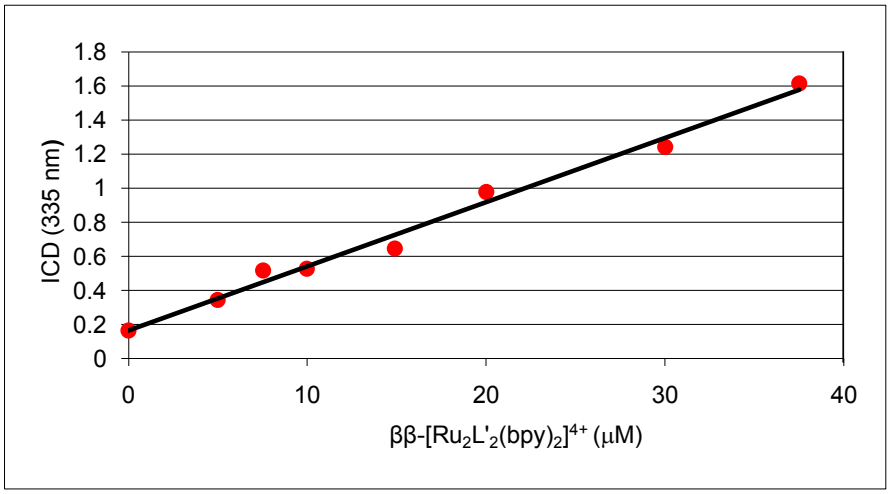

Figure 6. 12 Plot of induced CD signal against ββ-$[Ru_2L^2_2(bpy)_2]^{4+}$ concentration (μM).

There is a clear linear correlation, with induced CD signal increasing as the concentration of complex increases, suggesting only one binding mode of this cylinder to DNA. This linear correlation also exists for the other induced CD bands of this complex and is analogous to that of the triple stranded cylinder, $[Ru_2L_3]^{4+}$ at these concentrations. This

shows that ββ- $[Ru_2L^2_2(bpy)_2]^{4+}$ and $[Ru_2L_3]^{4+}$ may potentially have the same non-covalent binding mode.

6.2.3.2 Linear Dichroism

Linear dichroism (see section 2.4.3) was used to give information on the orientation of the DNA, hence binding, bending and coiling of the DNA upon increase in ββ-$[Ru_2L^2_2(bpy)_2]^{4+}$ concentration can be seen, Figure 6. 13.

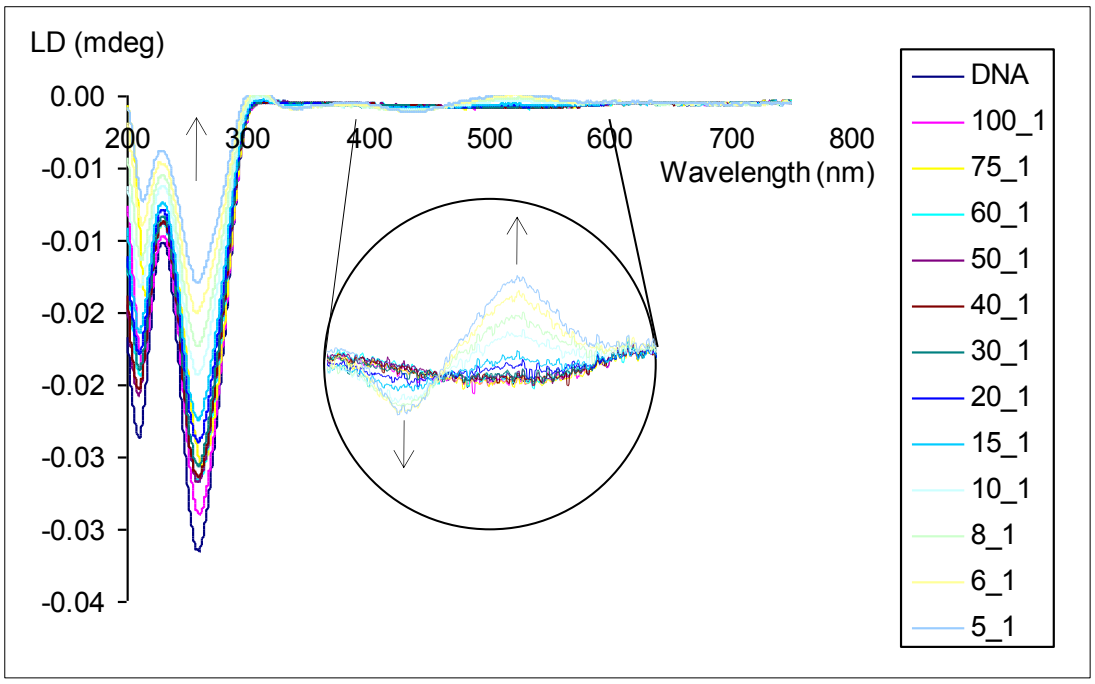

Figure 6. 13 LD spectra of ct-DNA (300 μM) in the presence of varying concentrations of ββ-$[Ru_2L^2_2(bpy)_2]^{4+}$. Mixing ratios are indicated as DNA bases to complex.

Upon addition of ββ-$[Ru_2L^2_2(bpy)_2]^{4+}$ to DNA, both positive and negative induced LD (ILD) signals can be seen in the metal to ligand charge transfer region (300-550 nm). Increasing the concentration of the complex leads to an increase of the ILD signal, indicating that as more compound is added more becomes oriented with the DNA. Furthermore, increasing the concentration of ββ-$[Ru_2L^2_2(bpy)_2]^{4+}$ increases the negative

DNA LD signal, between 200-300 nm, consistent with loss of DNA orientation due to bending or coiling.

A plot of ILD signal at 512 nm against concentration of ββ-$[Ru_2L^2_2(bpy)_2]^{4+}$, Figure 6. 14, shows one linear region.

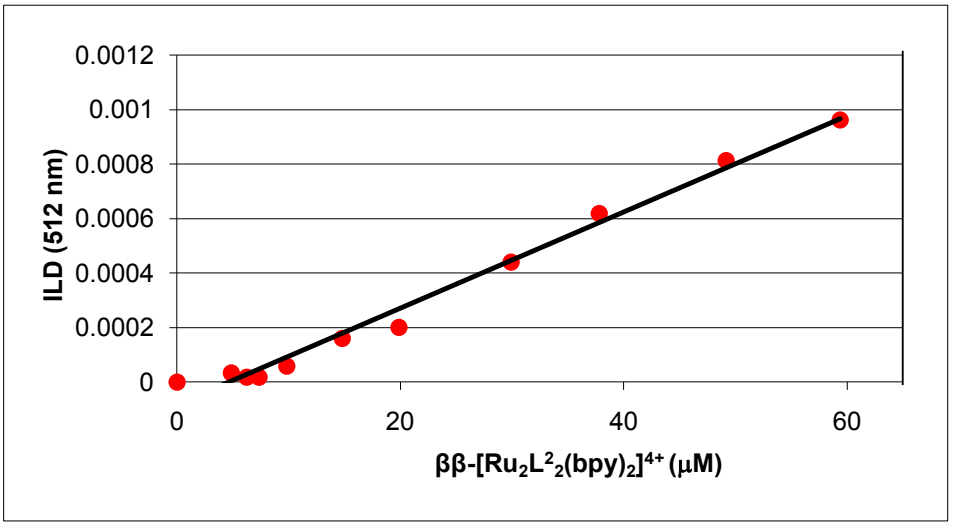

Figure 6. 14 Plot of induced LD signal at 512 nm versus $[Ru_2L^2_2(bpy)2]^{4+}$ concentration (μM).

This result is in agreement with circular dichroism, showing only one binding mode of ββ-$[Ru_2L^2_2(bpy)_2]^{4+}$ to DNA.

Focusing on the DNA band of the LD spectra, at 258 nm and plotting percentage LD against ββ-$[Ru_2L^2_2(bpy)_2]^{4+}$ concentration gives information on the loss of DNA orientation due to complex interactions. Figure 6. 15.

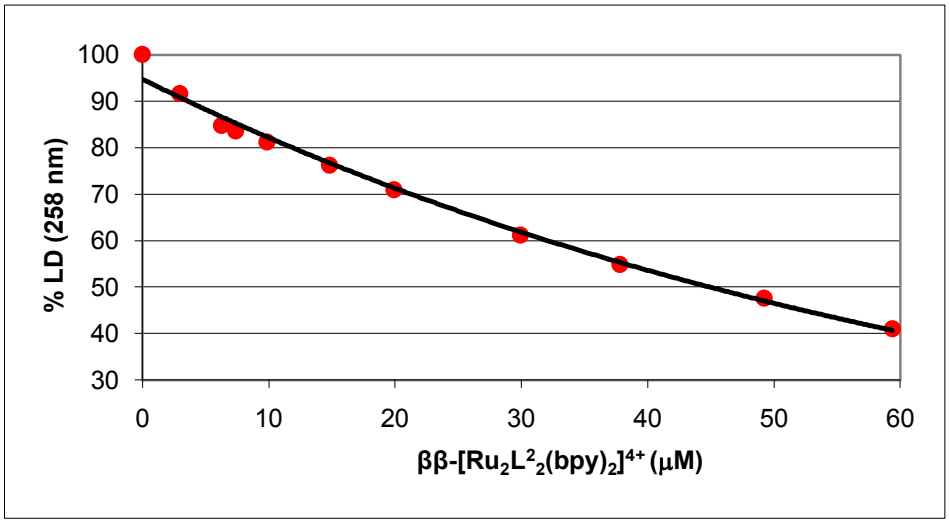

Figure 6. 15 Plot of percentage LD signal at 258 nm against ββ-$[Ru_2L^2{}_2(bpy)_2]^{4+}$ concentration (μM).

The effect of complex-DNA binding is significant, with 8 % of the DNA losing its orientation at a DNA base : complex ratio of 100:1, while at a ratio of 5:1 60 % of the DNA has lost its orientation. This effect is, however, not as profound as that of $[Ru_2L_3]^{4+}$ or $[Fe_2L_3]^{4+}$ [12], Figure 6. 16. In the case of ββ-$[Ru_2L^2{}_2(bpy)_2]^{4+}$, due to the presence of the bipyridine moiety on each metal atom, with coordination through two pyridine nitrogen atoms rather than one pyridine and one azo nitrogen atom, it is thought that ββ-$[Ru_2L^2{}_2(bpy)_2]^{4+}$ will be larger in diameter than the triple stranded cylinders. This result is therefore in agreement with results found previously where increasing the length of cylinders did not affect the DNA binding, but increasing the width significantly reduced DNA binding and coiling.[15]

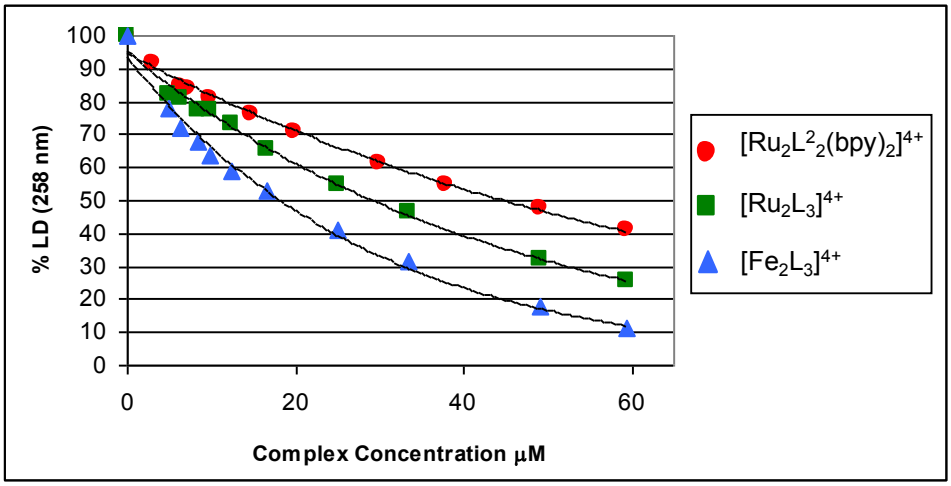

Figure 6. 16 Plot of percentage LD signal at 258 nm against complex concentrations (µM) of ββ-$[Ru_2L^2{}_2(bpy)_2]^{4+}$, $[Ru_2L_3]^{4+}$ and $[Fe_2L_3]^{4+}$.

For $[Ru_2L_3]^{4+}$ there is an orientation loss of 74 % at a 5 : 1 DNA base : complex ratio, however, the most severe loss of orientation occurs for $[Fe_2L_3]^{4+}$, with a loss in DNA orientation of ~90 % at a 5:1 ratio.

These results suggest that DNA binding is not only related to specific structure and rigidity of complexes but that the choice of metal ion may also play an important role.

6.2.3.3 DNA Emission Studies

ββ-$[Ru_2L^2{}_2(bpy)_2]^{4+}$ is coloured bright red, characteristic of a RuN_6 chromophore. The UV-Visible absorption spectrum (see section 2.4.1) shows two MLCT bands in the visible region of the spectrum (380-750 nm) centered at 388 nm and 512 nm. The UV area of the spectrum (200-350 nm) shows ligand centered $\pi - \pi^*$ transitions, Figure 6. 17.

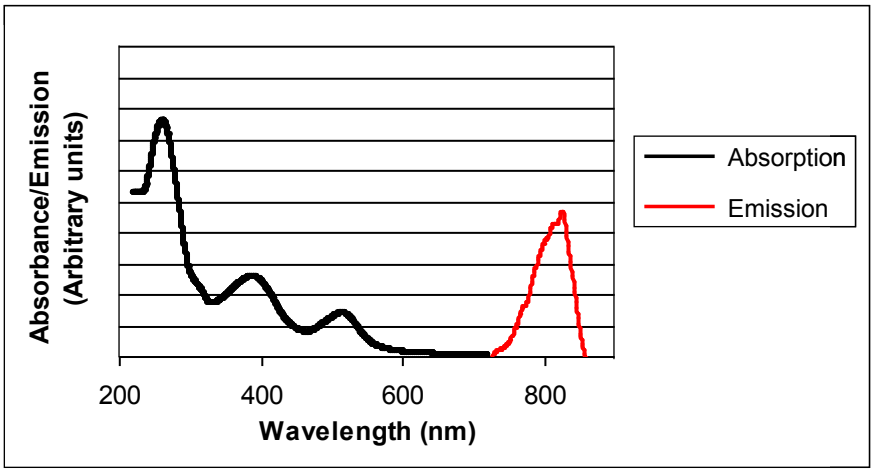

Figure 6. 17 UV-Visible spectrum of ββ-$[Ru_2L^2{}_2(bpy)_2]^{4+}$, with emission after excitation at 512 nm.

The complex itself is fluorescent in water, with excitation in the MLCT band at 512 nm leading to an emission at 820 nm (see section 2.4.5). This arises from a ^{3}MLCT triplet excited state. The abrupt decrease in emission is caused by a drop in PMT response at this wavelength. ct-DNA titrations were performed with ββ-$[Ru_2L^2{}_2(bpy)_2]^{4+}$ at a constant concentration, (19 μM) and emission after excitation at 512 nm was followed, Figure 6. 18.

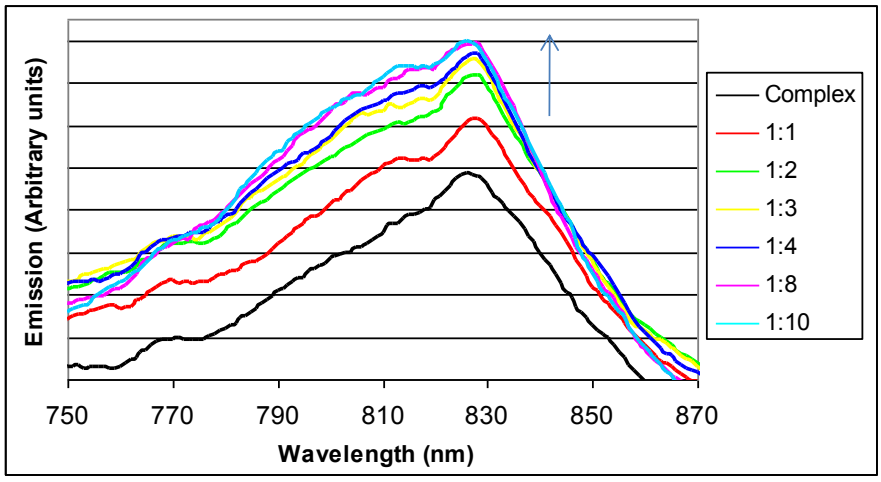

Figure 6. 18 Fluorescence response of ββ-$[Ru_2L^2{}_2(bpy)_2]^{4+}$ (19 μM) in the presence of increasing concentrations of DNA. Mixing ratios indicated as complex to DNA bases.

Successive additions of ct-DNA induced a luminescence enhancement in ββ-$[Ru_2L^2{}_2(bpy)_2]^{4+}$. The increase in emission can be followed at 820 nm, Figure 6. 19.

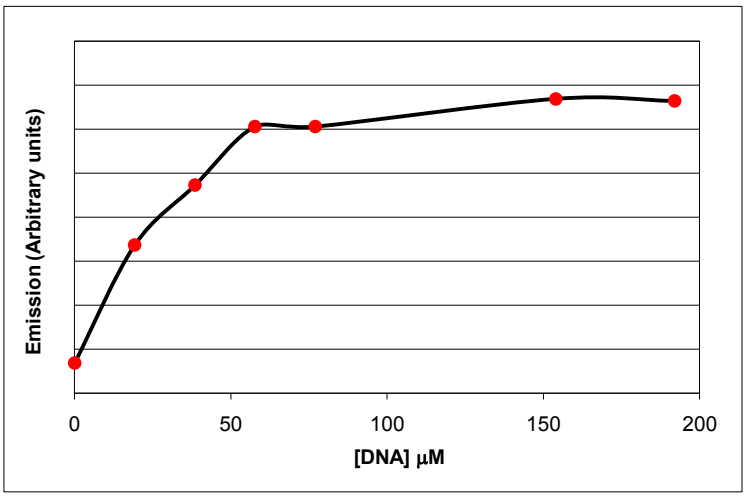

Figure 6. 19 Plot of emission at 820 nm after excitation at 512 nm of ββ-$[Ru_2L^2{}_2(bpy)_2]^{4+}$ (19 µM) against DNA concentration (µM).

There appears to be a maximum loading of the complex on the DNA, where there is no further increase in ββ-$[Ru_2L^2{}_2(bpy)_2]^{4+}$ emission, between a 1:4 to 1:8 complex : DNA base ratio. This is similar to the triple stranded $[Ru_2L_3]^{4+}$ helicate, where a clear maximum loading was seen at a 1:4 complex : DNA base ratio. The well documented "light switch" effect, where emission of a complex is increased upon DNA binding is not as prominent with ββ-$[Ru_2L^2{}_2(bpy)_2]^{4+}$ as with many other complexes, notably DNA intercalators.[16] This is due to the fact that ββ-$[Ru_2L^2{}_2(bpy)_2]^{4+}$ is emissive without the presence of DNA. The enhancement of emission upon DNA binding is caused by an increase in energy of the non-emissive (or in this case slightly emissive) state moving up in energy towards the emissive MLCT excited state, allowing energy transfer and thus enhancement of the luminescence. It is likely that in the ββ-$[Ru_2L^2{}_2(bpy)_2]^{4+}$ system, fluorescence quenching through hydrogen bonding of solvent molecules is prevented upon DNA binding.

In parallel with emission experiments, UV-Visible spectra were recorded after each DNA titration, Figure 6. 20. As the ββ-$[Ru_2L^2_2(bpy)_2]^{4+}$ concentration remains constant, the influence of the DNA on its structure can be monitored.

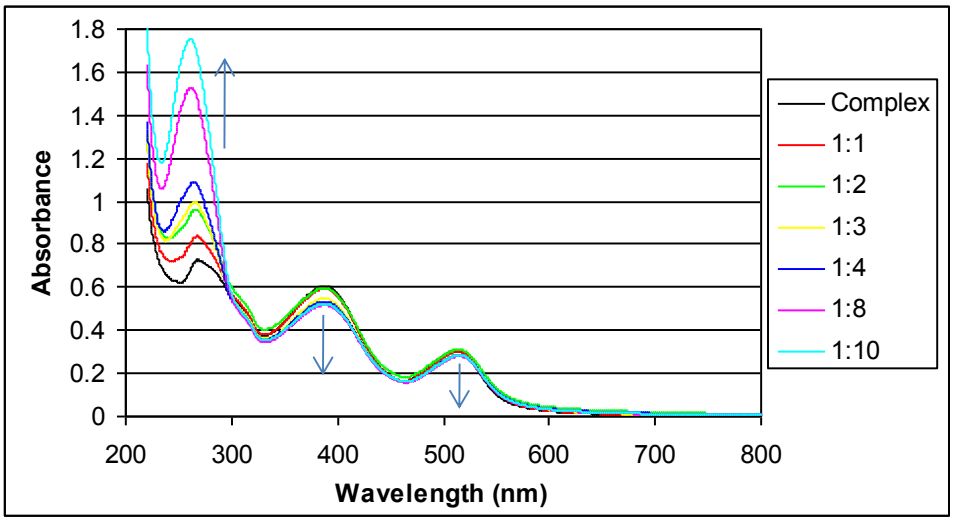

Figure 6. 20 UV-Visible spectra showing the influence of increasing DNA concentration on ββ-$[Ru_2L^2_2(bpy)_2]^{4+}$ structure. Mixing ratios are indicated as complex to DNA bases. (Spectra recorded in parallel with emission titration).

Throughout the titration no shift to red or blue (longer/shorter) wavelengths were observed for the ruthenium MLCT bands (300-600 nm). This indicates the complex ββ-$[Ru_2L^2_2(bpy)_2]^{4+}$ is retained throughout. The observed hypochromicity (decrease) of the ligand centred bands at 388 nm and 512 nm is attributed to the interaction between the complex and DNA. A decrease in these absorption bands is consistent with a stacking interaction involving the ligand.[12]

The binding constant of ββ-$[Ru_2L^2_2(bpy)_2]^{4+}$ to ct-DNA has been estimated using an ethidium bromide (EB) displacement assay (see section 2.4.4). ββ-$[Ru_2L^2_2(bpy)_2]^{4+}$ was able to displace EB from ct-DNA, with the distinctive EB-DNA fluorescence signal

decreasing in intensity on addition of ββ-$[Ru_2L^2{}_2(bpy)_2]^{4+}$. The binding constant of ββ-$[Ru_2L^2{}_2(bpy)_2]^{4+}$ was indicated to be ~ 1.1 x 10^8 M^{-1} and the binding constant of $[Fe_2L_3]^{4+}$ to ct-DNA has previously been estimated to be ~ 0.6 x 10^8 M^{-1}. [15] However, an accurate binding constant greater than that of EB cannot be calculated using this assay.

6.2.3.4 DNA Photocleavage Studies

In order to fully investigate the photophysical properties of the ββ-$[Ru_2L^2{}_2(bpy)_2]^{4+}$ ruthenium centre, DNA cleavage in the presence of UVA (320-400 nm) light was analysed, Figure 6. 21 (see section 2.4.6).

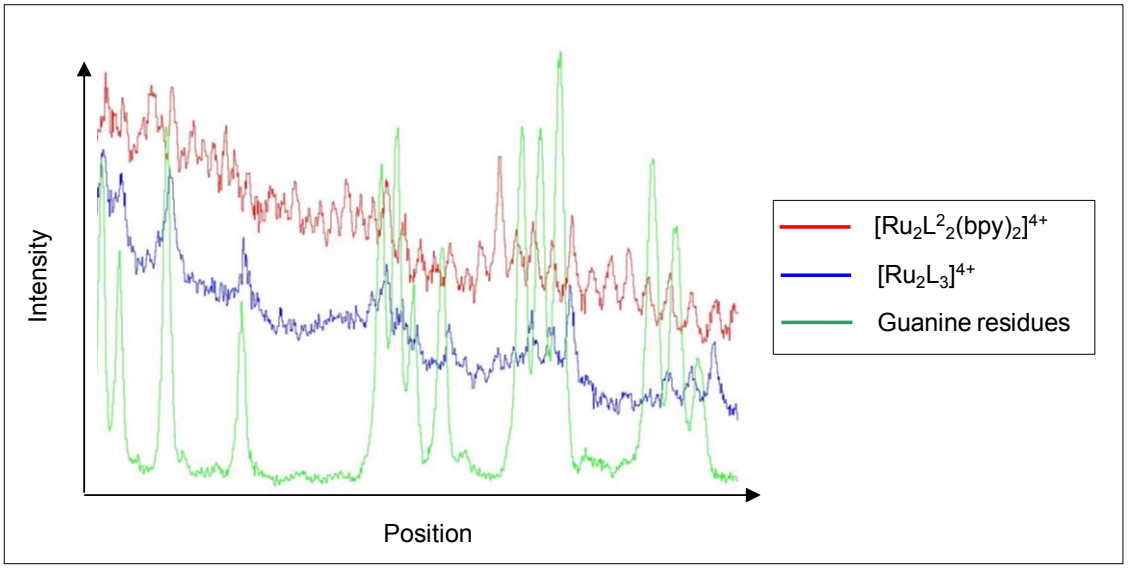

Figure 6. 21 Denaturing gel profile showing guanine residues, DNA cleavage after treatment with $[Ru_2L^2{}_2(bpy)_2]^{4+}$ and DNA cleavage after treatment with $[Ru_2L_3]^{4+}$ at a 20 : 1, DNA base : complex ratio.

The ββ-$[Ru_2L^2{}_2(bpy)_2]^{4+}$ gel profile shows DNA cleavage at every base (without post-treatment with piperidine or aniline). This is markedly different to the triple stranded $[Ru_2L_3]^{4+}$ gel profile which shows cleavage selective to guanine residues. This usually implies an oxygen mediated cleavage pathway, due to the higher reactivity of singlet

oxygen towards guanine as compared to thymine, adenine or cytosine bases. An oxygen mediated pathway cannot, however, be ruled out in the case of ββ-$[Ru_2L^2_2(bpy)_2]^{4+}$, as singlet oxygen is able to diffuse along the DNA helix. This could imply a longer excited state lifetime of ββ-$[Ru_2L^2_2(bpy)_2]^{4+}$ as compared to $[Ru_2L_3]^{4+}$, in order to sensitise more singlet oxygen. However, other explanations for this cleavage pattern exist, so it is not certain exactly which pathway is active here. The production of hydroxy radicals[17] (although usually associated with hydrogen peroxide treatment) and low energy electrons[18] are known to induce cleavage at every base.

6.2.4 Cell Line Testing

With DNA bending and coiling interactions arising from ββ-$[Ru_2L^2_2(bpy)_2]^{4+}$ binding, cell line tests (see section 2.5.5) were carried out in order to try and correlate any anticancer activity with these DNA binding interactions. Results are compared to those previously determined for $[Ru_2L_3]^{4+}$ [13] and $[Ru_2L(bpy)_4]^{4+}$ [19] in order for a comparison on how specific structure is related to cytotoxic activity to be made.

The stability of ββ-$[Ru_2L^2_2(bpy)_2]^{4+}$ in aqueous medium was recorded over the time period of the cell tests (72 hours), at 37 °C in order to check that the compound remains stable in solution for this period, Figure 6. 22 (see section 2.4.1).

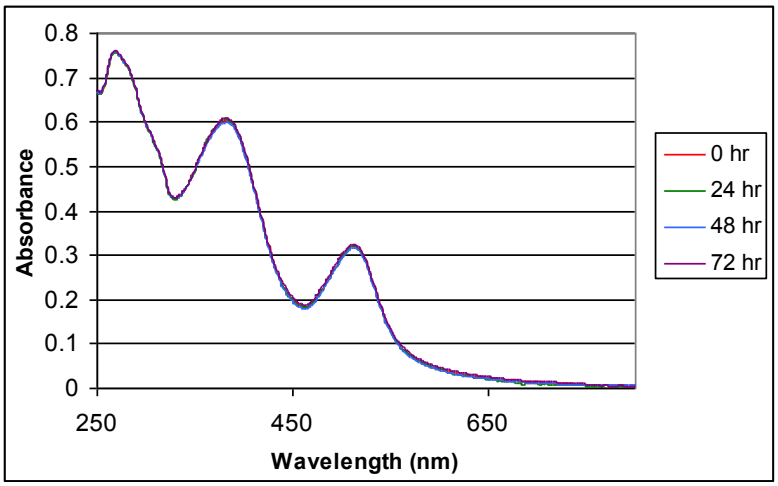

Figure 6. 22 UV- Visible spectra of 17 μM ββ-$[Ru_2L^2{}_2(bpy)_2]^{4+}$ over a 72 hr time period at 37 °C in water.

It is clear from the spectrum that ββ-$[Ru_2L^2{}_2(bpy)_2]^{4+}$ remains stable throughout the 72 hr period.

The human ovarian cancer cell line A2780-P was chosen for these cell tests as there also exists an engineered cisplatin resistant strain, A2780-R. These cell lines are important to study as there is a clinical need for drugs not susceptible to the same resistance mechanisms as cisplatin. T47D was chosen as a representative breast cancer cell line, in order to investigate the effects of ββ-$[Ru_2L^2{}_2(bpy)_2]^{4+}$ on different tumour types, Table 6. 2.

	A2780-P	A2780-R	T47D
ββ-$[Ru_2L^2{}_2(bpy)_2]^{4+}$	30.7 ± 6.0	> 100[ii]	33.4 ± 7.8
$[Ru_2L_3]^{4+}$ [13]	72.0 ± 3.3	> 100[ii]	53.0
Cisplatin	4.4 ± 0.8	19.3 ± 1.8	28.0 ± 1.7

Table 6. 2 IC_{50} values (μM) in the ovarian cancer cell lines, A2780-P/R and the breast cancer cell line T47D of ββ-$[Ru_2L^2{}_2(bpy)_2]^{4+}$ and $[Ru_2L_3]^{4+}$ with cisplatin as control following a 72 hour incubation, as assessed using the MTT assay. Data are reported as mean IC_{50} values ± SD from three independent experiments.

ββ-$[Ru_2L^2{}_2(bpy)_2]^{4+}$ has comparable activity to cisplatin in the breast cancer cell line, T47D. Activity in the ovarian A2780-P line is comparable to that of T47D, however lower than that of cisplatin (higher IC_{50}). ββ-$[Ru_2L^2{}_2(bpy)_2]^{4+}$ is also inactive, at these concentrations, against the cisplatin resistant A2780-R cell line, showing that it may be susceptible to the resistance mechanisms present in this cell line.

Interestingly, as the DNA binding of $[Ru_2L_3]^{4+}$ is clearly distinct to that of ββ-$[Ru_2L^2{}_2(bpy)_2]^{4+}$, with $[Ru_2L_3]^{4+}$ having a greater effect on the DNA as shown through CD and LD binding studies, it may be expected to have greater cellular toxicity. However, this does not appear to be the case and these studies show that DNA binding interactions are not the only important factor in determining cellular toxicity and a compromise between

[ii] Due to comparisons being drawn with cisplatin a maximum concentration of 100 μM was tested for all compounds. Therefore above this value compounds are classed as inactive, and an accurate IC_{50} value cannot be calculated.

rigidity of structure and DNA binding interactions needs to be found in order to find the optimum drug candidate.

The single stranded complex, $[Ru_2L(bpy)_4]^{4+}$ did not display activity in any of the cell lines tested.[19] With the most flexible structure and weakest DNA binding interactions of all the complexes discussed this is not an unexpected result, but again highlights the importance of finding the correct flexibility in compound structure for optimum cytotoxic activity of this range of complexes.

It is also interesting to compare the cytotoxic activity of the ruthenium complexes to that of the iron triple stranded parent cylinder, $[Fe_2L_3]^{4+}$, Figure 6. 23.

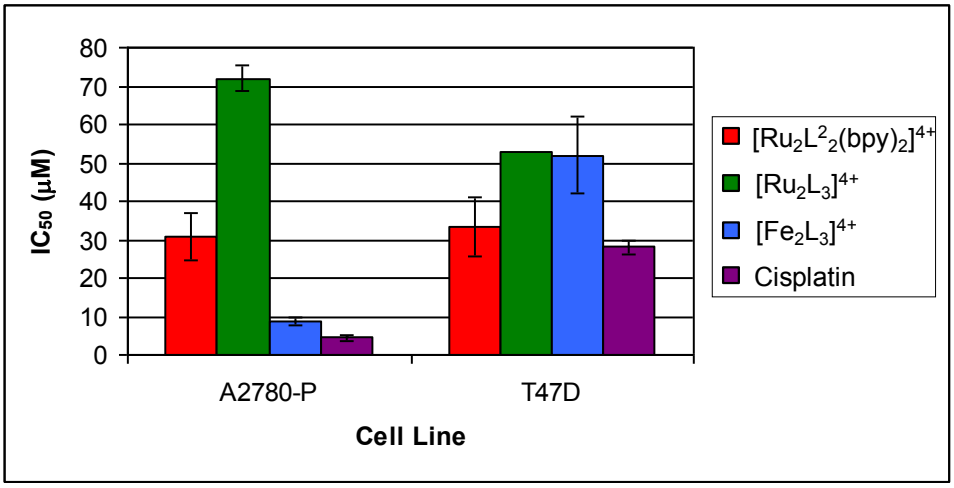

Figure 6. 23 Comparison of IC_{50} values (μM) of ββ-$[Ru_2L^2{}_2(bpy)_2]^{4+}$, $[Ru_2L_3]^{4+}$ and $[Fe_2L_3]^{4+}$ with cisplatin in the A2780-P and T47D cell lines, following a 72 hour incubation, as assessed using the MTT assay. Data are reported as mean IC_{50} values ± SD from three independent experiments.

With $[Ru_2L_3]^{4+}$ having similar DNA binding activity to $[Fe_2L_3]^{4+}$, as assessed by CD and LD studies, the greater activity of the iron cylinder in the A2780-P cell line would correlate

with results previously found where in certain instances the metal centre also plays an important role in cytotoxicity. This is not the case in the T47D cell line however, where both $[Fe_2L_3]^{4+}$ and $[Ru_2L_3]^{4+}$ display a similar activity, less than that of ββ-$[Ru_2L^2{}_2(bpy)_2]^{4+}$. These results show that the criteria for cytotoxic activity is clearly very different in different cell lines, and may indicate that the mechanism of action of this range of complexes differs in each cell line. In the cell lines investigated, cisplatin displayed the highest activity.

6.3 Conclusions and Further Work

The novel ruthenium(II) complex, ββ-$[Ru_2L^2{}_2(bpy)_2]^{4+}$ has been synthesised and studied using a variety of chemical, biophysical and biological techniques. The results have been compared to analogous single and triple stranded ruthenium(II) helicates in order to probe DNA binding interactions and the effects specific surface structures have on cytotoxicity.

It was initially thought that increased DNA binding interactions (bending/coiling) would correlate with increased cellular toxicity. However, this was found not to be the case and the results discussed herein imply that the specific ligand surface, rigidity of structure and the choice of metal centres are incredibly important to consider when designing DNA binding drug molecules. The investigation of novel DNA binding agents with anticancer activity, as well as other useful properties such as luminescence and a tunable ligand surface are important in order to increase understanding in the field of molecular drug design.

ββ-$[Ru_2L^2{}_2(bpy)_2]^{4+}$ is helical, and exists as a racemic mixture of enantiomers. Due to the chiral nature of DNA it is hypothesised that the two enantiomers of this compound may

show different DNA binding interactions and potentially distinct anticancer activity. In order to understand the nature of these interactions fully, the separation and biological studies of the enantiomers would be beneficial to carry out in the future.

Although only ββ-$[Ru_2L^2_2(bpy)_2]^{4+}$ has been discussed herein, it is anticipated that due to the synthetic route developed for this complex the attachment of ligands such as malonate, oxalate, phenanthroline or dppz to each ruthenium(II) centre, in place of the bipyridine moieties in ββ-$[Ru_2L^2_2(bpy)_2]^{4+}$ will be possible. This will allow the creation of a range of compounds with differing ligand surfaces which can be used to study DNA binding interactions. The synthesis of ββ-$[Ru_2L^2_2(ox)_2]$ and ββ- $[Ru_2L^2_2(mal)_2]$ has been attempted, however to date only the oxalate compound has been characterized through ESI mass spectrometry, Figure 6. 24, showing retention of a di-ruthenium(II) complex in solution. Synthesis of larger quantities needs to be carried out for complete characterisation of these complexes.

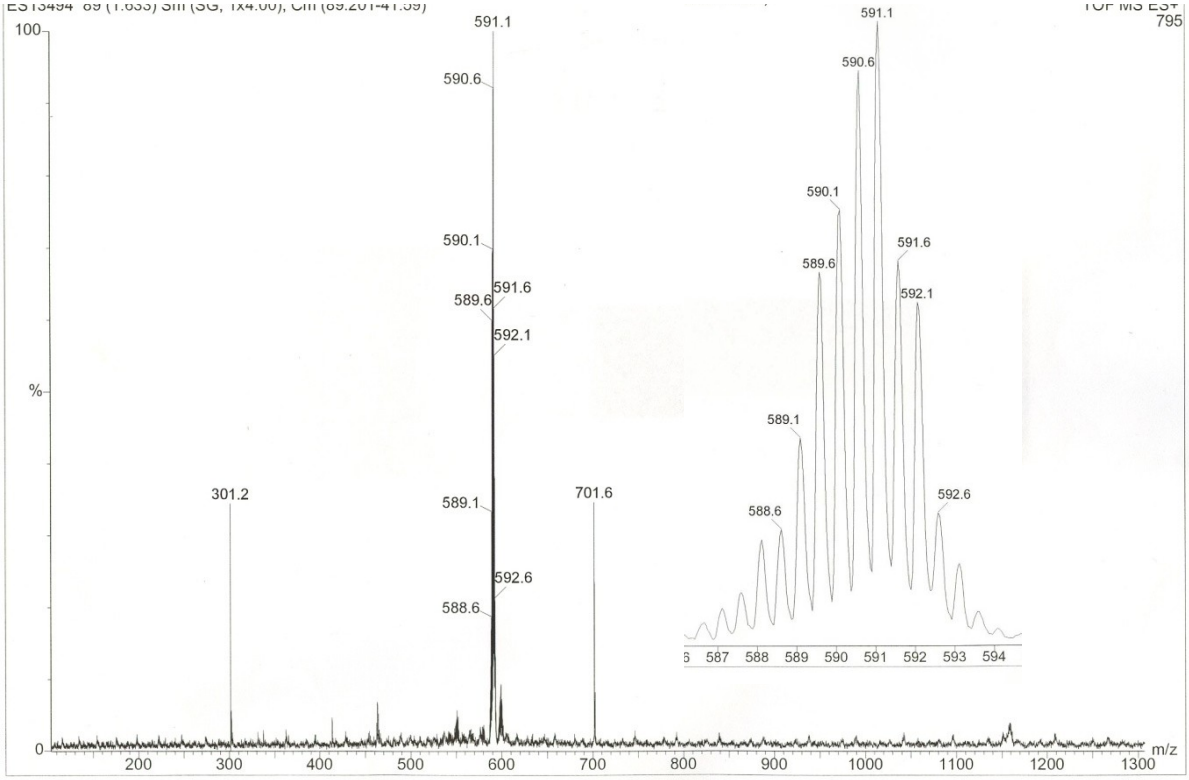

Figure 6. 24 ESI mass spectrum of $[(Ru_2L^2{}_2(ox)_2) + Na_2]^{2+}$ *Inset shows the main peak expanded.*

6.4 References

[1] M. J. Hannon, *Chem. Soc. Rev*., 2006, **35**, 1–18.

[2] J. Reedijk, *Macromol. Symp*., 2008, **270**, 193–201.

[3] E. Corral, A. C. G. Hotze, H. den Dulk, A. Leczkowska, A. Rodger, M. J. Hannon and J.Reedijk, *J. Biol. Inorg. Chem*., 2009, **14**, 439–448.

[4] V. Brabec and O. Novakova, *Drug Resistance Updates*, 2006, **9**, 111–122.

[5] J. Barton, *Chem. Rev*., 1999, **99,** 2777-2795.

[6] A. H. Velders, H. Kooijman, A. L. Spek, J. G. Haasnoot, D. De Vos and J. Reedijk, *Inorg. Chem*., 2000, **39**, 2966.

[7] A. C. G. Hotze, PhD Thesis, University of Leiden, 2003.

[8] M. J. Clarke, *Coord. Chem. Rev.*, 2002, **232**, 69 - 93.

[9] A. C. G. Hotze, E. P. L. van der Geer, S. E. Caspers, H. Kooijman, A. L. Spek, J. G. Haasnoot and J. Reedijk, *Inorg. Chem.,* 2004, **43**, 4935-4943.

[10] U. McDonnell, M. R. Hicks, M. J. Hannon and A. Rodger, *J. Inorg. Biochem.,* 2008, **102**, 2052–2059.

[11] G. I. Pascu, A. C. G. Hotze, C. Sanchez-Cano, B. M. Kariuki and M. J. Hannon, *Angew. Chem. Int. Ed*., 2007, **46**, 4374 –4378.

[12] G. Pascu, PhD Thesis, Univeristy of Birmingham, 2008.

[13] C. Sanchez-Cano, PhD Thesis, University of Birmingham, 2009.

[14] A. L. Harris, J. J. Ryan and N. Farrell, *Mol. Pharmacol.,* 2006, **69**, 666-672.

[15] J. C. Peberdy, J. Malina, S. Khalid, M. J. Hannon and A. Rodger, *J. Inorg. Biochem.,* 2007, **101**, 1937-1945.

[16] D. A. Lutterman, A. Chouai, Y. Liu, Y. Sun, C. D. Stewart, K. R. Dunbar and C. Turro, *J. Am. Chem. Soc.,* 2008, **130**, 1163-1170.

[17] S. Kawanishi, S. Inoue and S. Sano, *J. biol. chem.*, 1986, **261**, 5952-5958.

[18] X. Li, L. Sanche, M. D. Sevilla, *Rad. Res.*, 2006, **165**, 721-729.

[19] U. McDonnell, J. M. C. A. Kerchoffs, R. P. M. Castineiras, M. R. Hicks, A. C. G. Hotze, M. J. Hannon and A. Rodger, *Dalton Trans.*, 2008, 667–675.

Chapter 7

Conclusions and Future Work

In this thesis, biological and DNA binding studies have been carried out on a number of supramolecular helicates containing both iron and ruthenium metal centres. Analogous single, double and triple stranded helicates have been compared. This work has concluded that there are a number of factors affecting the DNA binding of these metal complexes, including the metal centre, ligand structure and the specific ligand surface which changes flexibility of the overall structure. All these factors must be taken into consideration when designing novel metal containing helical drug agents.

This thesis has also advanced knowledge on the biological properties of these complexes and their interactions with cancer cell lines through a number of biological assays, a number of which have not previously been reported in the literature and which have shown very interesting and important results.

Three way junction binding, a novel DNA binding mode, representing the replication fork of living cells has been investigated and a possible link has been found between the stabilisation of this structure by a the parent iron helicate and its ability to kill cancer cells *in vitro*. This is a link which had not previously been established and is therefore very important to help understand existing helical drugs and to design new ones.

Cell line testing of the parent complex showed the influence of parameters not previously thought to be important when determining cytotoxicity. Results obtained have shown that extra care needs to be taken when assessing cytotoxicity for complexes of this nature with an unknown mode of action. This will affect the way cell line testing is carried out in the future. Time-lapse microscopy of cells *in vitro* showed a potential new mode of action of

this range of helical complexes not previously considered or investigated, relating to the cellular cytoskeleton.

Genotoxicity and mutagenicity studies confirmed that double stranded, unsaturated ruthenium complexes do not cause DNA strand breaks or mutations, important results for these promising drug agents to progress further towards the clinic.

Finally, a novel supramolecular drug agent with a tunable ligand surface was synthesised and investigated. This is important to be able to understand effects of ligand and structure flexibility on DNA binding and anticancer activity.

Further work, spanning all chapters of this thesis must be in the elucidation of the exact mode of action of this family of complexes. The work herein has identified key areas to investigate including interactions of complexes with cell membranes and the cytoskeleton, stability of complexes especially those with different metal centres and further DNA binding studies.

Further work arising from chapter three needs to be carried out in order to confirm exact reasons for differing anticancer activities of parent and methyl substituted iron cylinders. Does the inactive methyl substituted cylinder interact with the cell membrane, as images would suggest and does this play a more important role than originally thought on lack of anticancer activity. Synthesis of the ruthenium analogue of this methyl substituted iron cylinder would also be beneficial in order to assess the importance of the metal centre in

this complex on cytotoxic activity and also to investigate the role of stability of the various helicates on anticancer action.

From chapter four the need arises to elucidate the exact mode of action of the parent complex. It appears from results herein that this iron helicate may have a mode of action distinct to that of known anticancer agents and that its effect on the cellular cytoskeleton is more significant than previously thought. These experiments may take the form of live imaging in cells to assess the uptake of the iron helicate and further biological assays to assess the full extent of cytoskeleton disruption. Comparison with the analogous ruthenium cylinder is also important as these complexes display similar DNA binding but have distinct anticancer actions.

Chapter five poses further questions about the ruthenium nitrate substituted helicate, again related to interactions with cell membranes. This needs to be investigated further and may link the mode of action of the double and triple stranded helicates, important for the understanding and design of new agents.

Chapter six discussed one complex in a possible range of many unique supramolecular structures and further work should therefore be carried out to synthesise a full range of complexes using this design and method of synthesis. Bipyridine moieties should be replaced with other ligand surfaces, such as DNA intercalators, to investigate how DNA binding and anticancer activities can be modified.